

Assessing the likelihood and magnitude of volcanic explosions based on seismic quiescence

Diana C. Roman^{a*}, Mel Rodgers^b, Halldor Geirsson^{c,1}, Peter C. LaFemina^c, Virginia Tenorio^d

a. Dept. of Terrestrial Magnetism, Carnegie Institution of Washington, Washington, D.C., USA

b. Dept. of Earth Sciences, Oxford University, Oxford, United Kingdom

c. Dept. of Geosciences, The Pennsylvania State University, University Park, Pennsylvania, USA

d. Instituto Nicaraguense de Estudios Territoriales (INETER), Nicaragua

*Corresponding author. Email address: droman@carnegiescience.edu (D.C. Roman)

1. Present address: Institute of Earth Sciences, University of Iceland, Reykjavik, Iceland

Abstract

Volcanic eruptions are generally forecast based on strong increases in monitoring parameters such as seismicity or gas emissions above a relatively low background level (e.g., Voight, 1988; Sparks, 2003). Because of this, forecasting individual explosions during an ongoing eruption, or at persistently restless volcanoes, is difficult as seismicity, gas emissions, and other indicators of unrest are already in a heightened state. Therefore, identification of short-term precursors to individual explosions at volcanoes already in heightened states of unrest, and an understanding of explosion trigger mechanisms, is important for the reduction of volcanic risk worldwide. Seismic and visual observations at Telica Volcano, Nicaragua, demonstrate that a) episodes of seismic quiescence reliably preceded explosions during an eruption in May 2011 and b) the duration of precursory quiescence and the energy released in the ensuing explosion were strongly correlated. Precursory seismic quiescence is interpreted as the result of sealing of shallow gas pathways, leading to pressure accumulation and eventual catastrophic failure of the system, culminating in an explosion. Longer periods of sealing and pressurization lead to greater energy release in the ensuing explosion. Near-real-time observations of seismic quiescence at restless or erupting volcanoes can thus be useful for both timely eruption warnings and for forecasting the energy of impending explosions.

27

28 **Keywords:** Volcano monitoring, volcanic hazards, phreatic explosions, seismic quiescence, Telica Volcano

29

30 1. Introduction

31

32 It is well-established that volcanic eruptions are the end result of a long-term, crustal-scale process of magma
33 ascent, degassing, and pressurization (Sparks, 2003; Cashman and Sparks, 2013) that generally manifests in
34 monitoring data as a gradual-to-rapid increase in monitored signals (e.g., seismicity, gas emissions) over weeks
35 to months (e.g., Moran et al., 2008; Power et al., 2010). Consequently, observed increases in seismicity,
36 degassing, and/or ground deformation have formed the basis for successful and accurate forecasts of eruption
37 onset at previously quiescent volcanoes (e.g., Voight, 1988; Kilburn, 2003). However, forecasting individual
38 explosions during an ongoing eruption, or at persistently restless volcanoes, is difficult, as seismicity, gas
39 emissions, and other indicators of unrest are already in a heightened state. Thus, identification of short-term
40 precursors to individual explosions is important for the reduction of volcanic risk worldwide.

41

42 Our goal in this study is to determine whether systematic, internally-consistent detection of periods of seismic
43 quiescence could be used to forecast individual explosions, thus providing short-term warning of an impending
44 explosion. Several published studies (e.g., Fischer et al., 1994; Hotovec et al., 2012; Nishimura et al., 2013) have
45 documented instances of precursory quiescence preceding both phreatic and magmatic explosions, which have
46 been linked to sealing of normally-open shallow gas pathways, resulting in a buildup of subsurface pressure
47 ultimately leading to catastrophic failure of the seals and the release of accumulated pressure in the form of an
48 explosion. We focus our analysis on a recent well-monitored sequence of volcanic explosions at Telica Volcano,
49 Nicaragua, in 2011. The high level of both seismic and explosive activity at Telica Volcano makes it an ideal
50 case for assessing the usefulness of this phenomenon as a forecasting tool. Our results demonstrate a strong
51 predictive correlation between episodes of quiescence and explosion, and further show that a strong linear
52 correlation exists between the duration of the precursory quiescence and the energy of the ensuing explosion. In

53 combination, these two findings have important implications for volcano monitoring and eruption forecasting
54 that may be applicable to both magmatic and phreatic eruptions worldwide.

55

56 **2. Background**

57

58 Telica Volcano, Nicaragua, is a basaltic-andesitic stratovolcano located in the Maribios Range of the Central
59 American volcanic arc (Fig. 1). Telica is characterized by persistent restlessness (incandescence, high rates of
60 degassing, and hundreds of low-frequency (LF) seismic events/day), interrupted by VEI 1 Vulcanian phreatic
61 explosions every few years (e.g., in 2004, 2006, 2007, and 2013; Global Volcanism Program, 2009a; 2009b;
62 2014). More explosive (VEI 2) eruptions occurred in 1999, 2011, and 2015 (Rodgers et al., 2013; Geirsson et al.,
63 2014; Rodgers et al., 2015; Global Volcanism Program, 2015). Beginning in November 2009, we deployed the
64 TESAND (Telica Seismic and Deformation) network to record continuous broadband seismic, infrasound, and
65 GPS data with the aim of characterizing background and low-level eruptive processes at persistently restless
66 volcanoes. At the time of the 2011 eruption, the TESAND network consisted of six broadband seismic stations,
67 seven cGPS stations, and one pressure sensor in operation within 4 km of Telica's summit (Fig. 1). Overall,
68 measurements from the TESAND network revealed a lack of magmatic deformation, steady high rates of
69 seismicity during non-eruptive periods, and highly variable rates of seismicity during eruptive periods (Geirsson
70 et al., 2014; Rodgers et al., 2015).

71

72 The 2011 eruptive episode at Telica Volcano consisted of a ~1-month-long series of small-to-moderate ash
73 explosions resulting in ash columns with heights of 1-2 km above the crater rim. Analyses of eruptive products
74 reveal hydrothermally-altered, non-juvenile ash containing sulphate (anhydrite, gypsum, and bassanite), sulfur,
75 and oxide mineralization (Geirsson et al., 2014). A long-term, gradual decrease in rates of LF events began ~9
76 months before the eruption onset, accompanied by an increase in the rate of high-frequency (HF, or VT) events
77 (Geirsson et al., 2014; Rodgers et al., 2015). Multidisciplinary observations, data and analyses for the 2011
78 eruptive episode, in particular a lack of juvenile ash, a lack of deep deformation or seismicity indicating magma

79 ascent from depth, and small observed net changes in the SO₂ flux, indicated that the eruption was amagmatic
80 and likely driven by a transition from an open to a closed degassing system by sealing of the shallow
81 hydrothermal system (Geirsson et al., 2014; Rodgers et al., 2015).

82

83 **3. Data Analysis**

84

85 3.1 Explosion Detection

86

87 Explosions at Telica in May 2011 were detected using a combination of visual observations, infrasound data, and
88 analyses of continuous seismic data. Fieldwork conducted at and around Telica (by H.G.) from May 9-22
89 allowed limited visual observations and photographic documentation (Fig. S1) of individual explosions during
90 daylight hours. An infrasound sensor (Chaparral Physics Model 25V) and a Guralp 6T three-component
91 broadband (30 second) seismic sensor, both sampling at 100 Hz, were located at station TBCF (~200 m from
92 vent; Fig. 1), but were out-of-operation from January-May 2011 due to theft of the solar panels from the station
93 in January 2011. Power was restored to TBCF temporarily between May 11 (17:00 UTC) -15 (08:00 UTC), and
94 then permanently on May 20 at 15:00 UTC. However, only one large explosion (Explosion 38) is associated with
95 an unambiguous explosion signal in TBCF infrasound data (Fig. 2b), with a strongly impulsive onset and an N-
96 shaped waveform characteristic of Vulcanian explosions (Morrissey and Mastin, 2000). Therefore, the only
97 continuous record of explosions during the 2011 eruption is provided by the seismometer at station TBTN (Fig.
98 1; ~560 m from vent, with a Guralp CMG-6TD three-component broadband (30s) seismometer sampling at 50
99 Hz due to data storage limitations), which we use as the primary source of data for our analyses. Several
100 explosions during the 2011 eruption sequence were observed simultaneously by visual and seismic monitoring
101 (Fig. 2). Comparison of these independent records indicate that explosions are generally identifiable in raw
102 seismic data from TBTN as emergent, broadband (1-15 Hz), and long-duration (>1 minutes) high-amplitude
103 transients (Fig. 2), and more obviously as large spikes in seismic intensity (a physically-meaningful, instrument-
104 corrected version of the commonly-used RSAM signal - calculated following Taisne et al., 2011; e.g., Fig. 3.).

105

106 Following Taisne et al. (2011), a continuous seismic intensity time series for May 2011 (Figs. 3 and S2) was
107 derived from raw continuous seismic data from station TBTN (including removal of instrument response), and,
108 together with limited visual observations (Fig. S1), allows us to reconstruct a catalog of explosions during the
109 2011 eruption (Table 1). Raw seismic records from the vertical component (BHZ) of TBTN for the entire month
110 of May 2011 were bandpass-filtered from 0.5-20 Hz and converted to velocity seismograms (Haney et al., 2012).
111 The envelope of each seismogram was calculated by taking the absolute value of the Hilbert transform of the
112 seismogram and then smoothing it using a 15000-point (five minute) median filter. The continuous seismic
113 intensity data for the entire month was then scanned for explosions, defined empirically, based on visual
114 inspection of the data, as periods when seismic intensity remained above $1.5 \mu\text{m/s}$ for at least 10 minutes.

115

116 Based on our analysis of the continuous seismic intensity time series from TBTN combined with a record of
117 visual observations, we identified 50 discrete explosions (Table 1, Fig. 4a) during May 2011. A period of near-
118 continuous, relatively low-amplitude explosive activity accompanied by increased background seismicity
119 (referred to here as the 'transitional period' based on its occurrence during a transition from moderate to higher
120 rates of seismicity; Fig 4b) occurred from May 12-15, during which it is difficult to objectively identify the start
121 and/or end of individual explosions. Thus, our explosion catalog is known to be incomplete on these dates.
122 Furthermore, because visual observation was necessary to identify the smallest explosions within the seismic
123 data, and because the smallest visually observed explosion (40; Fig S1) does not correspond to any discernible
124 change in seismic signal (at TBTN, Fig S2., or TBCF), this catalog is likely missing some smaller explosions
125 during periods when visual observations are unavailable.

126

127 3.2 Quiescence Detection

128

129 Visual inspection of continuous seismic data confirms that explosions are preceded by short-term (minutes to
130 hours) periods of dramatically reduced seismicity rates on all components of all seismic stations in the TESAND

131 network (Figs. 3, 5, and S3). We use the continuous seismic intensity time series for May 2011 to detect periods
132 of seismic quiescence, defined empirically as variable-length periods when the peak-to-peak amplitude of
133 seismic intensity did not exceed $0.1 \mu\text{m/s}$ (Fig. S2). Based on our analysis of continuous seismic intensity, we
134 identify 46 periods of seismic quiescence lasting >30 minutes (Fig. S2). 35 of these immediately preceded one of
135 the 50 identified explosions (Fig. S2). Of the remaining 11 periods, nine occur between May 12-15 when our
136 explosion catalog is known to be incomplete. 15 of the cataloged explosions (Fig. S2 and Table 1) were not
137 immediately preceded by a >30 -minute period of seismic quiescence. Reanalysis of seismic intensity preceding
138 these 15 explosions indicated that 13 were immediately preceded by a period of seismic quiescence lasting at
139 least five minutes. Thus, only two of the 50 identified explosions (explosions 20 and 48) had no identifiable
140 precursory quiescence period.

141

142 3.3 Quiescence Duration and Explosion Energy

143

144 To assess the relationship between the duration of precursory quiescence and the energy of the ensuing
145 explosion, we determine the precise onset and end times of periods of seismic quiescence and explosions using
146 changepoint analysis (e.g., Fig. 5). Changepoint analysis was conducted using the changepoint package (Killick
147 and Eckley, 2014) in R to implement a standard binary segmentation algorithm (Edwards, 1965) to identify the
148 location of multiple statistically significant change points in the mean value of the seismic intensity time series.
149 For each detected quiescence/explosion pair (see above) we visually selected for changepoint analysis a segment
150 of the continuous seismic intensity time series that contained a representative period of pre-quiescence activity,
151 the quiescence and explosion events, and a representative period of post-explosion activity. Thus, the length of
152 the analyzed time series varies based on the relative timing of quiescence and explosion. We assume *a priori* that
153 each time series has exactly three temporal changepoints, corresponding to the quiescence start (QS), explosion
154 start (ES), and explosion finish (EF). We use the 300-second median filtered seismic intensity time series for
155 changepoint analysis for all but the three shortest sequences (Explosions 19, 34, and 39 in Table 1), which were
156 instead smoothed using a 500-point (10 second) median filter. The results of changepoint analysis for all 50

157 explosions in Table 1 are shown in Fig. S4.

158

159 Start times for QS, ES, and EF identified through changepoint analysis are given in Table 1. We calculate the
160 quiescence duration (QD) as the time in minutes between QS and ES (Table 1). QD ranges from 6 minutes prior
161 to Explosion 39 on May 21 at 22:32 to 619 minutes prior to Explosion 28 on May 17 at 05:19. Explosions have
162 variable durations (ED - the time in minutes between ES and EF) ranging from 2-150 minutes on station TBTN
163 (Table 1), and often consist of multiple pulses in rapid succession (Figs. 2 and S3).

164

165 Explosion energy (EE; Table 1) for all explosions is calculated following Johnson and Aster (2005):

166
$$E_{seismic} = 2\pi r^2 \rho_{earth} c_{earth} \frac{1}{A} \int S^2 U(t)^2 dt \quad , \quad (1)$$

167

168 where ρ is density, c is P-wave velocity, and $U(t)$ is the vertical component velocity seismogram. Velocity
169 seismograms were bandpass-filtered between 0.5-20 Hz and integrated over the time window between ES and
170 EF. Because we are interested primarily in internally consistent, rather than absolutely accurate, estimates of
171 explosion energy, we normalize the equation for our purposes by fixing seismic site response (S) and attenuation
172 (A) at unity. For analyses at TBTN, we set $r=560$ m (the horizontal distance from TBTN to the center of the
173 summit crater), $\rho=2000$ kg/m³ (the same value used by Johnson and Aster, 2005), and $c=2100$ m/s (the P-wave
174 velocity in the top layer of the velocity model used by Rodgers et al., 2015 to locate seismic events at Telica).

175

176 Normalized explosion energy ranges from 100-6067 kJ. There is no systematic trend in explosion energy
177 through the eruption (Fig. 4a), but all explosions with > 2000 kJ occur in the middle of the eruption, between
178 May 7-21. The largest (Explosion 28) in terms of energy release (6067 kJ) occurred on May 17, at 05:19 (all
179 times UTC), and was followed shortly by issuance of a Volcanic Ash Advisory Center warning for Telica (Global
180 Volcanism Program, 2011). Additional large explosions with > 3500 kJ energy release occurred on May 7 at

16:20 (Explosion 9), May 10 at 01:09 (Explosion 15) and 13:11 (Explosion 16), May 11 at 06:46 (Explosion 18), May 18 at 19:34 (Explosion 31), May 20 at 10:18 (Explosion 36) , and May 21 at 20:54 (Explosion 38). The May 21 explosion was documented photographically (Fig. S1), and was observed to deposit sizable lithic blocks up to 150 m away from the crater rim (Geirsson et al., 2014).

4. Discussion

4.1 Predictive relationship between quiescence and explosions at Telica

Results of data analysis demonstrate that individual explosions at Telica in May 2011 are consistently preceded by short-term (hours to minutes) episodes of seismic quiescence immediately beforehand, and that there is a strong linear relationship between the duration of precursory quiescence and the energy of the ensuing explosion. Assuming all explosions are cataloged, then 11 periods of seismic quiescence out of 46, or 24%, are false positive predictors of explosion (Fig. S2). However, given that our explosion catalog is almost certainly incomplete, the false positive rate is most likely lower in reality. Only two explosions (explosions 20 and 48) were not immediately preceded by a period of seismic quiescence, corresponding to a false negative rate of two out of 50, or 4%. Explosion 20 is, however, preceded by a statistically-significant increase in the variance of seismic intensity (Fig S2). Explosion 48 is an unremarkable moderate-energy explosion. Overall, we find that the occurrence of a period of seismic quiescence is a strong predictor of short-term eruption likelihood, with low rates of false prediction.

For the entire dataset, a strong linear correlation exists between QD and EE (Fig. 6), indicating that larger explosions are preceded by longer precursory periods of seismic quiescence, and thus that quiescence duration is a strong predictor of explosion energy. The relationship between QD and EE for our dataset is

$$EE = 9.09(QD) + 467.25 \quad (2)$$

206 which leads to $R^2=0.75$, $p<0.0001$). We note that the relationship contains a small offset term, which, if correct,
 207 implies that some small explosions could occur without precursory quiescence. As our observations indicate that
 208 explosions with energy lower than the offset in Eq (2) are preceded by precursory quiescence, the offset term in
 209 Eq (2) is probably not physically meaningful. If the line is forced to pass through the origin, the relationship
 210 between QD and EE becomes

$$211 \qquad \qquad \qquad EE=10.82(QD) \qquad \qquad (3)$$

212 with an $R^2=0.72$. We plot the relationship described by Eq (3) in Figure 6 and note that it is similar to that
 213 described by Eq (2). From here on, we refer to Eq (2) as 'the linear relationship', given that it requires fewer
 214 assumptions. We test whether the linear relationship between QD and EE could be used in real-time to forecast
 215 explosions. Because the first two explosions at minimum are required to define the linear relationship, it is not
 216 possible to forecast the energy of these explosions in real-time. For all subsequent explosions, it is possible to
 217 forecast a *minimum* energy for the impending explosion based on the linear relationship defined by all previous
 218 quiescence/explosion pairs and the current quiescence duration (the actual QD for each explosion can only be
 219 known in hindsight, after the explosion occurs). We demonstrate the use of the linear relationship between EE
 220 and QD in real-time using our explosion/quiescence catalog to forecast the energy of an explosion based on the
 221 QD/EE relationship defined by the previous explosion/quiescence pairs, and graph the forecast values vs actual
 222 values in Figure 7a. We note that the forecast value is generally close to the actual value and that the forecast and
 223 hindcast (the predicted values once the full data set can be used to establish the linear relationship) values
 224 converge towards the end of the eruption sequence (Figure 7b).

226 4.2 Observations and forecasts of precursory quiescence at other volcanoes

228 Similar observations of precursory seismic quiescence have long been noted anecdotally (Newhall & Endo,
 229 1987), and several published studies document instances of precursory quiescence preceding both phreatic and
 230 magmatic explosions. During a phreato-magmatic eruption at Copahue Volcano, Chile, episodes of seismic

quiescence were observed preceding individual explosions (Morales et al., 2015). A period of seismic quiescence also immediately preceded the April 2012 phreatic explosion at Masaya Volcano, Nicaragua (Global Volcanism Program, 2012). Magmatic examples include Suwanose-jima, Japan, where a log-log correlation between quiescence duration and the maximum amplitude of the explosion (a weak proxy for explosion energy) was also documented (Nishimura et al., 2013). Examples of precursory seismic quiescence preceding magmatic eruptions have also been documented at Galeras Volcano, Colombia, in 1993 (Stix et al., 1993; Fischer et al., 1994; Gil Cruz and Chouet 1997), Redoubt Volcano, Alaska, in 2009 (Hotovec et al., 2012); Piton de la Fournaise, la Reunion, in 2010 (Taisne et al., 2011); and Soufriere Hills Volcano, Montserrat, in July 2008 (immediately preceding the onset of eruption Phase 4 of Wadge et al., 2014).

The key challenge in applying the approach demonstrated here to other volcanoes exhibiting precursory seismic quiescence, such as those noted above, in a real-time forecasting context is that our approach requires several *a priori* threshold intensity parameters or values for what defines an "explosion" or "quiescence" that are not easily determined in advance. For our study, these parameters were empirically derived in hindsight, in large part to allow an objective and self-consistent analysis of the continuous dataset, and the threshold values used in this study are almost certainly station- or volcano-specific (and may also change at the same station/volcano from eruption to eruption). Thus, the same parameters would not necessarily work for other data sets, so for other eruptions it would be necessary to estimate the parameters using only the first few eruptions and then 'tune' the parameters through the course of the eruption as demonstrated in the preceding section. Ultimately, additional studies of precursory quiescence will demonstrate whether a set of universal parameters exist that can facilitate real-time quiescence detection and explosion forecasting.

4.3 Mechanism of precursory seismic quiescence

Several studies that document precursory seismic quiescence preceding magmatic explosions invoke a model involving shallow sealing of previously-open gas pathways due to formation of a shallow degassed plug of

newly-emplaced magma (Stix et al, 1993; Gil Cruz and Chouet, 1997; Nishimura et al., 2013), based on observations of long-period seismicity preceding the onset of quiescence (Stix et al., 1993; Gil Cruz and Chouet, 1997), followed by quiescence concurrent with inflationary tilt (Nishimura et al., 2012) and cessation of volcanic gas emissions (Nishimura et al., 2012; Stix et al., 1993). The general sealing-pressurization-explosion model put forward in previous studies explains our observations of precursory quiescence and the strong correlation between quiescence duration and explosion energy at Telica: the longer the gas pathways remain sealed, the more pressure builds up before these seals fail catastrophically, resulting in a larger energy release. We further note that most 'background' seismic events at Telica are low-frequency events commonly associated with gas or fluid flow through constricted pathways (Chouet and Matoza, 2013). The sealing-pressurization-explosion model is similar to that proposed for longer-term seismic quiescence prior to recent eruptive episodes at Telica (Rodgers et al., 2013; Geirsson et al., 2014; Rodgers et al., 2015), but also explains the observed relationship between the duration of the closed-system phase and the energy of the ensuing explosion.

The specific mechanism of gas-pathway sealing at Telica for pre-explosion quiescence is unclear. The amagmatic nature of the 2011 Telica eruption (Geirsson et al., 2014) precludes a mechanism involving formation of a plug or cap at the top of a magmatic conduit due to degassing-induced crystallization, as has been proposed for magmatic eruptions (Stix et al, 1993; Gil Cruz and Chouet, 1997; Nishimura et al., 2013). One possible mechanism applicable to phreatic explosions is sealing due to precipitation of anhydrite and sulfur mineral deposits in shallow fractures acting as gas pathways (e.g., Tenthorey et al., 1998; Edmonds et al, 2003). Geochemical and petrologic analysis of ash erupted during the 2011 explosions revealed hydrothermally-altered, non-juvenile ash containing sulphate (anhydrite, gypsum, and bassanite), sulfur, and oxide minerals (Geirsson et al., 2014). However, additional studies are required to determine whether mineral precipitation sufficient to seal fractures could occur in one or two hours (the minimum time separating the end of an explosion and the onset of quiescence (Figure S2). Alternatively, sealing may occur due to closure of fractures due to subsidence of the crater floor (Matthews et al., 1997), transport of low-porosity volumes of magma to the top of a shallow chamber during sluggish convection (Stix, 2007), or some combination of these mechanisms. Again, however, no

283 deformation or seismicity indicative of magmatic intrusion occurred during the 2011 eruptive episode,
284 precluding a magmatic process for sealing. Additional observations (e.g., high-resolution geodetic observations
285 of Telica's crater floor, continuous gas emission measurements) would be required to determine the exact
286 combination of mechanisms responsible for sealing.

288 5. Conclusions

290 Ultimately, the strong correlation between precursory seismic quiescence and explosion occurrence, and also
291 between precursory duration of quiescence and explosion energy during the 2011 Telica eruption, indicate that
292 careful monitoring of real-time seismic data could be used to formulate accurate short-term forecasts of
293 explosions at restless volcanoes. Declines in seismic event rate may signal impending explosive activity at
294 restless volcanoes worldwide, and longer periods of seismic quiescence at a recently seismically active volcano
295 may indicate a higher risk of energetic explosive activity. The growing number of observations of precursory
296 seismic quiescence before phreatic and magmatic explosions suggests that the sealing-pressure accumulation
297 model may be applicable to eruptions worldwide, including the 2011 eruption of Telica, though the detailed
298 mechanism – in particular the cause of sealing – will differ from system to system.

300 Acknowledgements

301 This study was supported by the National Science Foundation grants EAR-0911366 to D.C.R. and EAR-
302 0911546 to P.C.L. Work undertaken at Oxford by M.R. was completed while funded on NERC STREVA grant
303 NE/J020001/1. We acknowledge the assistance for this study from Polaris Energy (Magdalena Perez), Nuevas
304 Esperanzas, and the residents at Telica. We thank the staff at INETER for on-going assistance and support during
305 deployment of this network. In particular we thank Allan Morales (INETER) and Jim Normandeau (UNAVCO)
306 for assistance in network installation and Molly Witter (PSU) for additional assistance in visual observation of
307 the 2011 eruption. We are extremely grateful to two anonymous reviewers for carefully reviewing this
308 manuscript and providing constructive and thought-provoking criticism of our approach and interpretations. The

309 raw continuous seismic data analyzed in this paper are archived and accessible through the IRIS Data
310 Management Center.

311

312 **References**

313 Cashman, K.V., Sparks, R.S.J., 2013. How volcanoes work: A 25 year perspective. *GSA Bull.* 125, 664-690.

314 Chouet, B.A., Matoza, R.S., 2013. A multi-decadal view of seismic methods for detecting precursors of magma
315 movement and eruption. *J. Volcanol. Geotherm. Res.* 252, 108-175.

316 Edmonds, M., Oppenheimer, C., Pyle, D.M., Thompson, G., 2003. SO₂ emissions from Soufrière Hills Volcano
317 and their relationship to conduit permeability, hydrothermal interaction and degassing regime. *J. Volcanol.*
318 *Geotherm. Res.* 124, 23-43.

319 Edwards, A.W.F., Cavalli-Sforza, L.L., 1965. A Method for Cluster Analysis. *Biometrics* 21, 362-375.

320 Fischer, T.P., Morrissey, M.M., Calvache, V.M.L., Gómez, M.D., Torres, C.R., Stix, J., Williams, S.N., 1994.
321 Correlations between SO₂ flux and long-period seismicity at Galeras volcano. *Nature* 368, 135-137.

322 Geirsson, H., Rodgers, M., LaFemina, P., Witter, M., Roman, D.C., Munoz, A., Tenorio, V., Alvarez, J., Jacobo,
323 V.C., Nilsson, D., Galle, B., Feineman, M.D., Furman, T., Morales, A., 2014. Multidisciplinary
324 observations of the 2011 explosive eruption of Telica volcano, Nicaragua: Implications for the dynamics of
325 low-explosivity ash eruptions. *J. Volcanol. Geotherm. Res.* 271, 55-69.

326 Gil Cruz, F., Chouet, B. A., 1997. Long-period events, the most characteristic seismicity accompanying the
327 emplacement and extrusion of a lava dome in Galeras Volcano, Colombia, in 1991. *J. Volcanol. Geotherm.*
328 *Res.* 77, 121-158.

329 Global Volcanism Program, 2009a. Report on Telica (Nicaragua). In: Wunderman, R (ed.), *Bulletin of the Global*
330 *Volcanism Network*, 34:6. Smithsonian Institution. [http://dx.doi.org/10.5479/si.GVP.BGVN200906-](http://dx.doi.org/10.5479/si.GVP.BGVN200906-344040)
331 [344040](http://dx.doi.org/10.5479/si.GVP.BGVN200906-344040).

332 Global Volcanism Program, 2009b. Report on Telica (Nicaragua). In: Wunderman, R (ed.), *Bulletin of the Global*
333 *Volcanism Network*, 34:8. Smithsonian Institution. <http://dx.doi.org/10.5479/si.GVP.BGVN200908->

334 344040.

335 Global Volcanism Program, 2011. Report on Telica (Nicaragua). In: Wunderman, R (ed.), Bulletin of the Global
 336 Volcanism Network, 36:11. Smithsonian Institution. [http://dx.doi.org/10.5479/si.GVP.BGVN201111-](http://dx.doi.org/10.5479/si.GVP.BGVN201111-344040)
 337 [344040](http://dx.doi.org/10.5479/si.GVP.BGVN201111-344040).

338 Global Volcanism Program, 2012. Report on Masaya (Nicaragua). In: Wunderman, R (ed.), Bulletin of the
 339 Global Volcanism Network, 37:6. Smithsonian Institution. [http://dx.doi.org/10.5479/si.GVP.BGVN201206-](http://dx.doi.org/10.5479/si.GVP.BGVN201206-344100)
 340 [344100](http://dx.doi.org/10.5479/si.GVP.BGVN201206-344100).

341 Global Volcanism Program, 2014. Report on Telica (Nicaragua). In: Wunderman, R (ed.), Bulletin of the Global
 342 Volcanism Network, 39:2. Smithsonian Institution. [http://dx.doi.org/10.5479/si.GVP.BGVN201402-](http://dx.doi.org/10.5479/si.GVP.BGVN201402-344040)
 343 [344040](http://dx.doi.org/10.5479/si.GVP.BGVN201402-344040).

344 Global Volcanism Program, 2015. Report on Telica (Nicaragua). In: Sennert, S K (ed.), Weekly Volcanic Activity
 345 Report, 20 May-26 May 2015. Smithsonian Institution and US Geological Survey.

346 Haney, M.M., Power, J., West, M., Michaels, P., 2012. Causal instrument corrections for short-period and
 347 broadband seismometers. *Seismol. Res. Lett.* 83, 834-845.

348 Hotovec, A.J., Prejean, S.G., Vidale, J.E., Gomberg, J., 2012. Strongly gliding harmonic tremor during the 2009
 349 eruption of Redoubt Volcano. *J. Volcanol. Geotherm. Res.* 259, 89-99.

350 Johnson, J.B., Aster, R.C., 2005. Relative partitioning of acoustic and seismic energy during Strombolian
 351 eruptions. *J. Volcanol. Geotherm. Res.* 148, 334-354.

352 Kilburn, C.R.J., 2003. Multiscale fracturing as a key to forecasting volcanic eruptions. *J. Volcanol. Geotherm.*
 353 *Res.* 125. 271-289.

354 Killick, R., Eckley, I.A., 2014. changepoint: An R Package for Changepoint Analysis. *J. Statistical Software* 58:
 355 1-19.

356 Matthews, S.J., Gardeweg, M.C., Sparks, R.S.J., 1997. The 1984 to 1996 cyclic activity of Lascar Volcano,
 357 northern Chile: cycles of dome growth, dome subsidence, degassing and explosive eruptions. *Bull.*
 358 *Volcanol.* 59, 72-82.

359 Morales, S., Alarcón, A., Basualto, D., Bengoa, C., Bertín, D., Cardona, C., Córdova, M., Franco, L., Gil, F.,

360 Hernandez, E., Lara, L., Lazo, J., Mardones, C., Medina, R., Peña, P. , Quijada, J, San Martín, J.,
 361 Valderrama, O., 2015. The 2012-2014 eruptive cycle of Copahue Volcano, Southern Andes. Magmatic-
 362 hydrothermal system interaction and manifestations. EGU Gen. Assemb. Conf. Abs. 17, 976.
 363 Moran, S.C., Malone, S.D., Qamar, A.I., Thelen, W.A., Wright, A.K., Caplan-Auerbach, J., 2008. Seismicity
 364 associated with renewed dome building at Mount St. Helens, 2004-2005. In: Sherrod, D.R., Scott, W.E.,
 365 Stauffer, P.H. (Eds). A volcano rekindled: The renewed eruption of Mount. St. Helens, 2004-2006. U.S.G.S.
 366 Prof. Pap. 1750, 27-60.
 367 Newhall, C.G., Endo, E.T., 1987. Sudden seismic calm before eruptions: illusory or real? Hawaii Symposium on
 368 How Volcanoes Work Abstracts Volume, 190.
 369 Nishimura, T., Iguchi, M., Kawaguchi, R., Surono, Hendrasto, M., Rosadi, U., 2012. Inflations prior to
 370 Vulcanian eruptions and gas bursts detected by tilt observations at Semeru Volcano, Indonesia. Bull.
 371 Volcanol. 74, 903-911.
 372 Nishimura, T., Iguchi, M., Oikawa, J., Kawaguchi, R., Aoyama, H., Nakamichi, H., Ohta, Y, Tameguri, T., 2013.
 373 Mechanism of small vulcanian eruptions at Suwanosejima volcano, Japan, as inferred from precursor
 374 inflations and tremor signals. Bull Volcanol. 75, 779 (2013).
 375 Power, J.A., Lalla, D.J., 2010. Seismic Observations of Augustine Volcano, 1970-2007. In: Power J.A., Coombs,
 376 M.L., Freymuller, J.T. (Eds), The 2006 Eruption of Augustine Volcano, Alaska. U.S.G.S. Prof. Pap. 1769, 3-
 377 40.
 378 Rodgers, M., Roman, D.C., Geirsson, H., LaFemina, P., Munoz, A., Guzman, C., Tenorio, V., 2013. Seismicity
 379 accompanying the 1999 eruptive episode at Telica Volcano, Nicaragua. J. Volcanol. Geotherm. Res. 265,
 380 39-51.
 381 Rodgers, M., Roman, D.C., Geirsson, H., LaFemina, P., McNutt, S.R., Munoz, A., Tenorio, V., 2015. Stable and
 382 unstable phases of elevated seismic activity at the persistently restless Telica Volcano, Nicaragua. J.
 383 Volcanol. Geotherm. Res. 290, 63-74.
 384 Sparks, R. S. J., 2003. Forecasting volcanic eruptions. Ear. Plan. Sci. Lett. 210, 1-15.
 385 Stix, J., 2007. Stability and instability of quiescently active volcanoes: The case of Masaya, Nicaragua.

Geology, 35, 535-538.

Stix, J., Zapata G., J.A., Calvache V., M., Cortés J., G.P., Fischer, T.P., Gómez M., D. , Narvaez, M., L. Ordoñez, V., M., Ortega E., A., Torres C., R., Williams, S.N., 1993. A model of degassing at Galeras Volcano, Colombia, 1988-1993. *Geology* 21, 963-967.

Taisne, B., Brenguier, F., Shapiro, N.M., Ferrazzini, V., 2011. Imaging the dynamics of magma propagation using radiated seismic intensity. *Geophys. Res. Lett.* 38, L04304.

Tenthorey, E., Scholz, C.H., Aharonov, E., Léger, A., 1998. Precipitation sealing and diagenesis. 1. Experimental results. *J. Geophys. Res.* 103, 23-951.

Voight, B., 1988. A method for prediction of volcanic eruptions. *Nature* 332, 125-130.

Wadge, G., Voight, B., Sparks, R.S.J., Cole, P.D., Loughlin, S.C., Robertson, R.E.A., 2014. An overview of the eruption of Soufriere Hills Volcano, Montserrat from 2000 to 2010. *Geol. Soc., Lond. Mem.* 39, 1-40.

Figure and table captions

Figure 1: Location of Telica Volcano in Nicaragua (inset maps), and location of Telica's active vent (star) and seismic, GPS, and pressure stations in the TESAND network during the 2011 eruption (green triangles).

Figure 2. Example of an explosion (corresponding to explosion 38 in Table 1) as seen in (a) photographic, (b) infrasonic, and (c-e) seismic records from TBCF and TBTN. Seismic (BHZ) and infrasound (BDF) records in b-d are unfiltered; the spectrogram in e is generated from a bandpass-filtered (0.5-20 Hz) seismic record from TBTN (BHZ).

Figure 3. Example day (May 21) of analysis of continuous median-filtered seismic intensity from a bandpass-filtered (0.5-20 Hz) seismic record from TBTN (BHZ). Red stars mark explosions indicated by periods of seismic intensity above 1.5 $\mu\text{m/s}$ for at least ten minutes – the star at 20:54 corresponds to explosion 38 (Table 1 and Figure 2). Dark blue inverted triangles mark periods of seismic quiescence indicated by periods of at least 30 minutes during which the peak-to-peak amplitude of seismic intensity did not exceed 0.1 $\mu\text{m/s}$. Pale blue

triangles mark pre-explosion periods of seismic quiescence lasting at least 5 minutes. See Supplementary Figure 2 for entire (May 2011) analysis.

Figure 4. (a) Timing and energy of detected explosions and (b) the number of automatically-detected seismic events (all volcano-seismic event types) per 30 minute period for the entire month (details of the automatically-detected seismic event catalog are given in Rodgers et al. 2015). The gray box in (a-b) denotes a transitional period during which explosions occurred frequently but with energy released over a longer period, resulting in seismic intensities below our explosion detection threshold (see also Fig. S2).

Figure 5. Example seismic data and the results of changepoint analysis of explosion intensity (for Explosion 7 on May 6, 2011). Seismic waveforms in both the time (a) and frequency (b) domain have been bandpass-filtered between 0.5 and 20 Hz. (c) shows median-filtered seismic intensity (blue) derived from the filtered waveform as well as the mean value (horizontal red lines) for segments defined by changepoint analysis. In (b), QS is quiescence start, QD is quiescence duration, ES is explosion start, ED is explosion duration, and EF is explosion finish. Light gray regions are periods of 'background' seismicity, the white region is the period of pre-explosion quiescence, and the dark gray region is the explosion period.

Figure 6. Quiescence duration (QD) vs. explosion energy (EE) from Table 1. Solid line is the linear best-fit to the entire data set given by Eq (2) showing strong positive correlation between QD and EE. Dashed line is the linear best-fit to the entire data set given by Eq (3), showing a similarly strong positive correlation.

Figure 7. a) Example of real-time forecasting of explosion energy based on a continuously updated linear relationship between quiescence duration and explosion energy. For each explosion for which QD and ED are available (explosion numbers correspond to those in Table 1) the best-fit linear relationship for all previous explosions (line not forced through the origin) is used to forecast explosion energy based on the measured quiescence duration (blue asterisks). This forecast is compared to the actual (measured *post-hoc*) value for

explosion energy (yellow triangles) and the 'hindcast' value based on Eq (2) (red crosses). Note that the forecast value is generally close to the actual value and that the forecast and hindcast values converge towards the end of the eruption sequence. In a true forecasting context where QD can only be known *post hoc*, only forecasts of minimum energy given the current QD are possible. b) Absolute value of residuals for the real-time forecast and hindcast (vs actual). Note the convergence of the two series towards the end of the explosion sequence.

Table 1: Composite catalog of explosions, listing all seismically-detected (Fig. S2) and photographically-documented ('X' in Visual column, see photos in Fig. S1) explosions. Gray-shaded regions in Visual and Infra columns indicate periods for which visual and/or infrasound observations are not available. An 'X' in the Infra column indicates that a characteristic 'N-wave' (an infrasonic wave comprised of a sharp upward pulse (compression) followed by a sharp downward pulse (rarefaction), similar in appearance to the letter N) is visible in continuous infrasound data, and an 'X' in the Seismic column indicates that a period of elevated seismic intensity corresponding to the explosion was identified during changepoint analysis. Date and time (UTC) given is the date for quiescence start (QS). Explosions starting or finishing the day after the corresponding QS are indicated by (+1). QS, ES (explosion start), and EF (explosion finish) are measured to the nearest second using changepoint analysis – see Section 3.3 for details and Fig. S4 for individual analyses. Quiescence duration (QD) is the difference between QD and ES in minutes and explosion duration (ED) is the difference between ES and EF in minutes. Explosion energy (EE) is calculated for the period between ES and EF – see Methods for details of calculation. In several cases, QS, ES, and/or EF could not be detected (N/D) thus QD, ED, and/or EE could not be calculated (N/C) – see Supplementary Information for detail on individual explosions. Explosion 40 was not detected seismically; therefore visually observed times are included for ES and EF.

Supplementary Information

Supplementary Figure 1: Photos of visually-observed explosions (Explosion numbers correspond to those in Table 1). All photos taken by H.G.

Supplementary Figure 2: Continuous median-filtered seismic intensity from TBTN during May 2011. Red stars

mark explosions indicated by periods of seismic intensity above $1.5 \mu\text{m/s}$ for at least ten minutes. Yellow stars indicate visually-observed explosions not accompanied by sustained elevated seismic intensity. Explosion numbers correspond to those in Table 1. Dark blue inverted triangles mark periods of seismic quiescence indicated by periods of at least 30 minutes during which the peak-to-peak amplitude of seismic intensity did not exceed $0.1 \mu\text{m/s}$. Pale blue triangles mark pre-explosion periods of seismic quiescence lasting at least 5 minutes (but less than 30 minutes). Identified periods of seismic quiescence not immediately followed by an explosion (false positives) are marked with blue arrows – note that all but two of these occur between May 12-15. Two tectonic earthquakes producing spikes in seismic intensity are marked with green diamonds. Finally, periods during which maintenance work on station TBTN resulted in high seismic noise are marked with gray boxes.

Supplementary Figure 3: Example of a quiescence/explosion cycle (Explosion 41) on vertical and horizontal components of TBTN and on vertical components of other stations in the TESAND network (see Fig 1. for station locations). The timing of QS, ES, and EF determined through changepoint analysis of the time series from TBTN_BHZ (Table 1) is shown with vertical red lines. Note that precursory quiescence is apparent on all stations/channels and the timing of QS, ES, and EF is similar on all stations/channels.

Supplementary Figure 4: Analyses of 50 individual explosions at TBTN. Top panel for each explosion shows bandpass-filtered (0.5-20 Hz) and instrument-corrected velocity seismogram (blue) and three identified changepoints (red vertical lines). Bottom panel for each explosion shows median-filtered seismic intensity (blue) and means for each of four segments (background activity, precursory quiescence, explosion, background activity) identified by changepoint analysis (horizontal red lines). Inset in top panel gives explosion number, calculated QD, and calculated EE. N/A indicates that the information cannot be determined because of station maintenance or a failure to identify segment(s) through changepoint analysis. Gray regions for explosions 17, 22, and 35 show periods of station maintenance at seismic station TBTN. Note that for explosions 11 and 21-26 there is no detectable explosion finish and therefore no calculated EE, and for explosions 20 and 48, there is no precursory seismic quiescence and therefore no calculated QD. Explosion 40 was visually observed (during the time indicated by the yellow shaded region) but does not correspond to any detectable change in seismicity (no QS, ES, or EF).

Figure_1

[Click here to download Figure: Figure_1_revised.pdf](#)

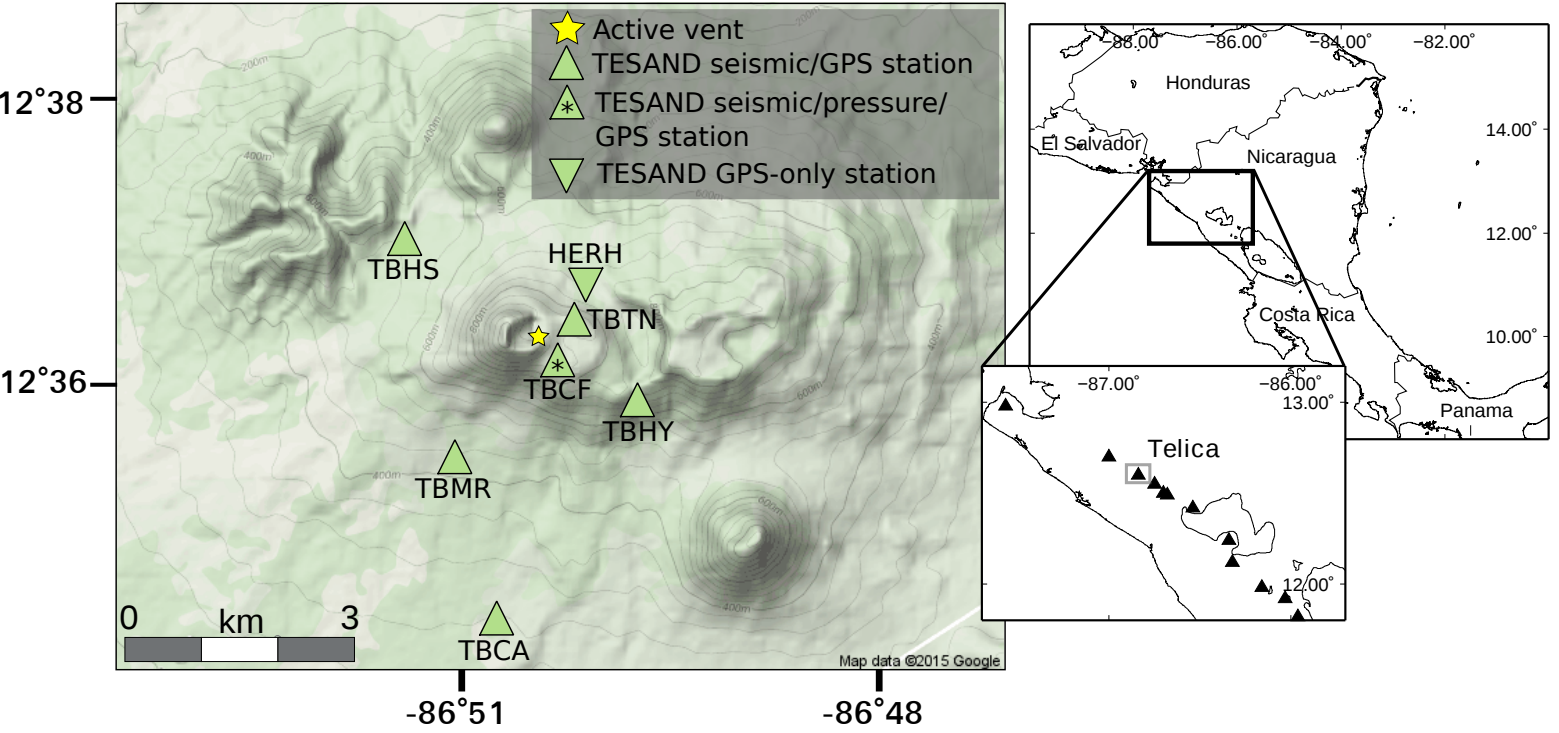


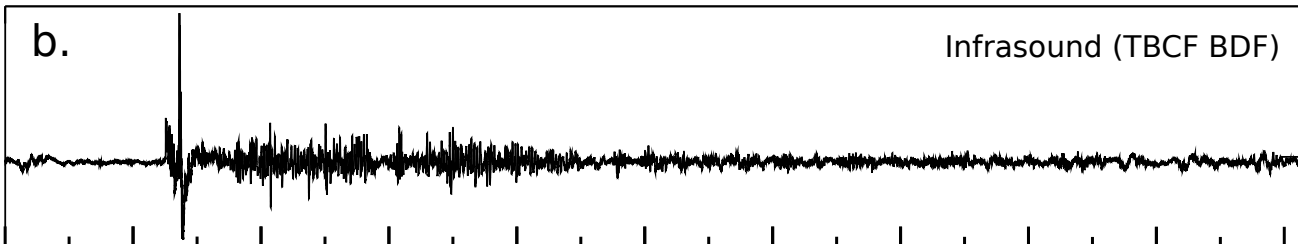
Figure_2
[Click here to download Figure: Figure_2.pdf](#)

a.



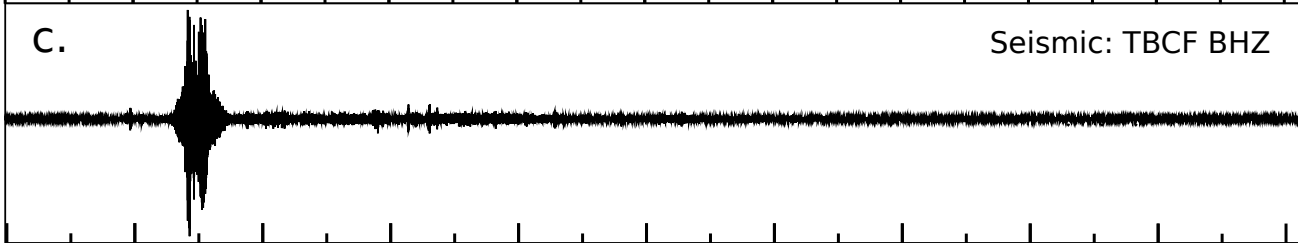
b.

Infrasound (TBCF BDF)



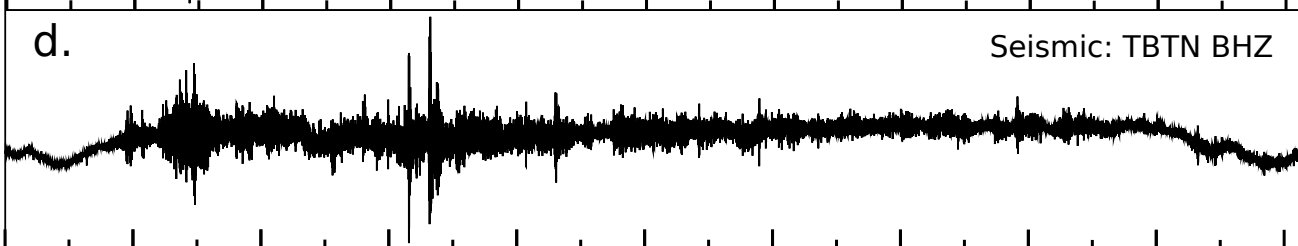
c.

Seismic: TBCF BHZ



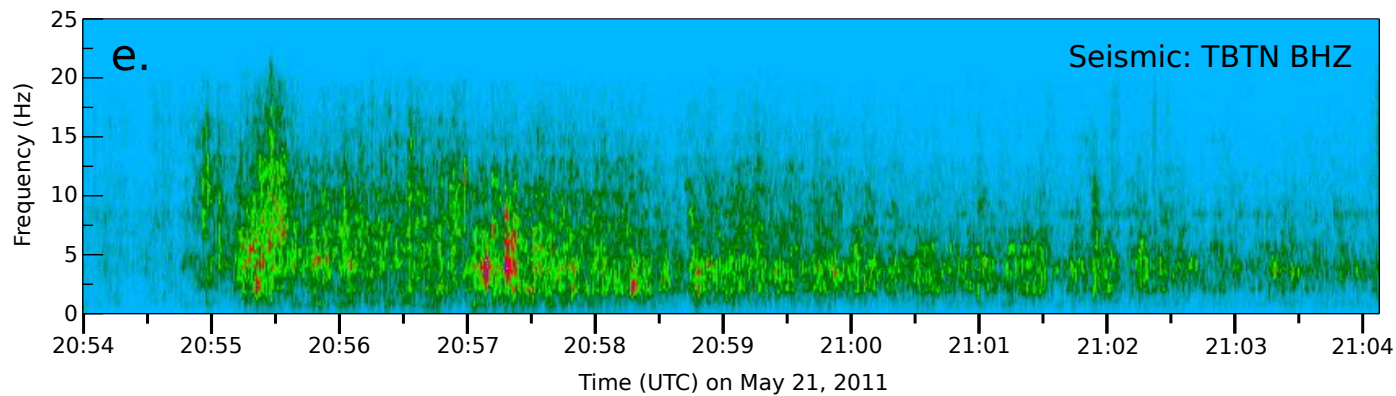
d.

Seismic: TBTN BHZ

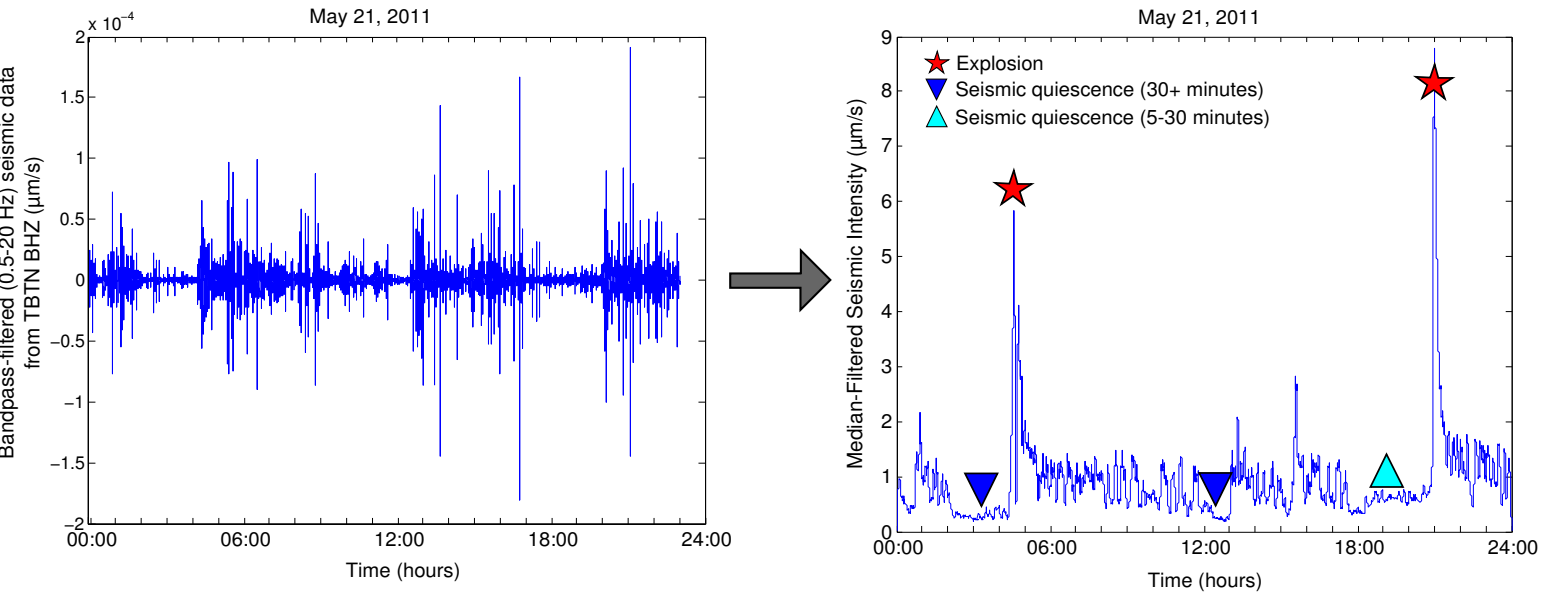


e.

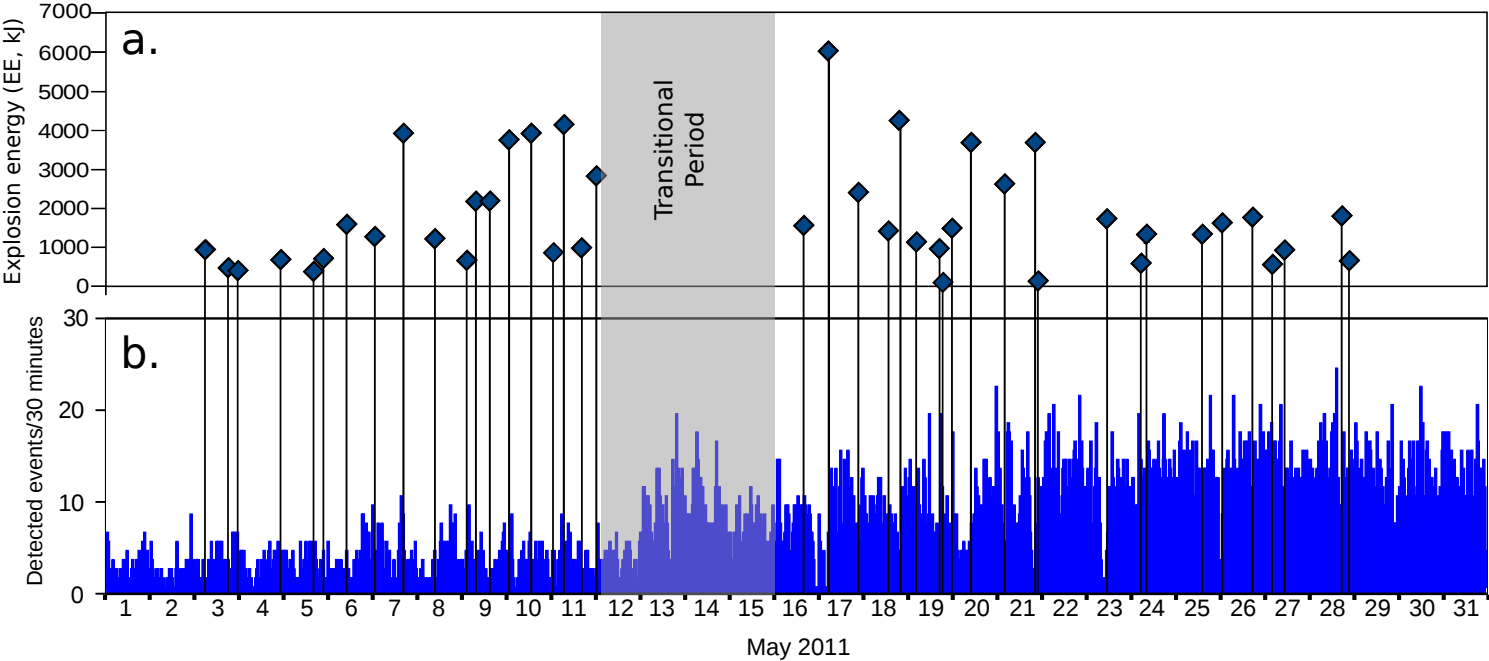
Seismic: TBTN BHZ



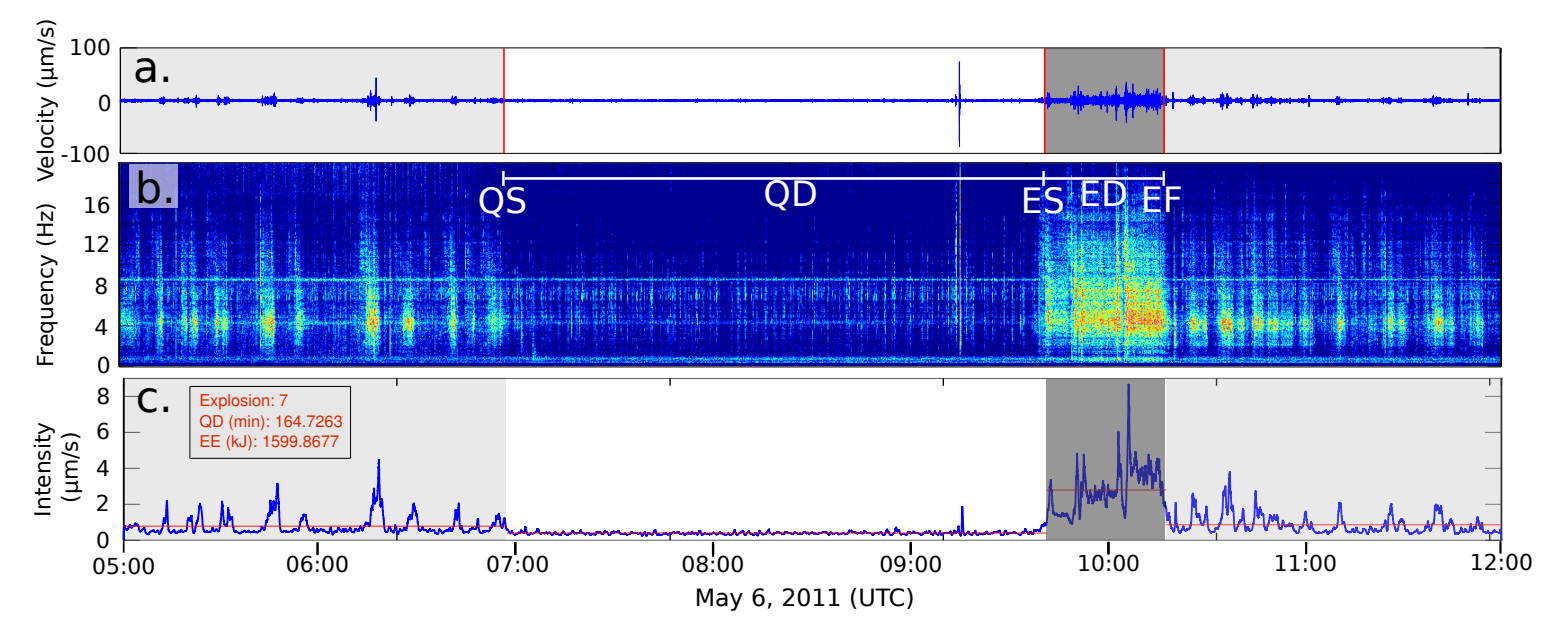
Figure_3
[Click here to download Figure: Figure_3_revised.pdf](#)

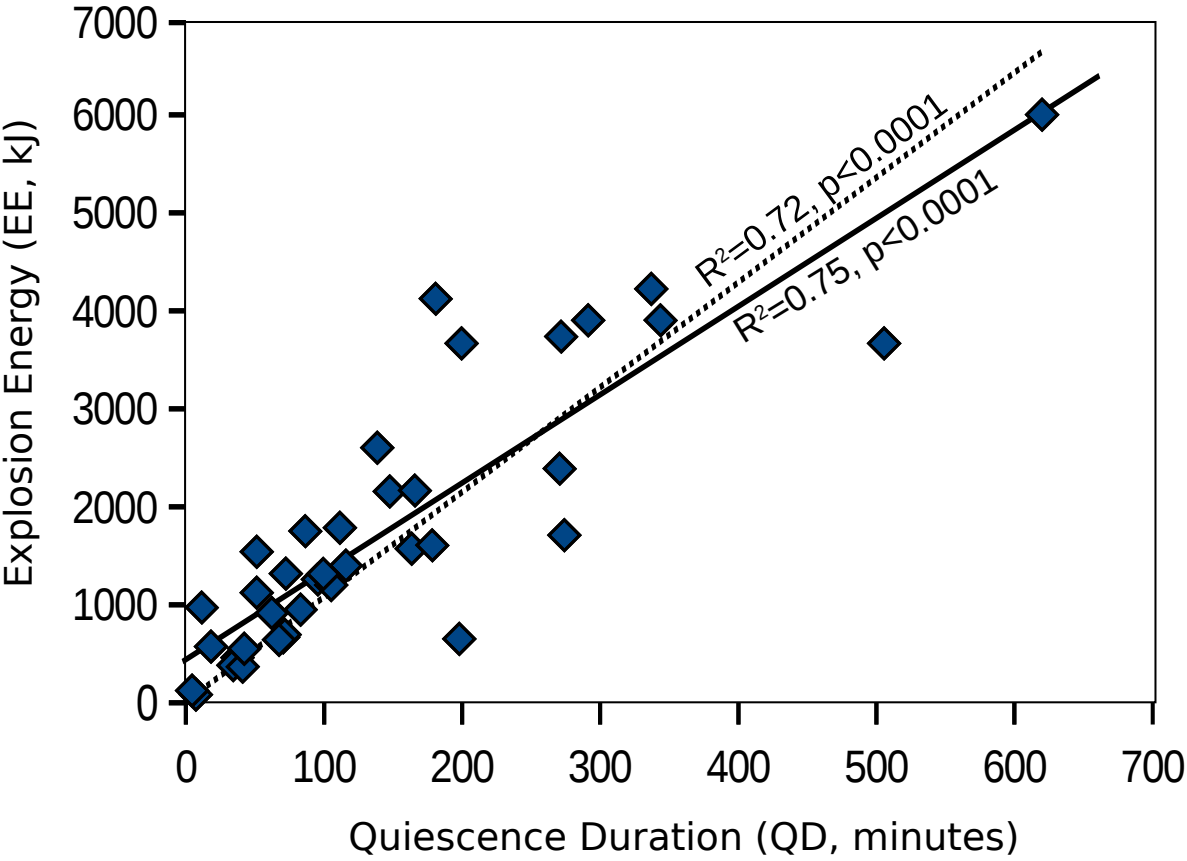


Figure_4
[Click here to download Figure: Figure_4.pdf](#)



Figure_5
[Click here to download Figure: Figure_5_revised.pdf](#)





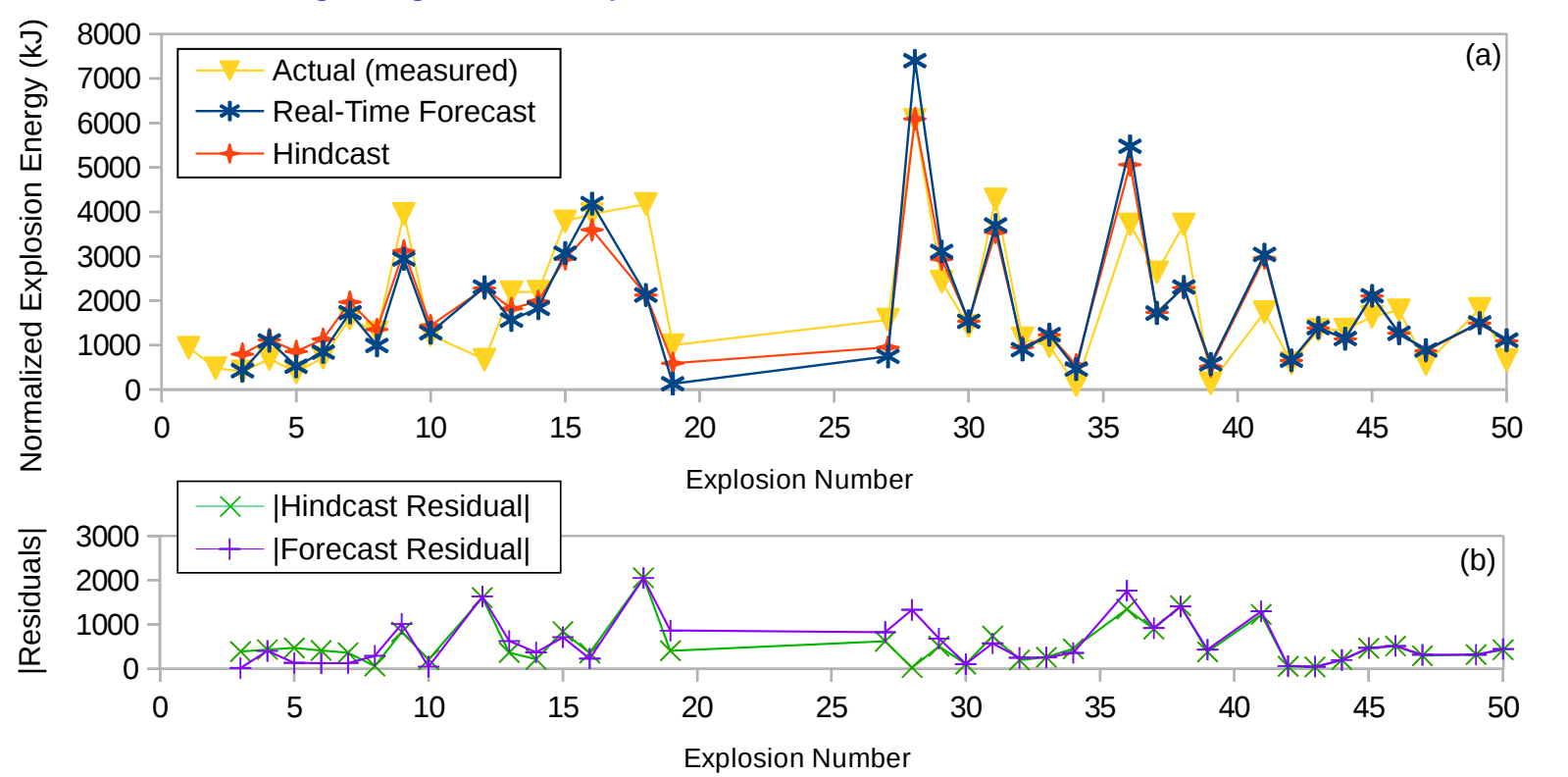


Table_1

Click here to download Table: Formatted_T1.pdf

#	Date	Visual	Infra	Seismic	Quiescence Start	Explosion Start	Explosion Finish	Quiescence Duration	Explosion Duration	Explosion Energy
	(dd/mm/yy)				(QS, UTC)	(ES, UTC)	(EF, UTC)	(QD, minutes)	(ED, minutes)	(EE, kJ)
1	03/05/11			X	04:34:53	05:38:39	06:36:49	64	58	940
2	03/05/11			X	17:08:34	17:47:46	18:56:08	39	68	479
3	03/05/11			X	22:33:07	23:09:38	23:54:40	36	45	403
4	04/05/11			X	21:05:56	22:17:54	22:43:08	72	25	688
5	05/05/11			X	15:09:41	15:52:14	16:04:41	43	12	386
6	05/05/11			X	20:00:58	21:13:36	21:39:13	73	26	716
7	06/05/11			X	06:57:00	09:41:43	10:18:08	165	36	1600
8	06/05/11			X	23:15:03	00:52:01 (+1)	01:08:50 (+1)	97	17	1285
9	07/05/11			X	11:28:30	16:20:18	16:46:20	292	26	3953
10	08/05/11			X	07:28:11	09:14:51	10:07:25	107	52	1228
11	08/05/11			X	13:21:24	16:53:55	N/D	213	N/C	N/C
12	08/05/11			X	23:07:02	02:26:24 (+1)	02:44:00 (+1)	199	18	672
13	09/05/11			X	04:47:51	07:16:44	08:07:00	149	50	2190
14	09/05/11			X	12:00:00	14:47:31	15:27:36	167	40	2200
15	09/05/11			X	20:36:56	01:09:19 (+1)	01:46:12 (+1)	272	37	3784
16	10/05/11			X	07:27:20	13:11:27	14:01:53	344	51	3952
17	11/05/11			X	N/D (maint.)	01:14:10	03:44:00	N/C	150	870
18	11/05/11			X	03:43:49	06:46:02	07:30:47	182	43	4173
19	11/05/11			X	15:58:09	16:11:29	16:25:48	13	14	995
20	11/05/11			X	N/D	12:20:16 (+1)	12:59:01 (+1)	N/C	39	2847
21	13/05/11			X	03:44:57	08:09:06	N/D	264	N/C	N/C
22	13/05/11	X		X	16:29:08	17:55:28	N/D	86	N/C	N/C
23	14/05/11			X	06:51:40	09:14:20	N/D	143	N/C	N/C
24	14/05/11	X		X	12:55:49	17:58:43	N/D	303	N/C	N/C
25	15/05/11			X	01:06:12	05:10:40	N/D	244	N/C	N/C
26	15/05/11			X	10:29:42	14:01:07	N/D	210	N/C	N/C
27	16/05/11	X		X	15:14:32	16:07:05	16:47:25	53	40	1570
28	16/05/11			X	18:59:58	05:18:54 (+1)	05:51:35 (+1)	619	37	6067
29	17/05/11			X	17:02:54	21:34:11	22:52:55	271	79	2425
30	18/05/11			X	11:50:27	13:47:35	13:58:51	117	11	1426
31	18/05/11			X	13:57:10	19:34:41	20:17:44	338	43	4276
32	19/05/11			X	04:01:58	04:54:31	05:19:19	53	25	1148
33	19/05/11	X		X	15:48:46	17:13:23	17:37:41	85	24	974
34	19/05/11	X		X	19:02:59	19:12:14	19:15:33	9	3	100
35	19/05/11	X		X	N/D (maint.)	23:09:45	23:38:36	N/C	18	1497
36	20/05/11			X	01:52:32	10:17:51	10:55:35	505	37	3713
37	21/05/11			X	02:06:37	04:26:34	05:09:07	140	43	2638
38	21/05/11	X	X	X	17:33:23	20:54:08	21:21:46	201	28	3714
39	21/05/11			X	22:26:14	22:32:40	22:34:32	6	2	141
40	22/05/11	X			N/D	N/D (obs 21:55)	N/D (obs 21:56)	N/C (obs 1)	N/C	N/C
41	23/05/11			X	06:50:03	11:24:44	12:31:12	275	66	1739
42	24/05/11			X	05:41:25	06:01:04	06:21:11	20	20	593
43	24/05/11			X	07:16:20	08:57:31	09:24:12	101	16	1342
44	25/05/11			X	13:47:33	15:01:26	15:13:25	74	12	1345
45	26/05/11			X	22:42:00	01:41:33 (+1)	02:18:37 (+1)	180	38	1637
46	26/05/11			X	16:35:37	18:03:09	18:20:19	88	17	1782
47	27/05/11			X	04:04:41	04:48:48	05:02:03	44	13	571
48	27/05/11			X	N/D	11:23:42	11:45:41	N/C	22	934
49	28/05/11			X	16:28:23	18:21:11	18:40:38	113	19	1817
50	28/05/11			X	21:10:26	22:19:30	22:29:20	69	10	664

Figure_S1

[Click here to download Supplementary material for online publication only: Figure_S1_revised.pdf](#)



Explosion 22 - May 13, 2011



Explosion 24 - May 14, 2011



Explosion 27 - May 16, 2011



Explosion 33 - May 19, 2011



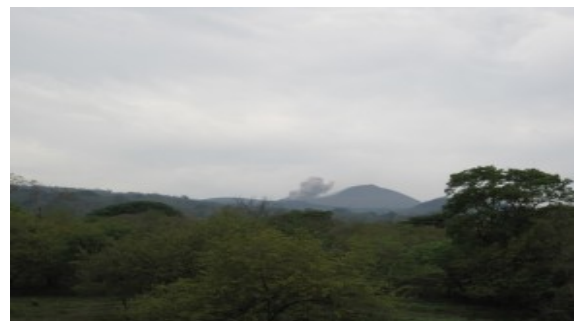
Explosion 34 - May 19, 2011



Explosion 35 - May 19, 2011



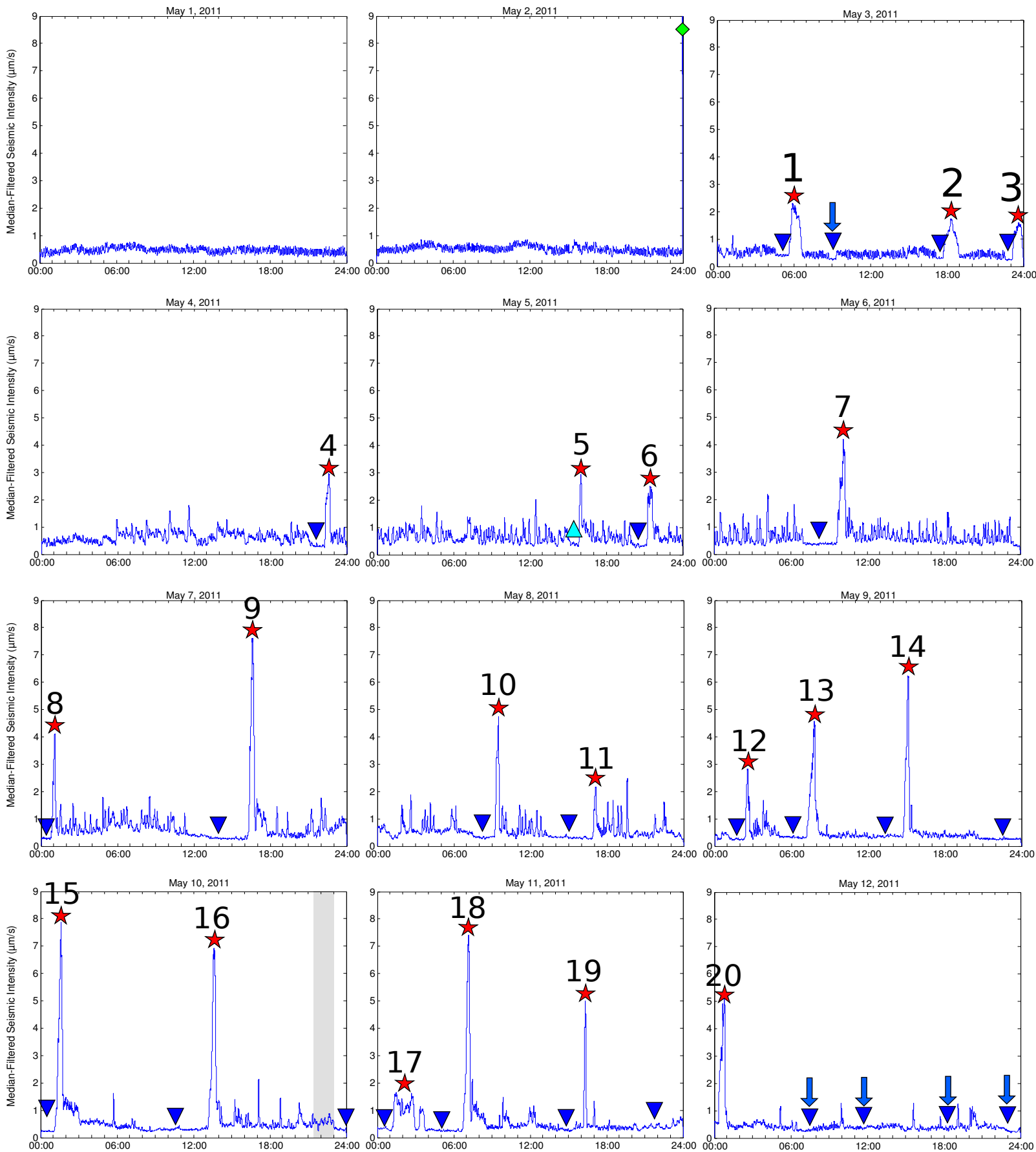
Explosion 38 - May 21, 2011



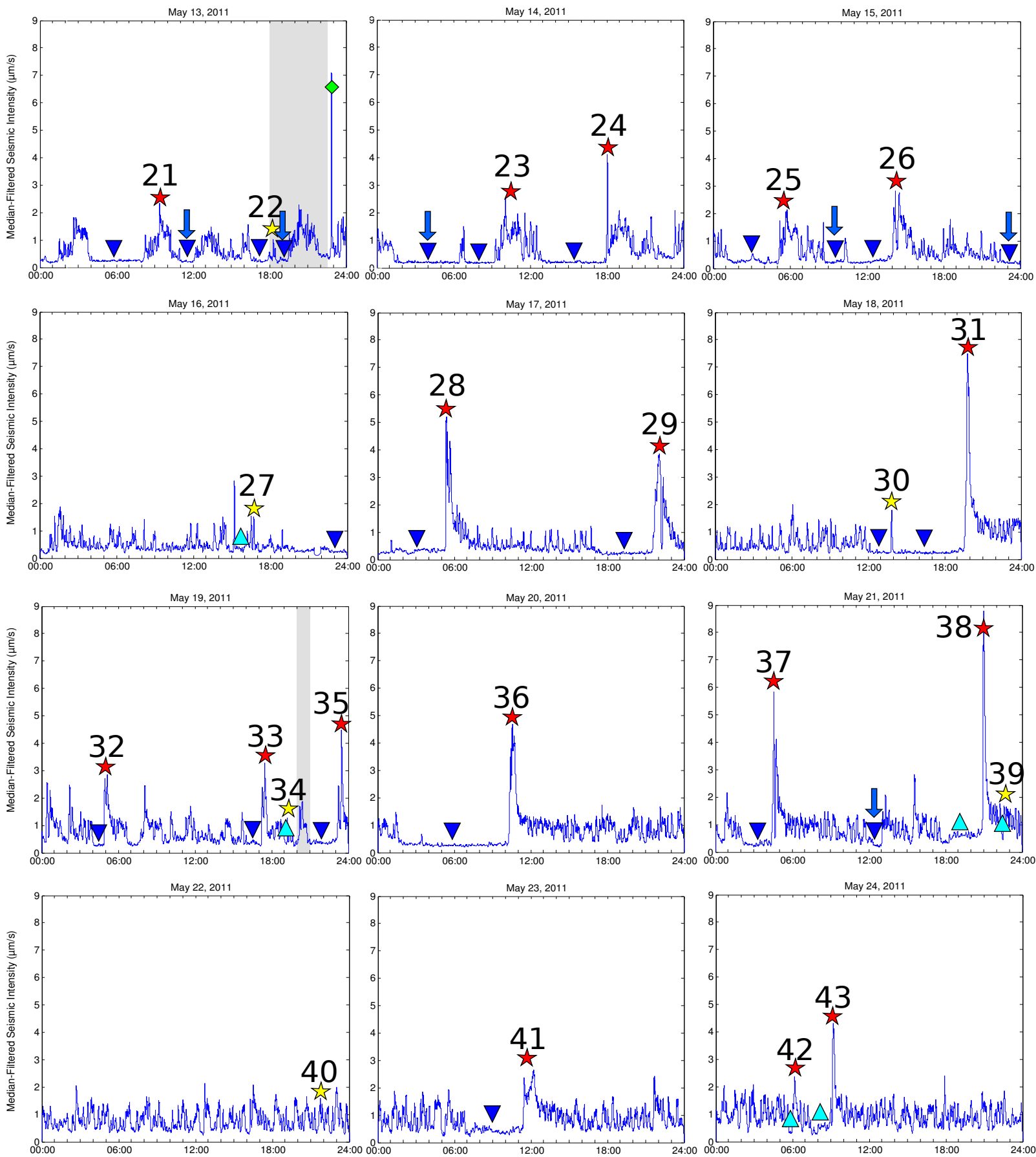
Explosion 40 - May 22, 2011

Figure_S2

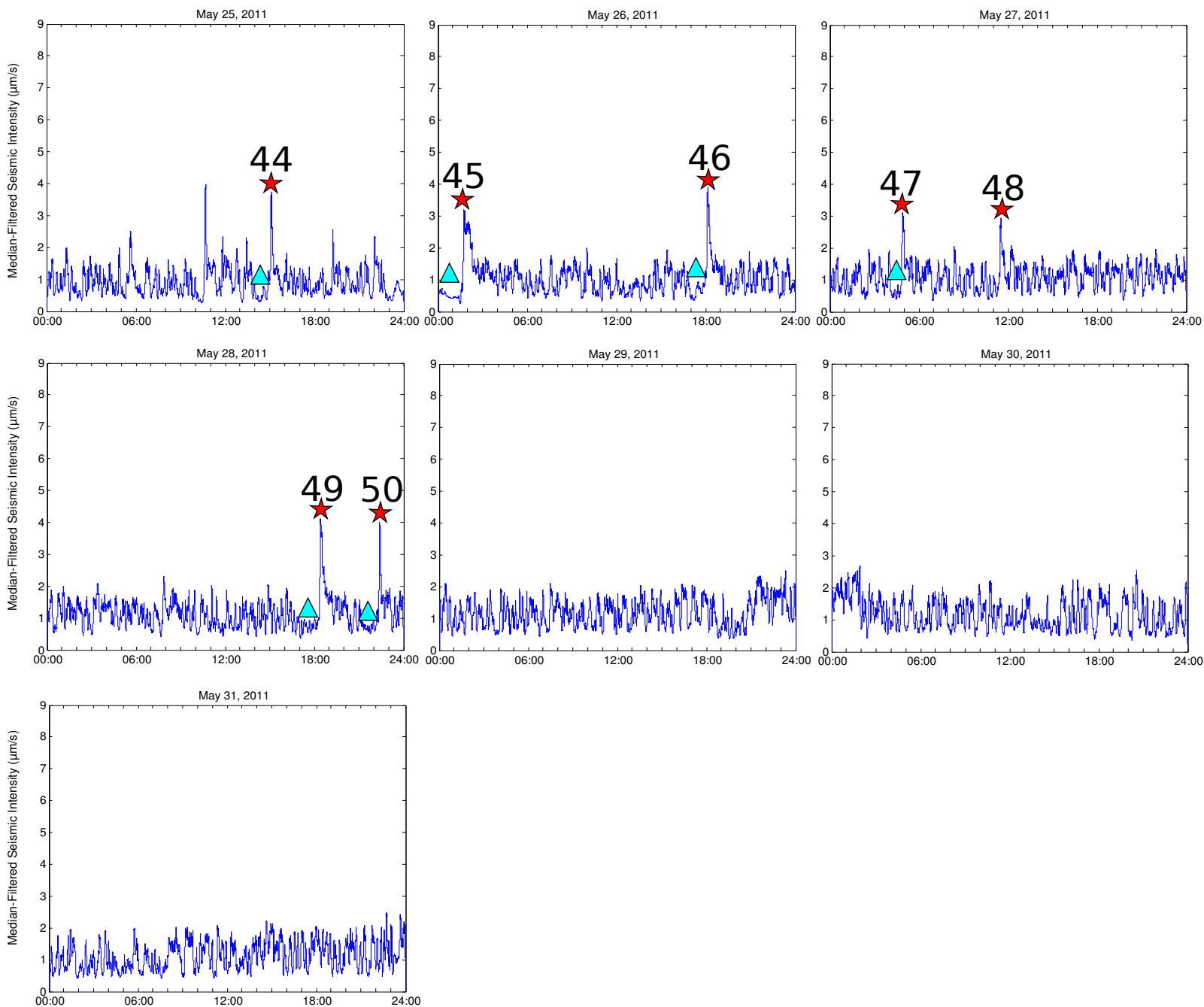
[Click here to download Supplementary material for online publication only: Figure_S2_revised.pdf](#)



- | | |
|--|---|
| ★ Explosion: Seismic intensity above 1.5 $\mu\text{m/s}$ for 10+ minutes | ★ Explosion: Photographically documented |
| ▼ Period of absolute quiescence: Seismic intensity within 0.1 $\mu\text{m/s}$ for 30+ minutes (analysis run on entire dataset) | ▼ Period of absolute quiescence: Seismic intensity within 0.1 $\mu\text{m/s}$ for 5+ minutes (analysis run only prior to explosions w/o 30+ min quiescence) |
| ⬇ False Positive: Quiescence not followed by explosion | |
| ■ Period of high seismic noise due to station maintenance | ◆ Seismic intensity spike due to tectonic earthquake |



- ★ Explosion: Seismic intensity above $1.5 \mu\text{m/s}$ for 10+ minutes
- ★ Explosion: Photographically documented
- ▼ Period of absolute quiescence: Seismic intensity within $0.1 \mu\text{m/s}$ for 30+ minutes (analysis run on entire dataset)
- ↘ False Positive: Quiescence not followed by explosion
- Period of high seismic noise due to station maintenance
- ▲ Period of absolute quiescence: Seismic intensity within $0.1 \mu\text{m/s}$ for 5+ minutes (analysis run only prior to explosions w/o 30+ min quiescence)
- ◆ Seismic intensity spike due to tectonic earthquake

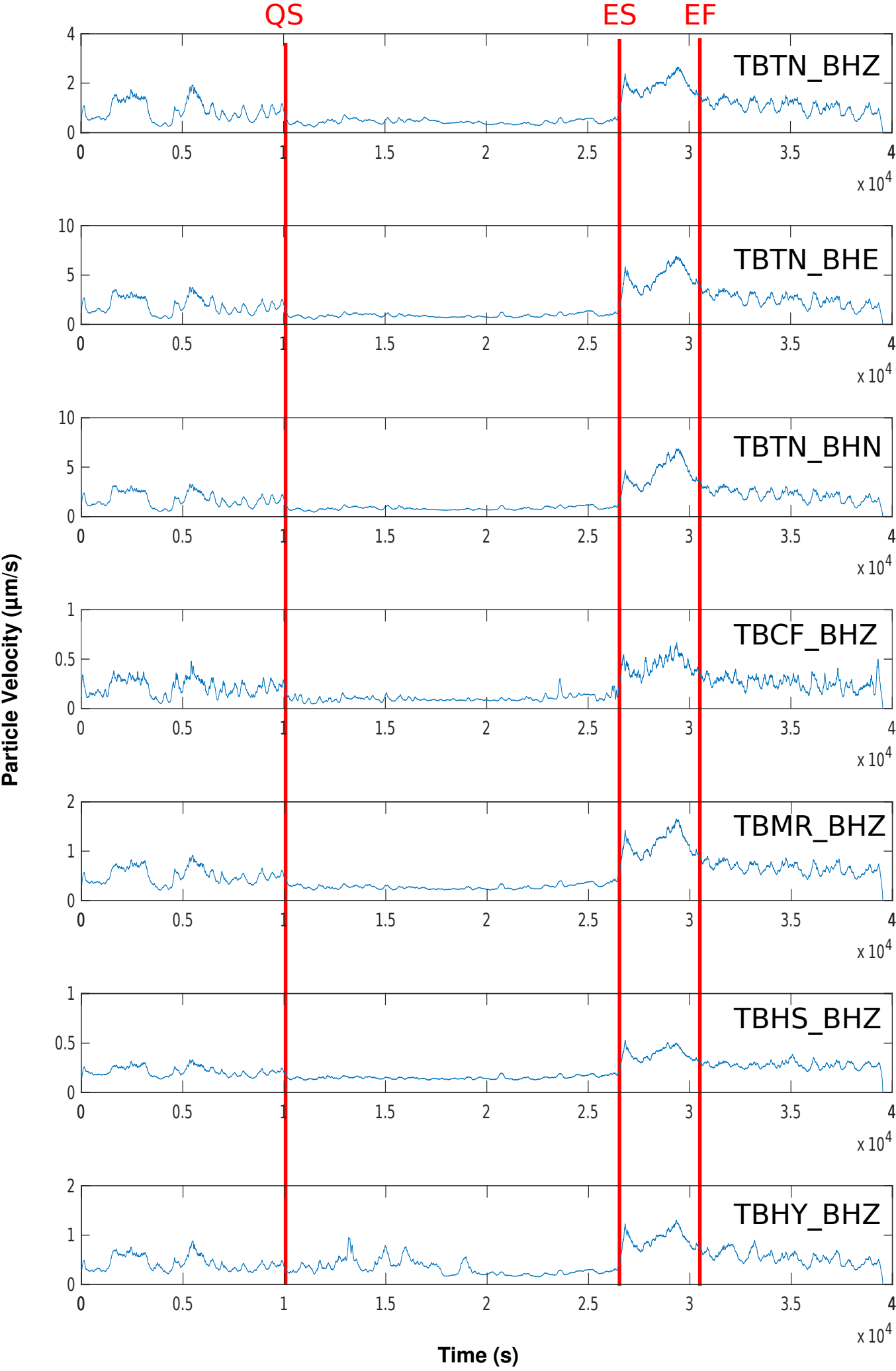


- | | |
|--|---|
| ★ Explosion: Seismic intensity above 1.5 $\mu\text{m/s}$ for 10+ minutes | ★ Explosion: Photographically documented |
| ▼ Period of absolute quiescence: Seismic intensity within 0.1 $\mu\text{m/s}$ for 30+ minutes (analysis run on entire dataset) | ▼ Period of absolute quiescence: Seismic intensity within 0.1 $\mu\text{m/s}$ for 5+ minutes (analysis run only prior to explosions w/o 30+ min quiescence) |
| ⬇ False Positive: Quiescence not followed by explosion | ◆ Seismic intensity spike due to tectonic earthquake |
| ■ Period of high seismic noise due to station maintenance | |

Figure_S3

[Click here to download Supplementary material for online publication only: Figure_S3.pdf](#)

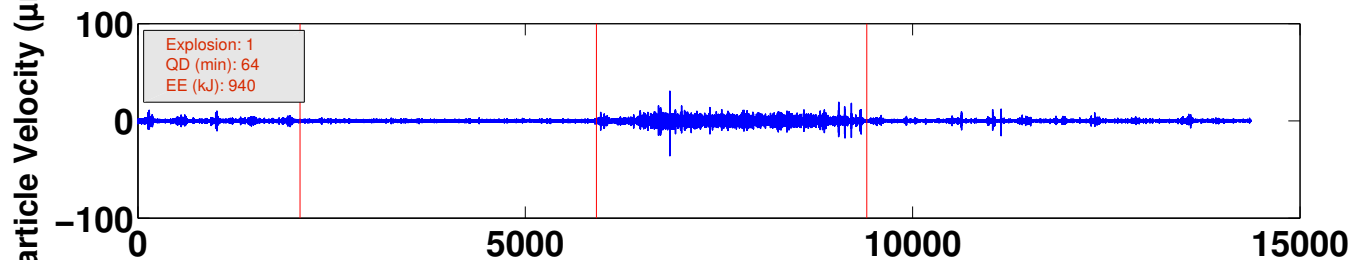
May 23, 2011 (Explosion 41)



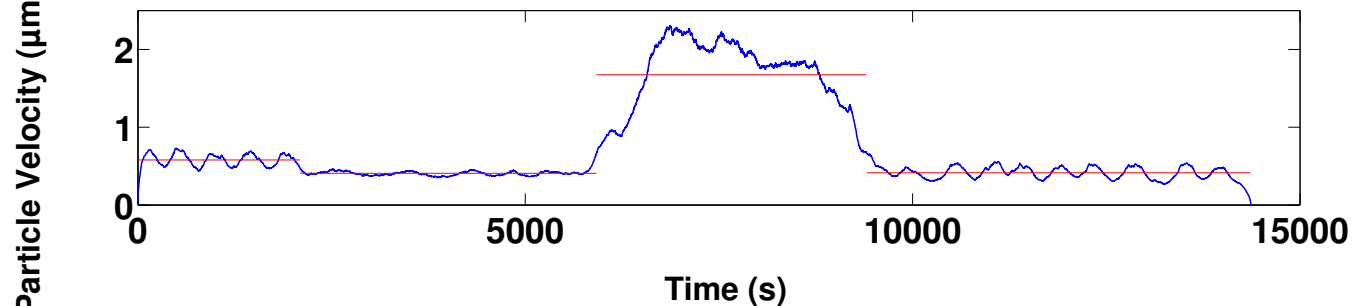
Figure_S4

[Click here to download Supplementary material for online publication only: Figure_S4.pdf](#)

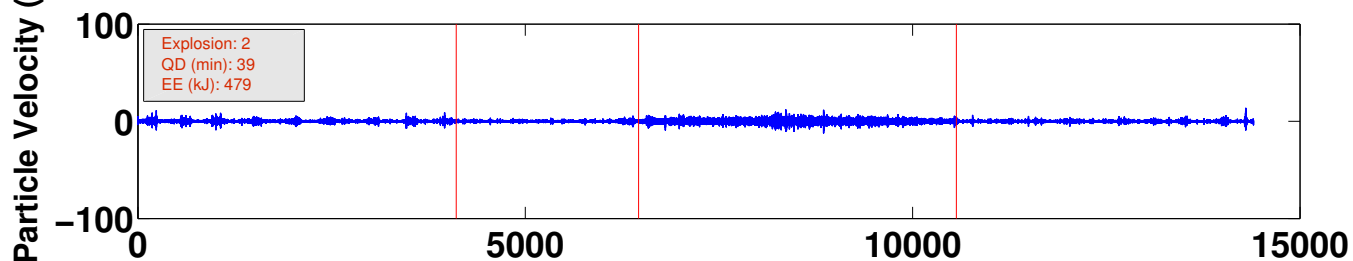
Instrument-Corrected Velocity Seismogram (0.5-20 Hz, blue) and changepoints (red)



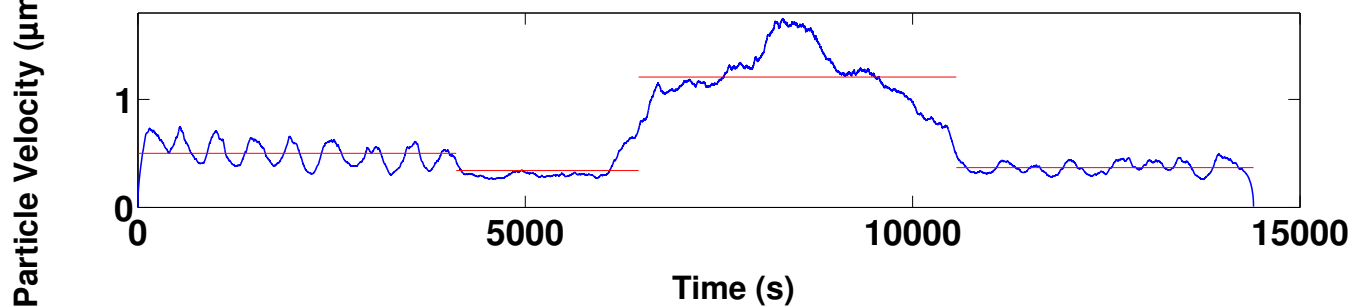
Median-Filtered Seismic Intensity (blue) and changepoint analysis (red)

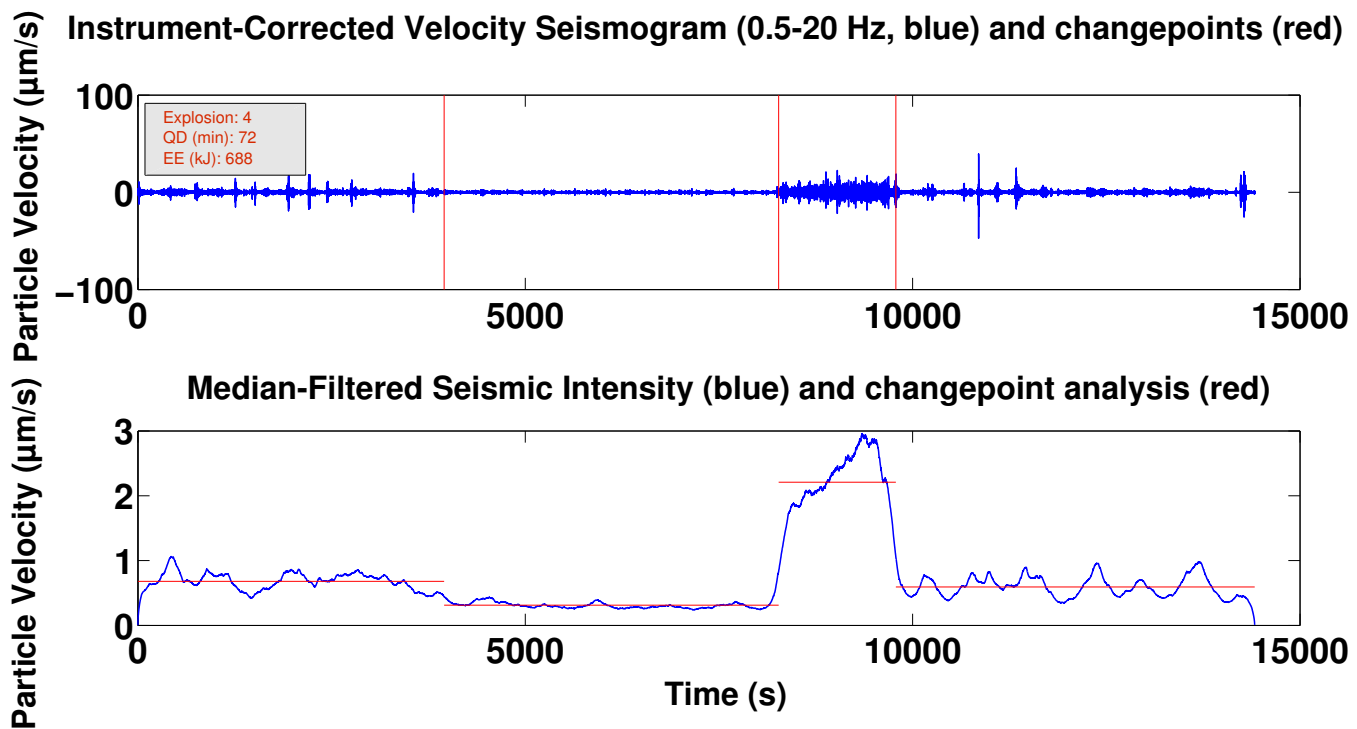
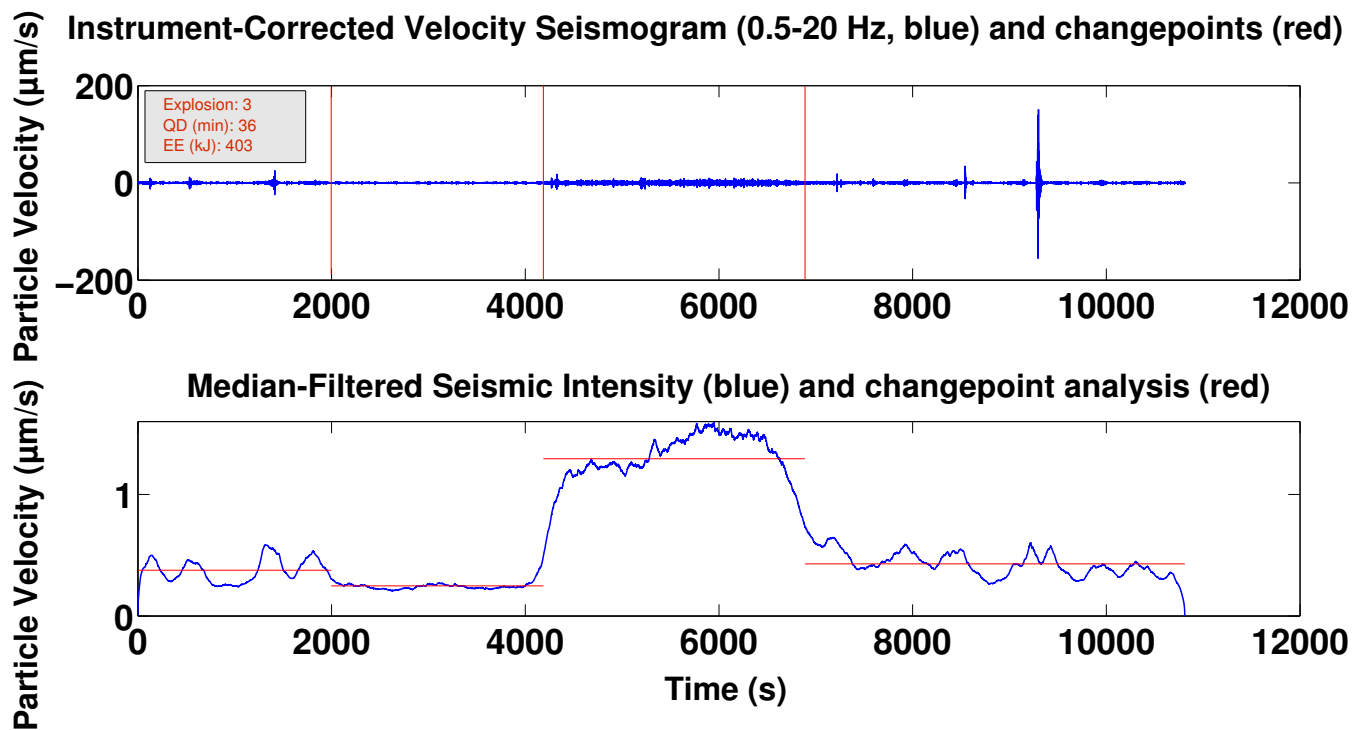


Instrument-Corrected Velocity Seismogram (0.5-20 Hz, blue) and changepoints (red)

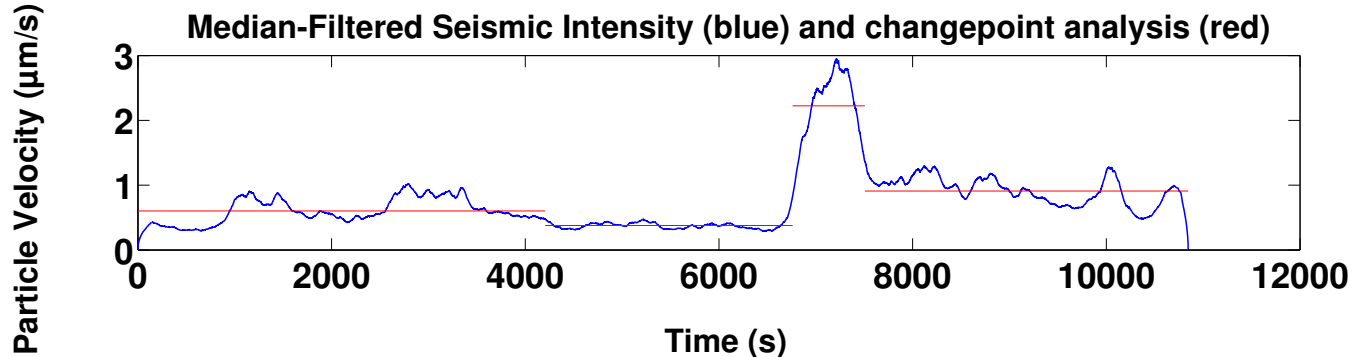
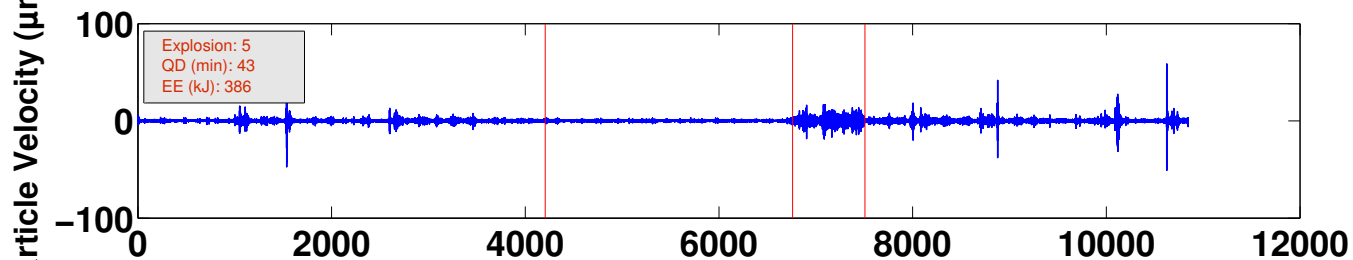


Median-Filtered Seismic Intensity (blue) and changepoint analysis (red)

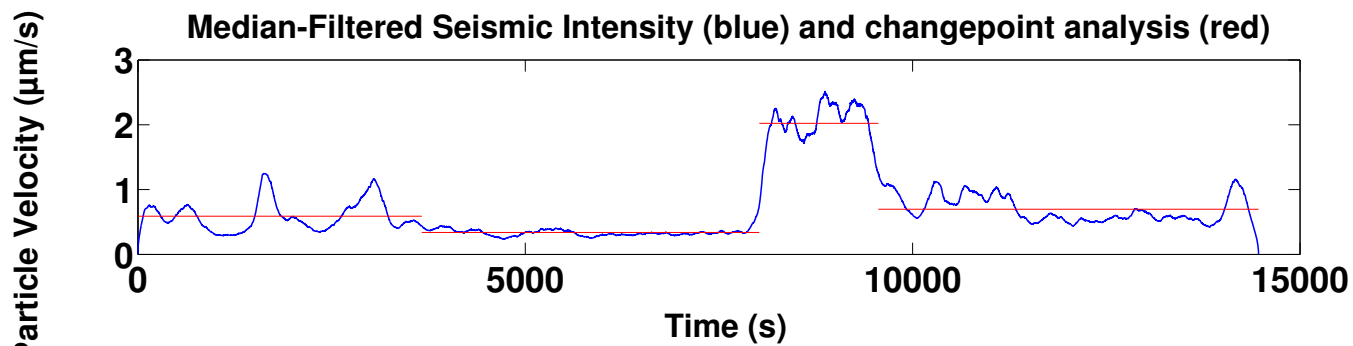
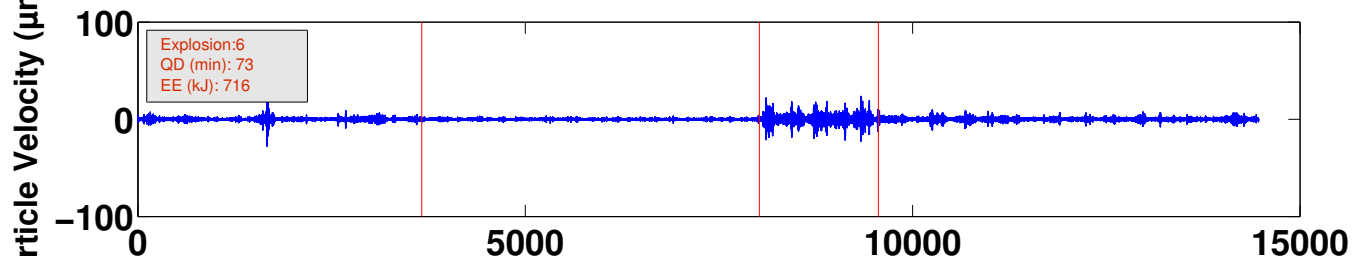




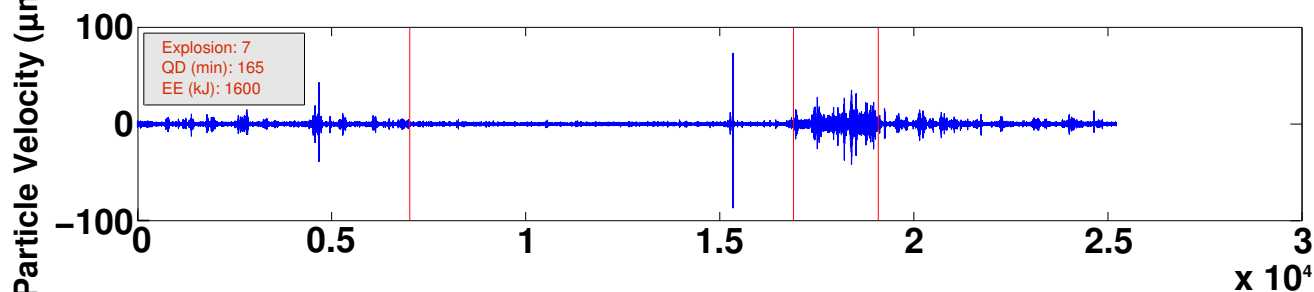
Instrument-Corrected Velocity Seismogram (0.5-20 Hz, blue) and changepoints (red)



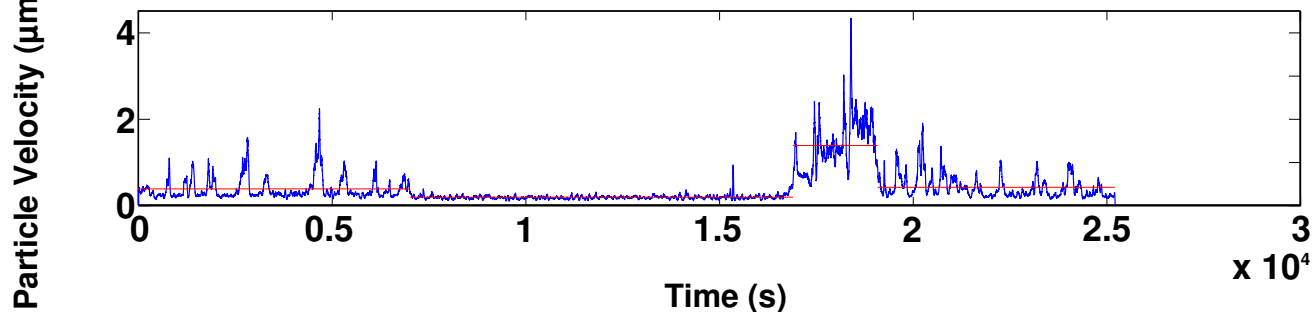
Instrument-Corrected Velocity Seismogram (0.5-20 Hz, blue) and changepoints (red)



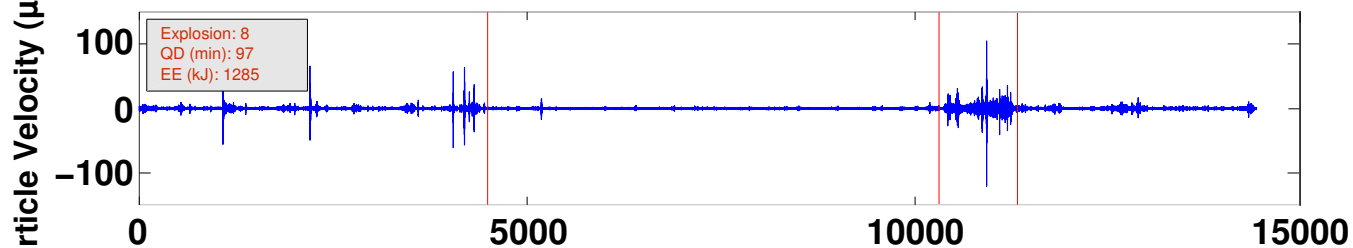
Instrument-Corrected Velocity Seismogram (0.5-20 Hz, blue) and changepoints (red)



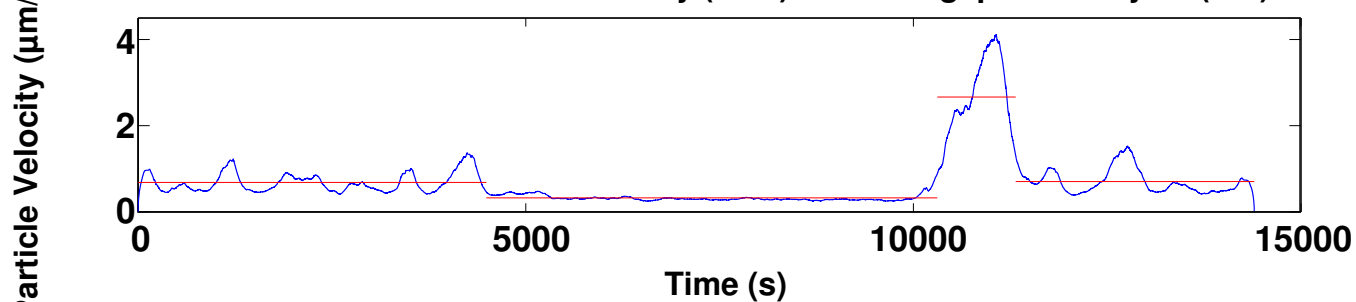
Median-Filtered Seismic Intensity (blue) and changepoint analysis (red)

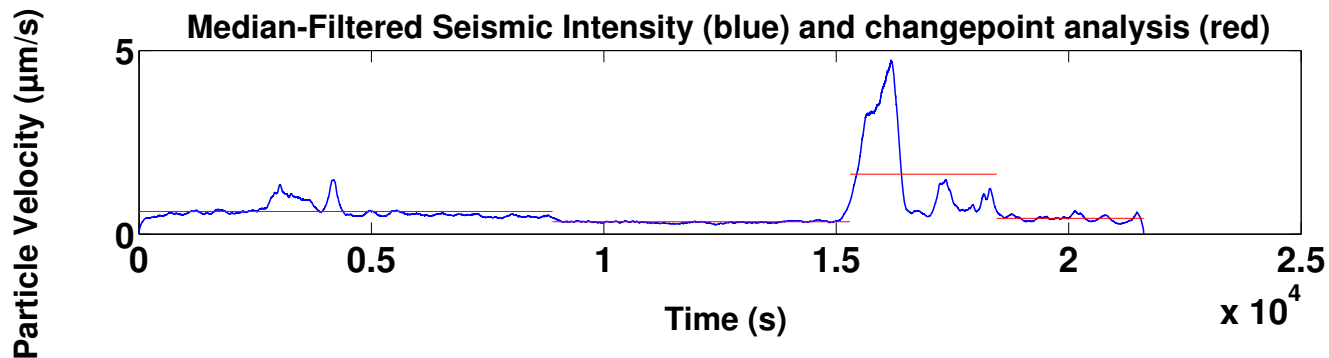
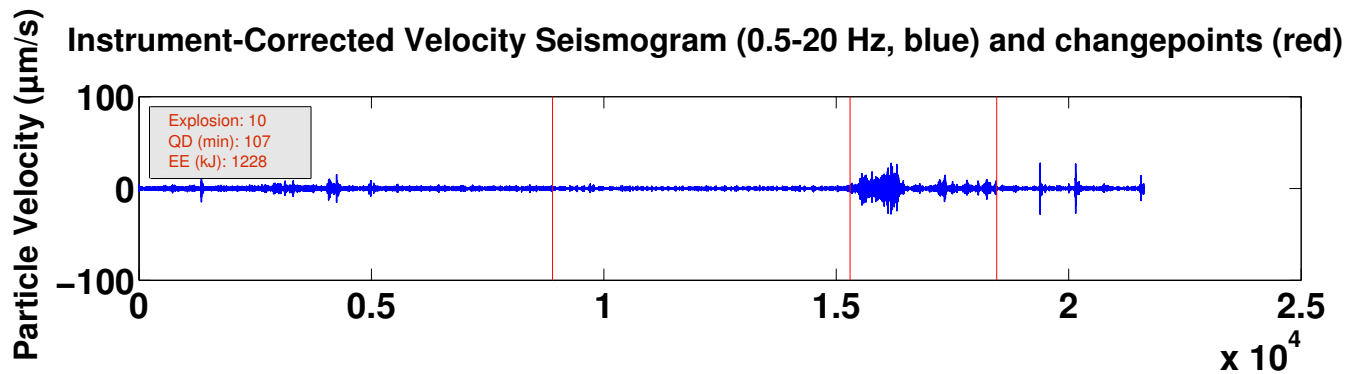
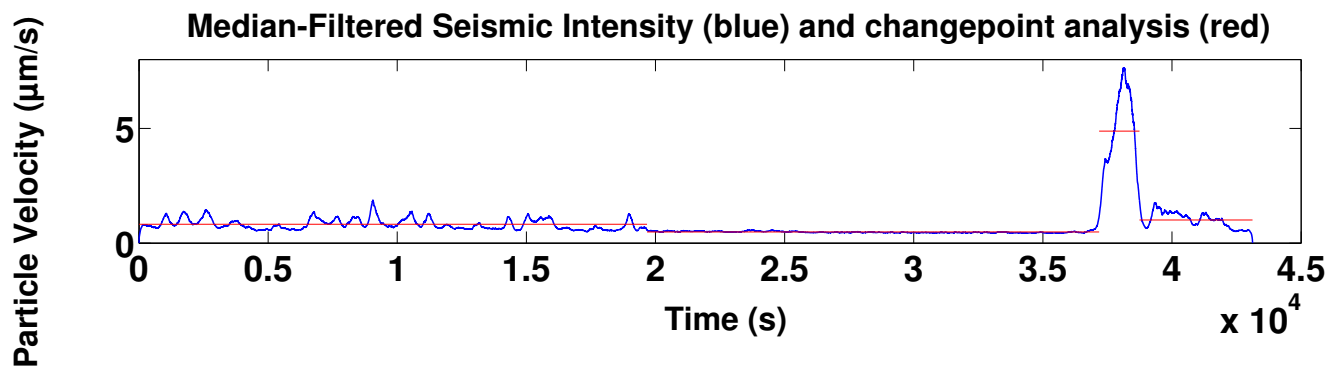
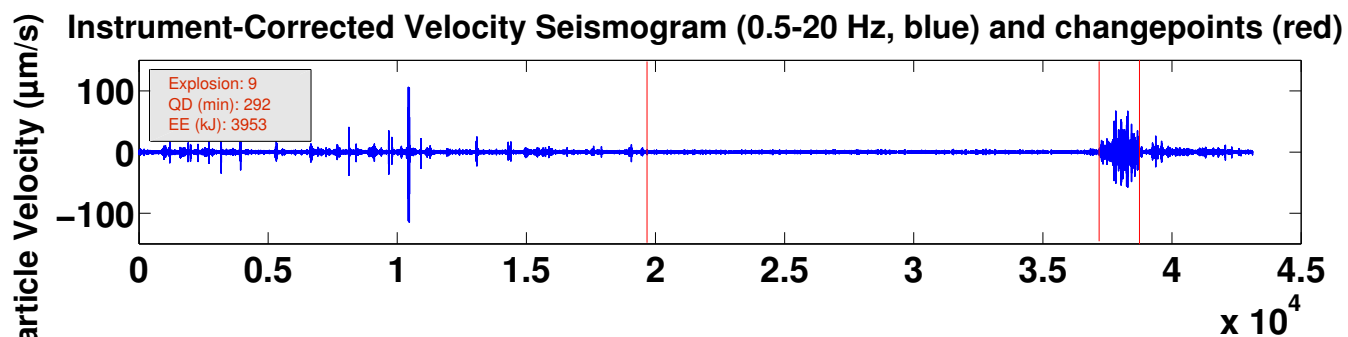


Instrument-Corrected Velocity Seismogram (0.5-20 Hz, blue) and changepoints (red)

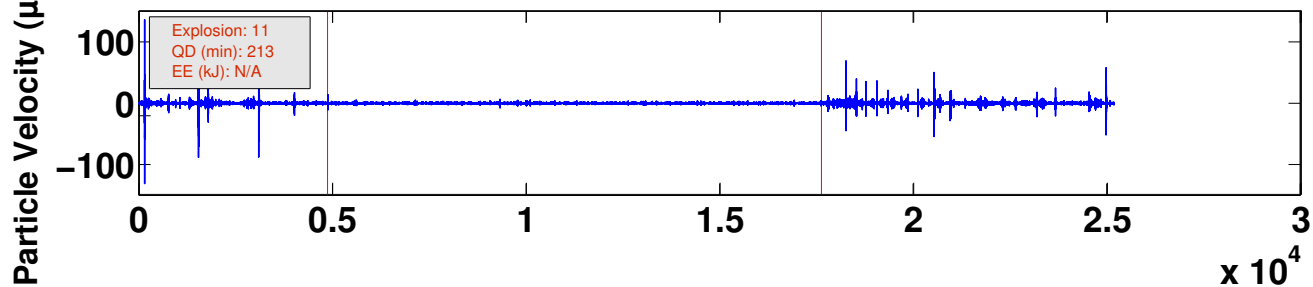


Median-Filtered Seismic Intensity (blue) and changepoint analysis (red)

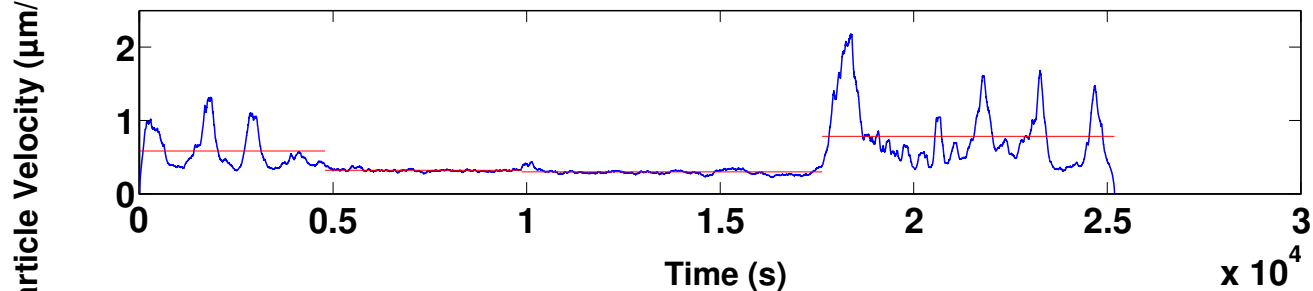




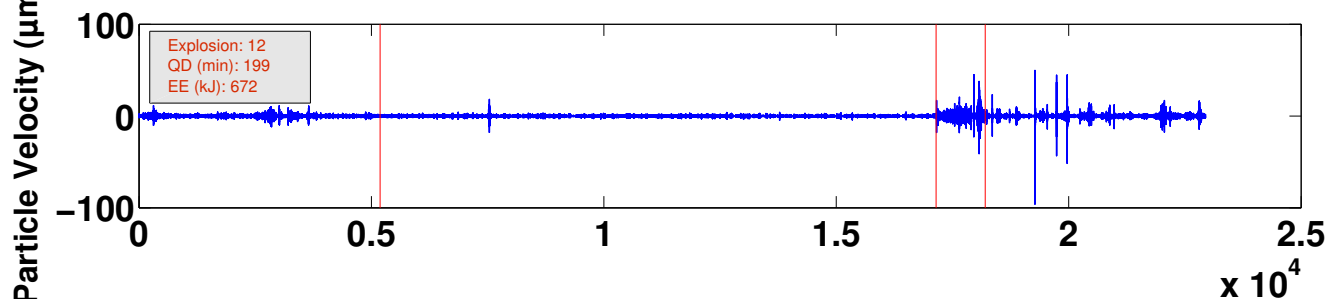
Instrument-Corrected Velocity Seismogram (0.5-20 Hz, blue) and changepoints (red)



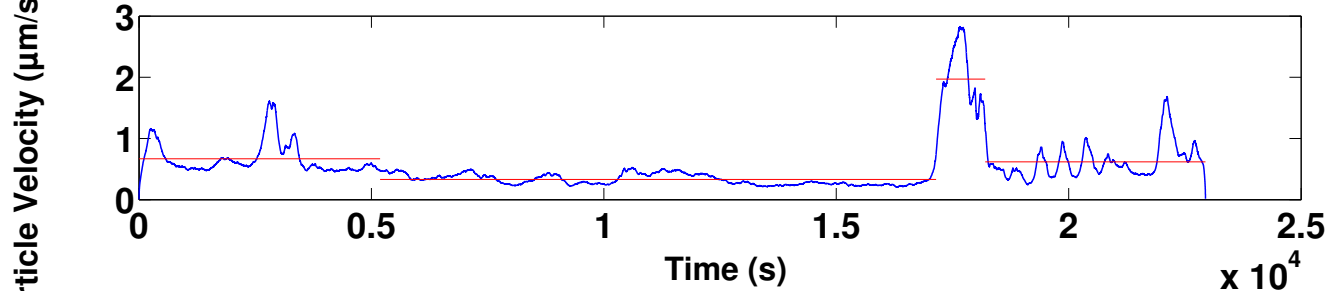
Median-Filtered Seismic Intensity (blue) and changepoint analysis (red)



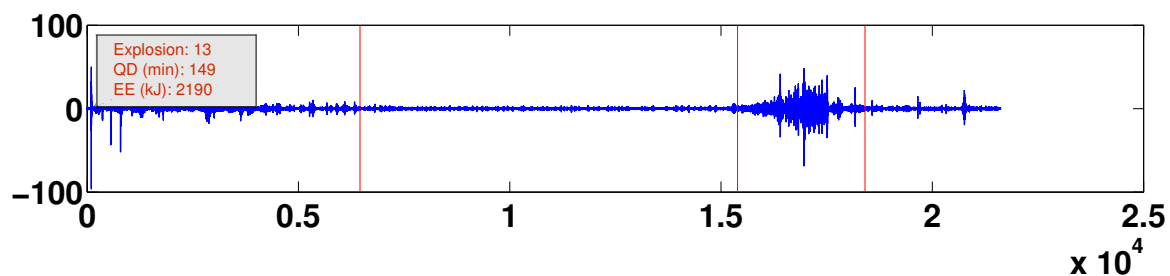
Instrument-Corrected Velocity Seismogram (0.5-20 Hz, blue) and changepoints (red)



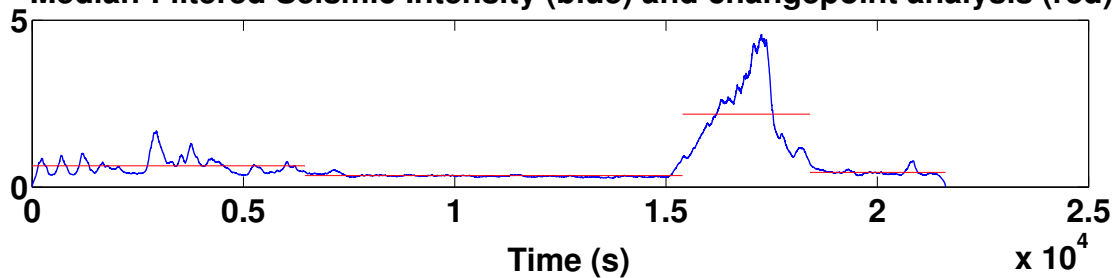
Median-Filtered Seismic Intensity (blue) and changepoint analysis (red)



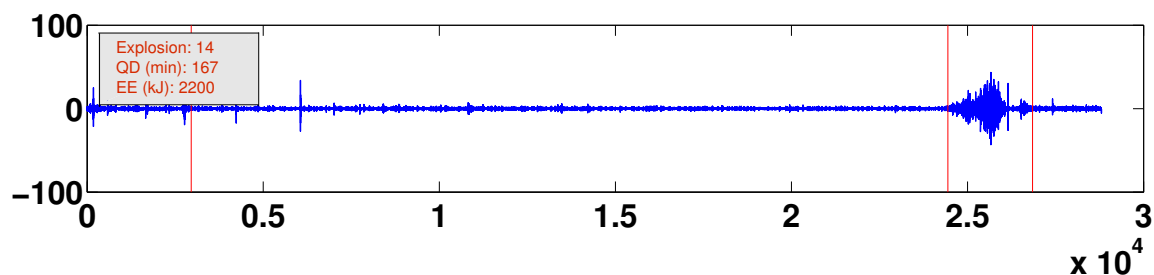
Instrument-Corrected Velocity Seismogram (0.5-20 Hz, blue) and changepoints (red)



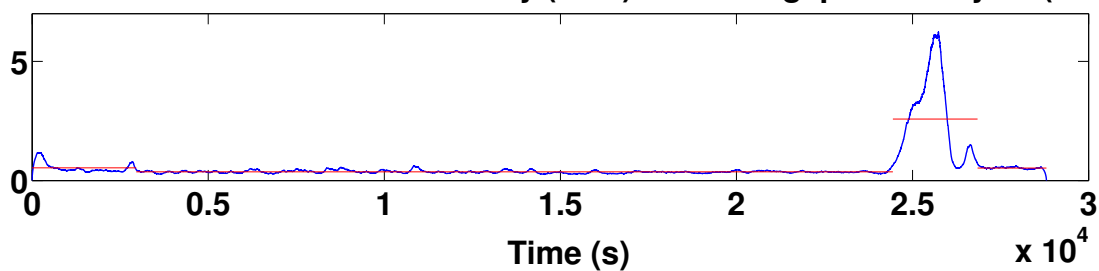
Median-Filtered Seismic Intensity (blue) and changepoint analysis (red)

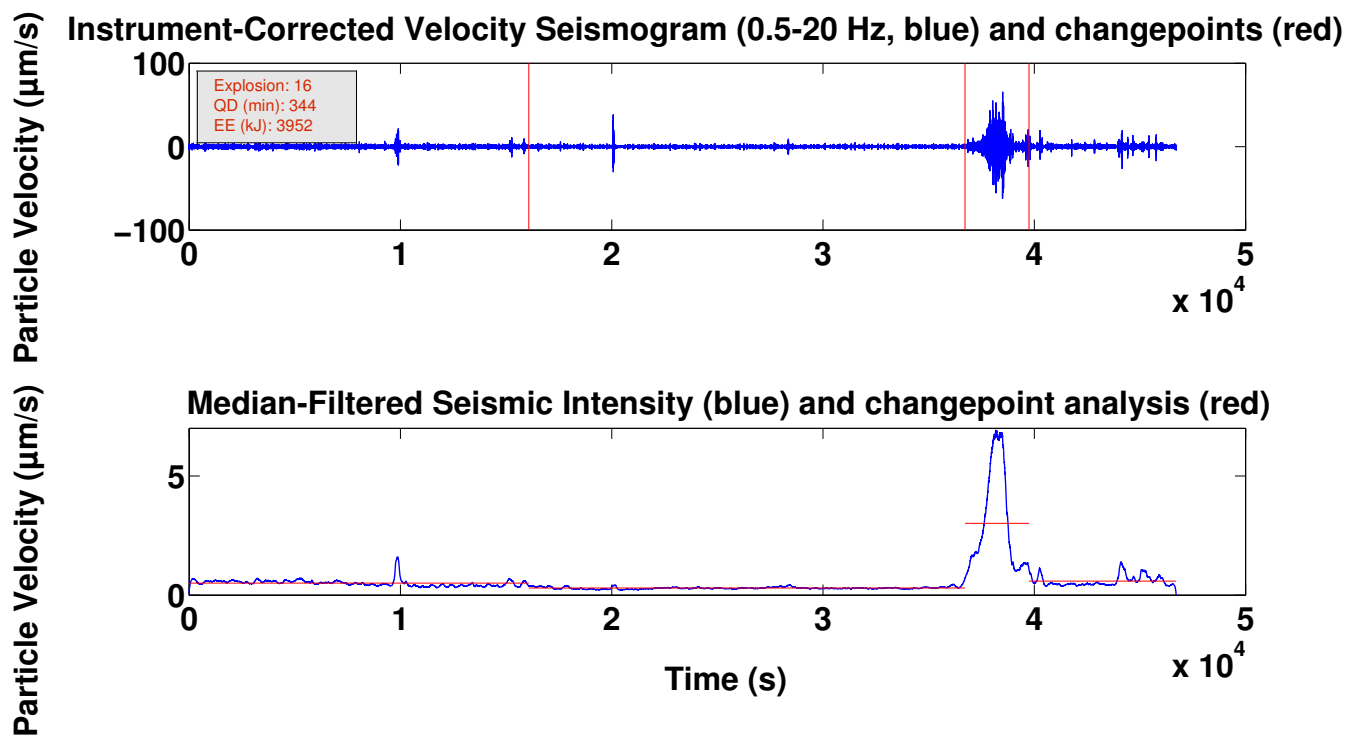
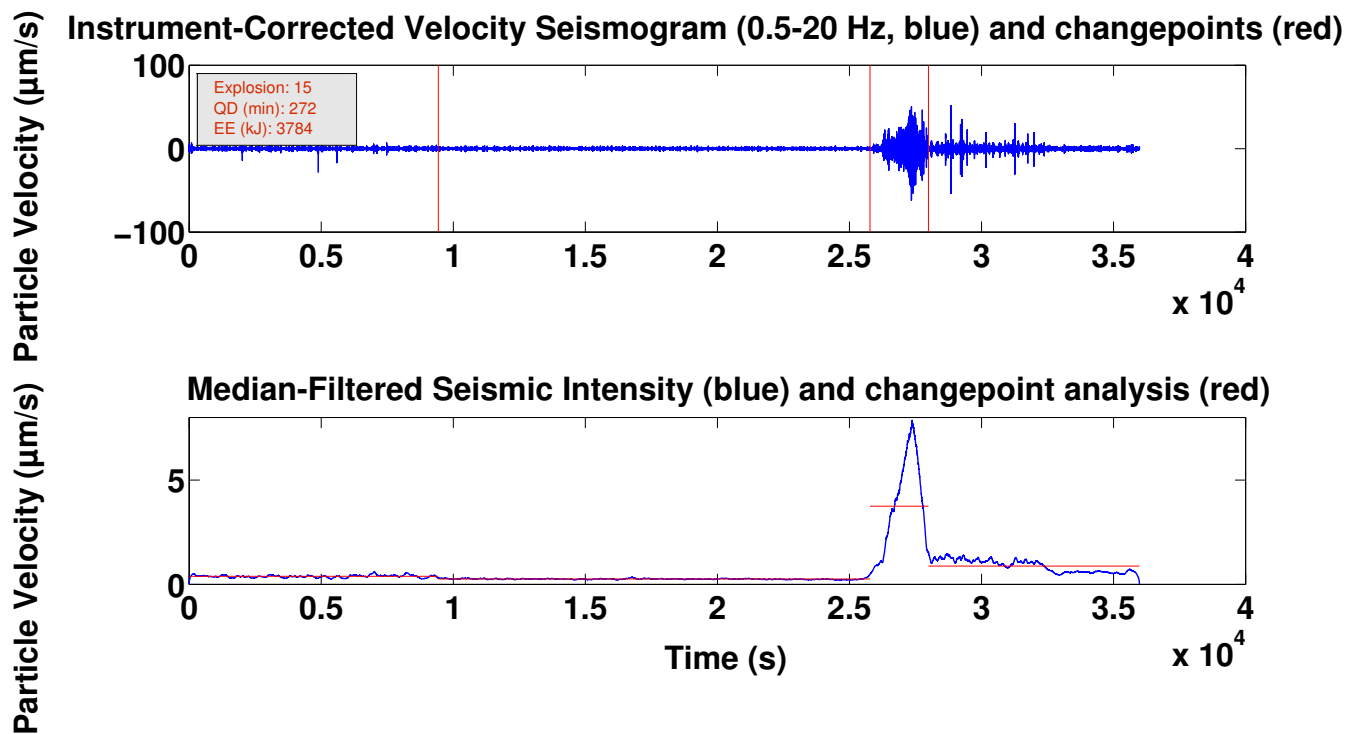


Instrument-Corrected Velocity Seismogram (0.5-20 Hz, blue) and changepoints (red)

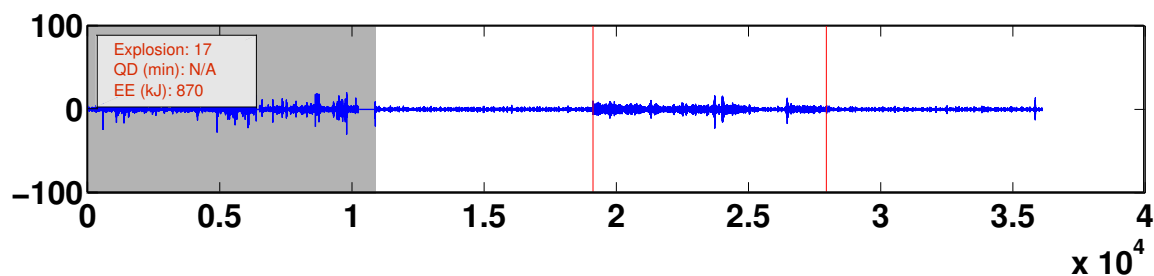


Median-Filtered Seismic Intensity (blue) and changepoint analysis (red)

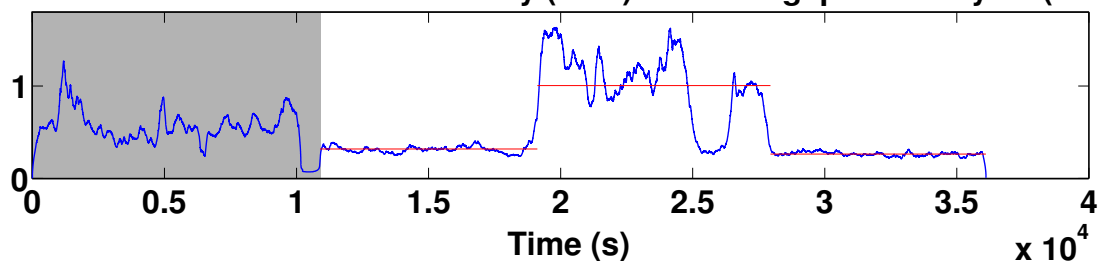




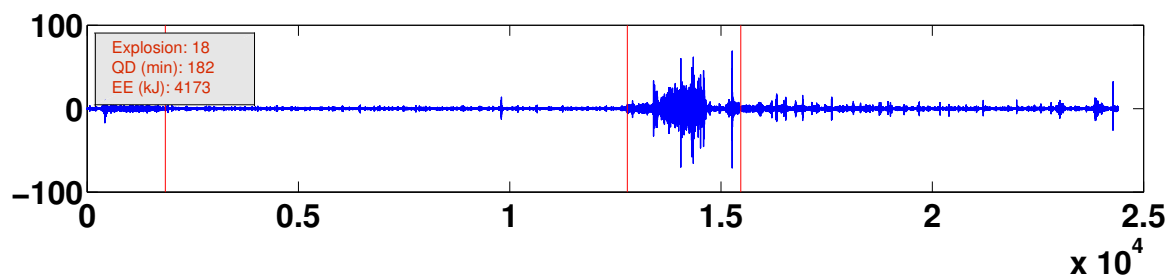
Instrument-Corrected Velocity Seismogram (0.5-20 Hz, blue) and changepoints (red)



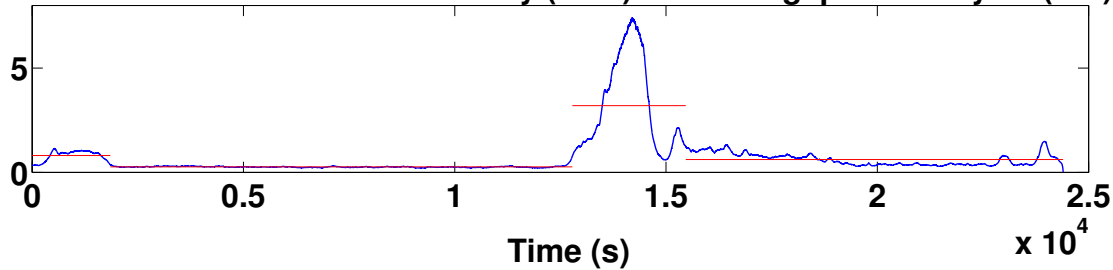
Median-Filtered Seismic Intensity (blue) and changepoint analysis (red)

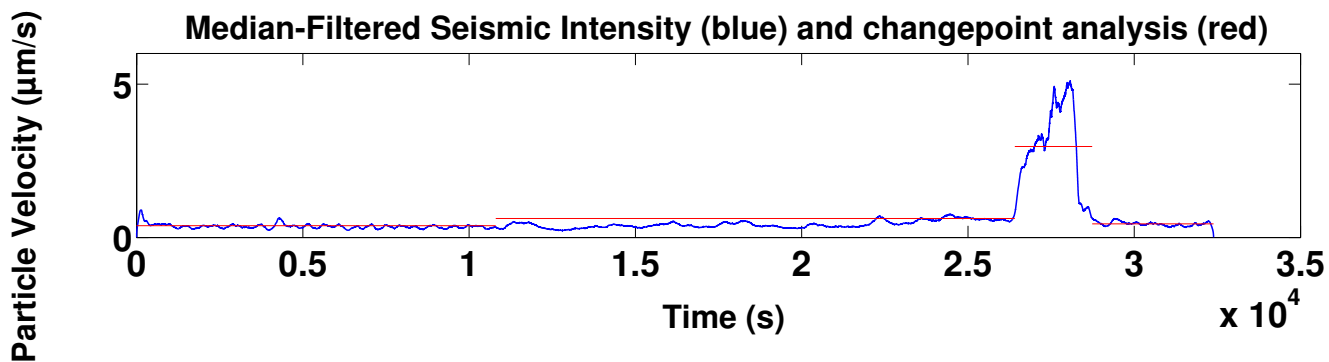
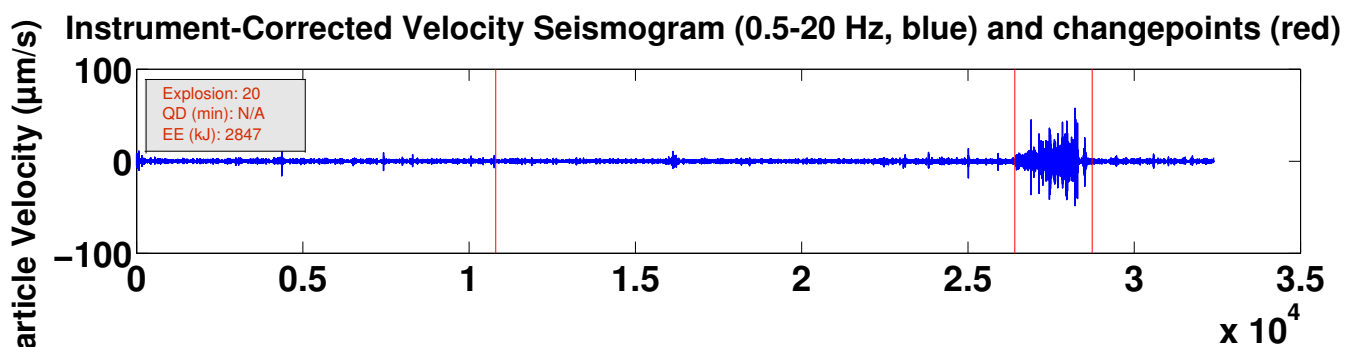
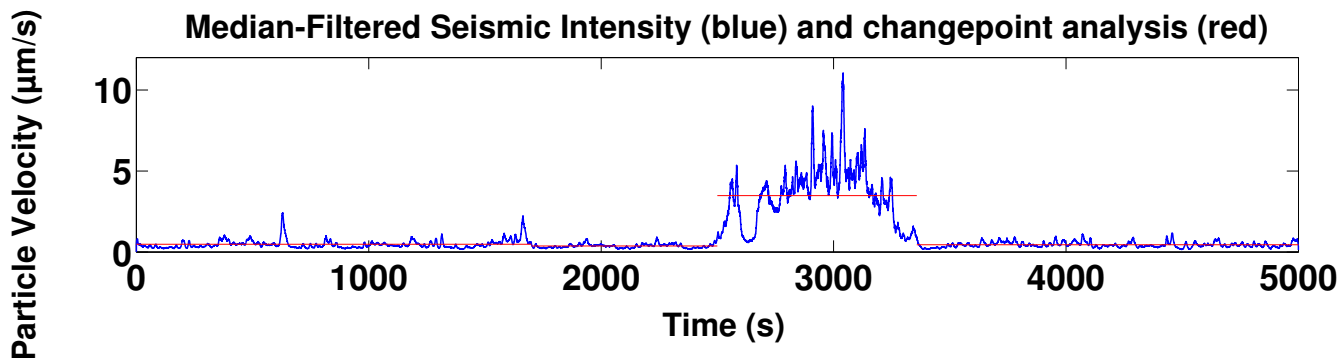
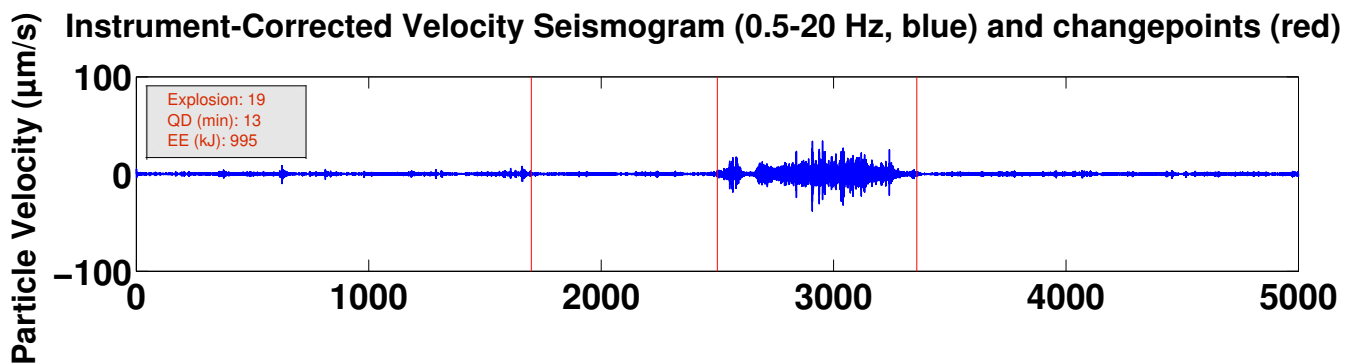


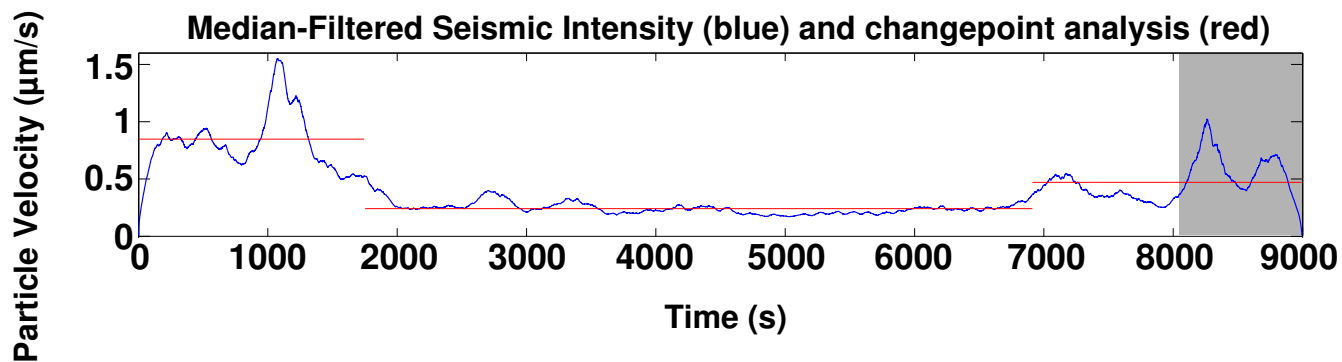
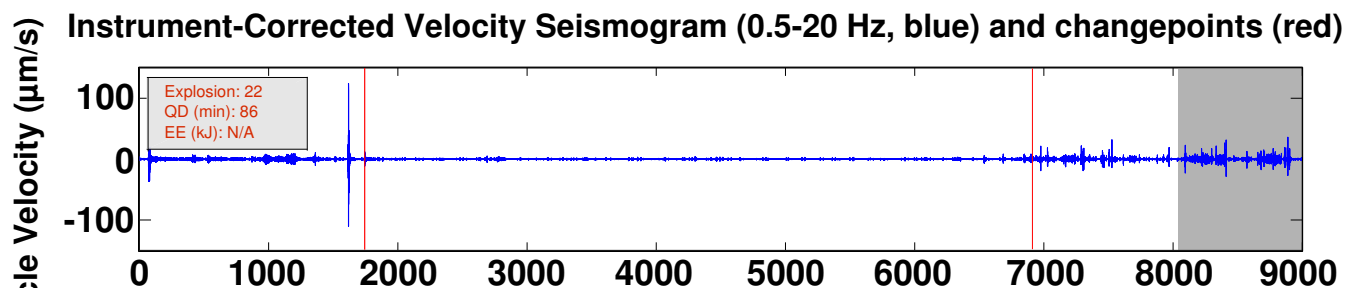
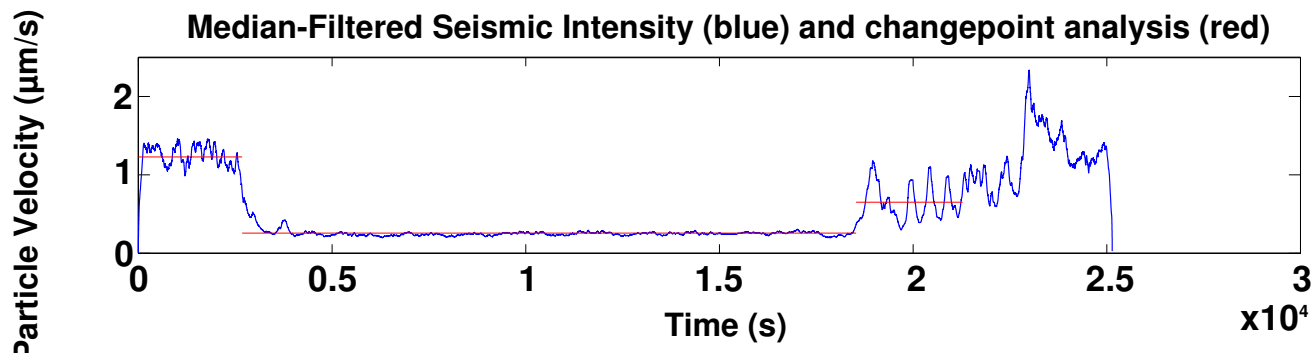
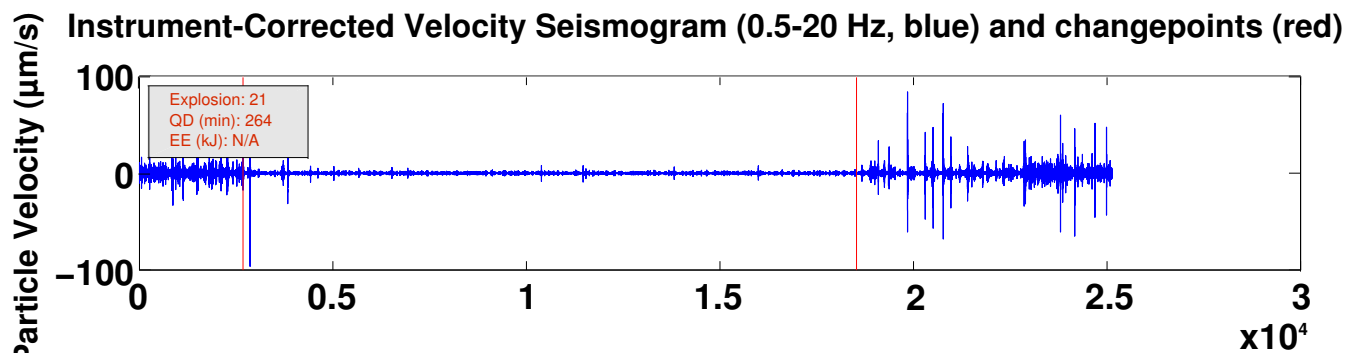
Instrument-Corrected Velocity Seismogram (0.5-20 Hz, blue) and changepoints (red)



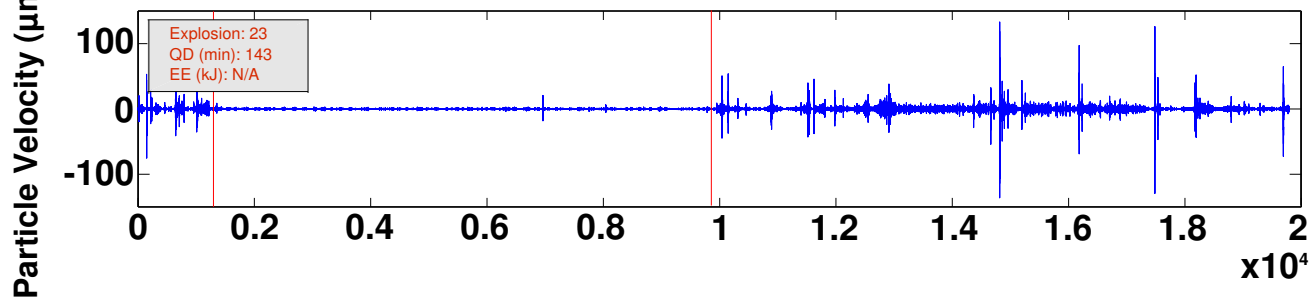
Median-Filtered Seismic Intensity (blue) and changepoint analysis (red)



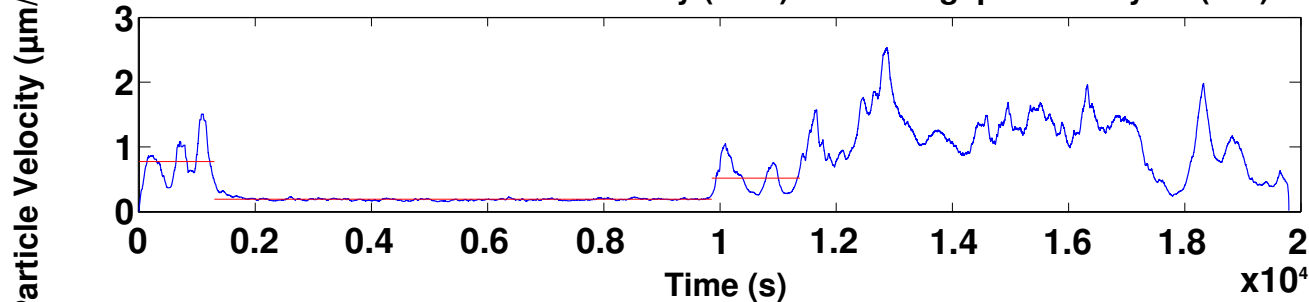




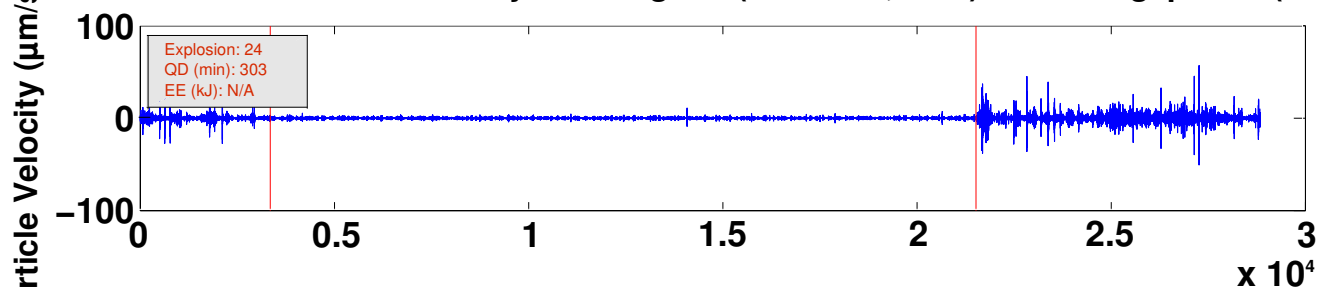
Instrument-Corrected Velocity Seismogram (0.5-20 Hz, blue) and changepoints (red)



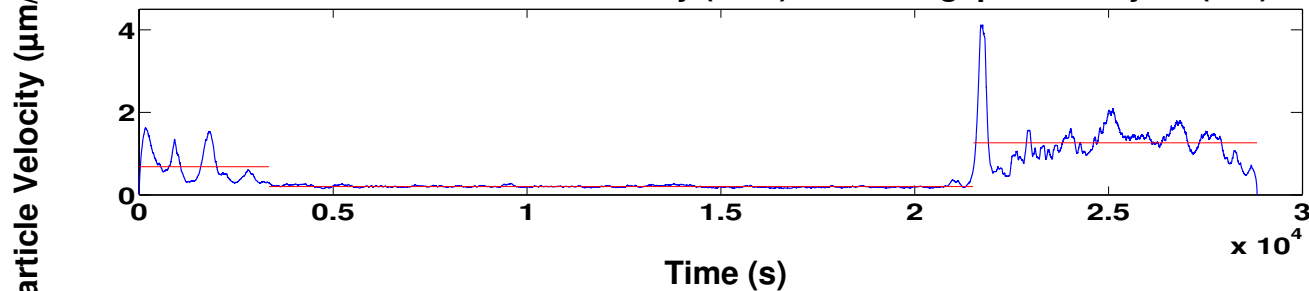
Median-Filtered Seismic Intensity (blue) and changepoint analysis (red)



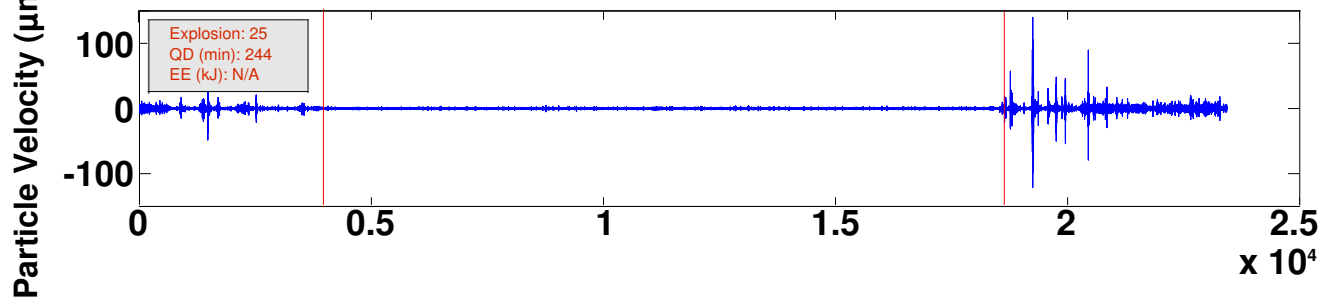
Instrument-Corrected Velocity Seismogram (0.5-20 Hz, blue) and changepoints (red)



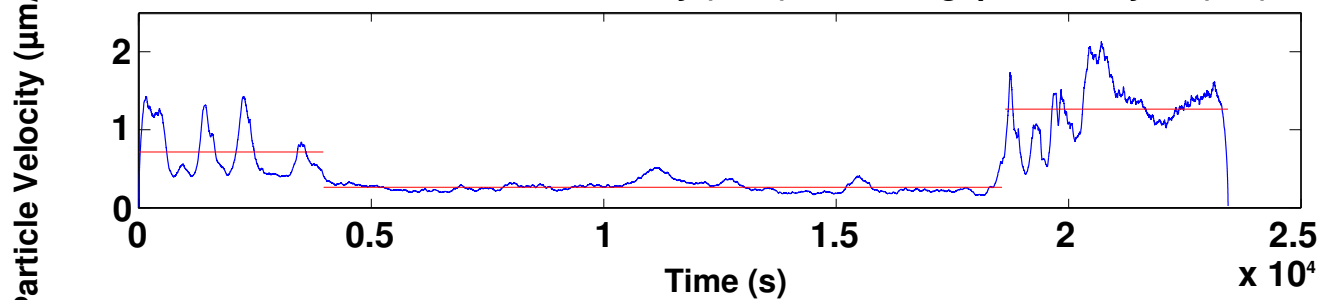
Median-Filtered Seismic Intensity (blue) and changepoint analysis (red)



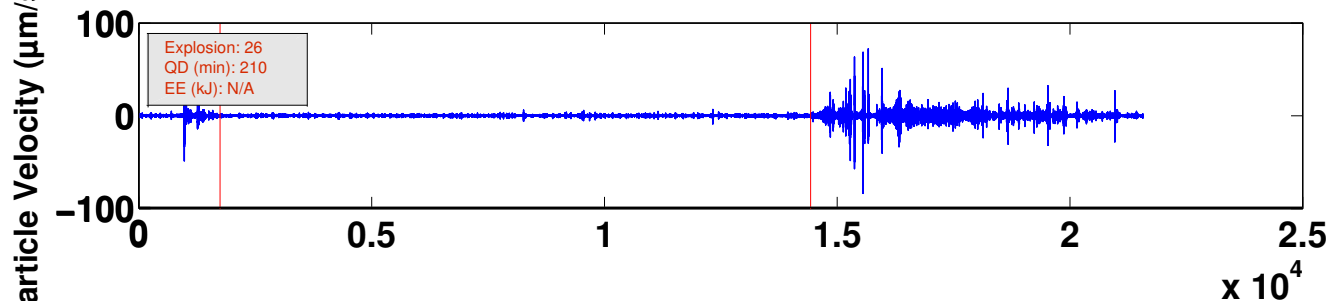
Instrument-Corrected Velocity Seismogram (0.5-20 Hz, blue) and changepoints (red)



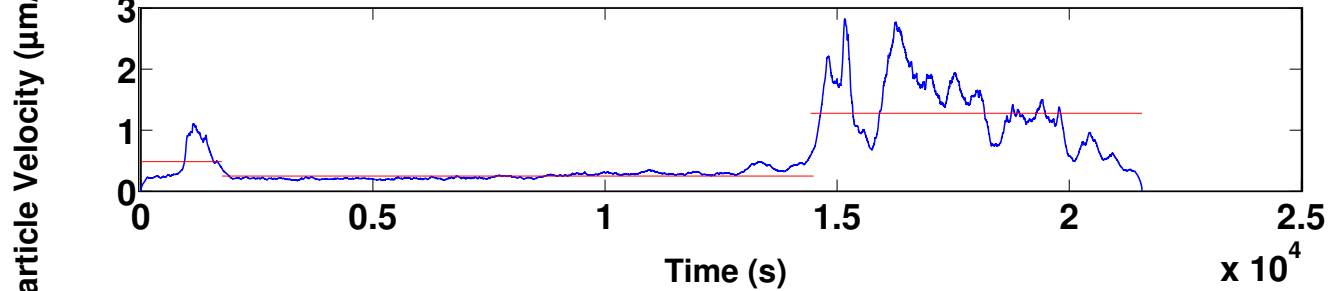
Median-Filtered Seismic Intensity (blue) and changepoint analysis (red)

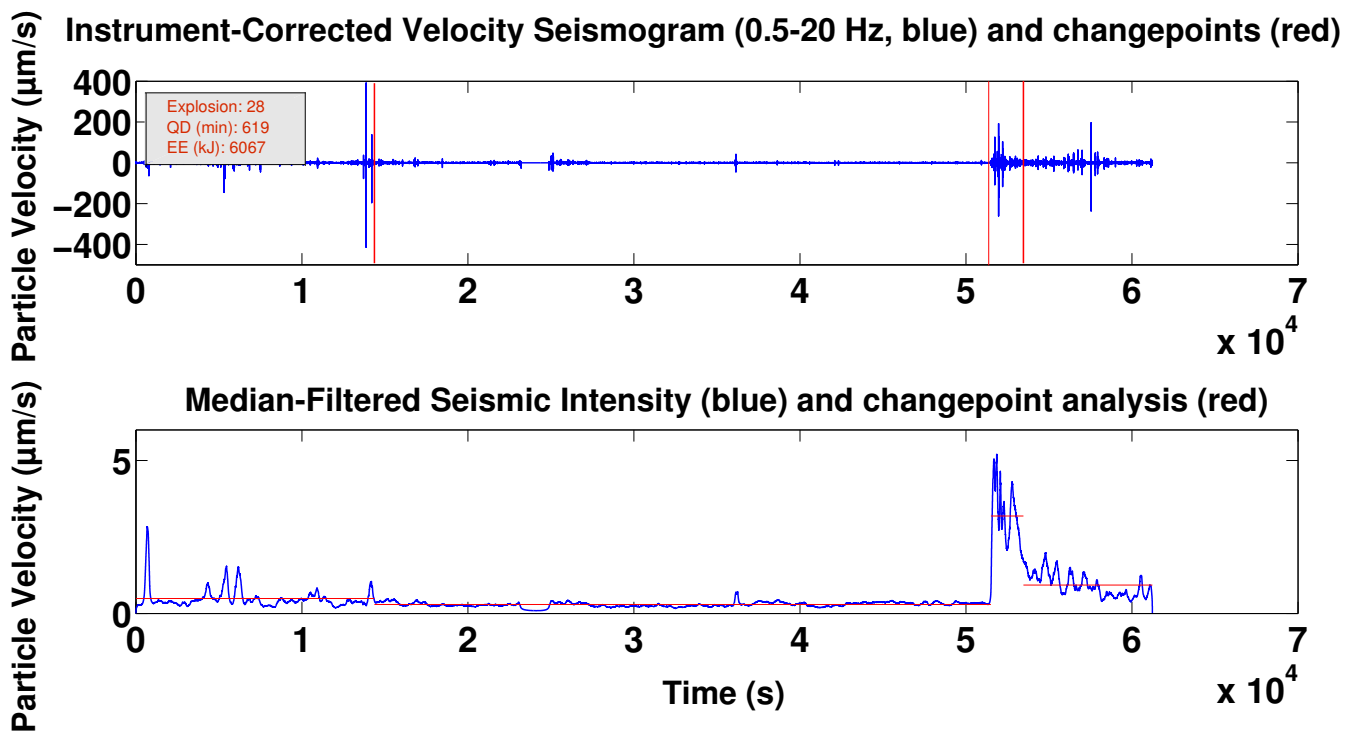
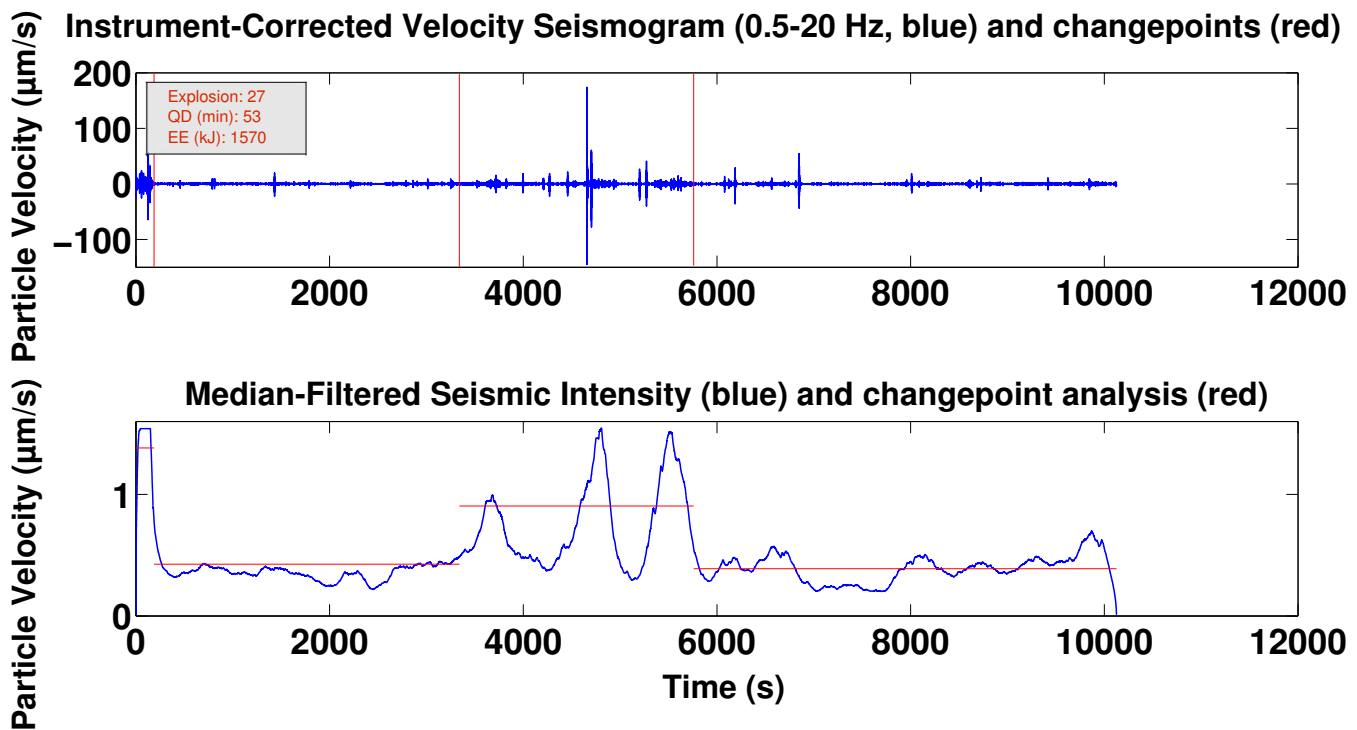


Instrument-Corrected Velocity Seismogram (0.5-20 Hz, blue) and changepoints (red)

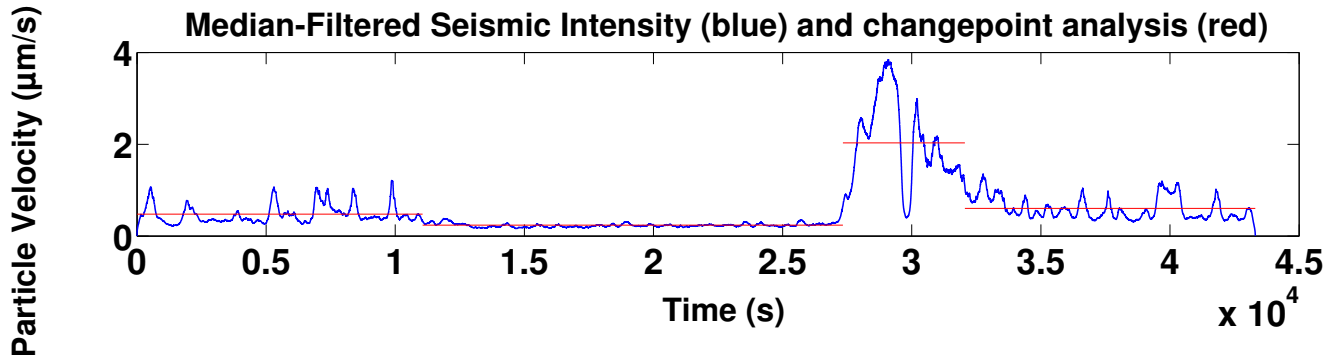
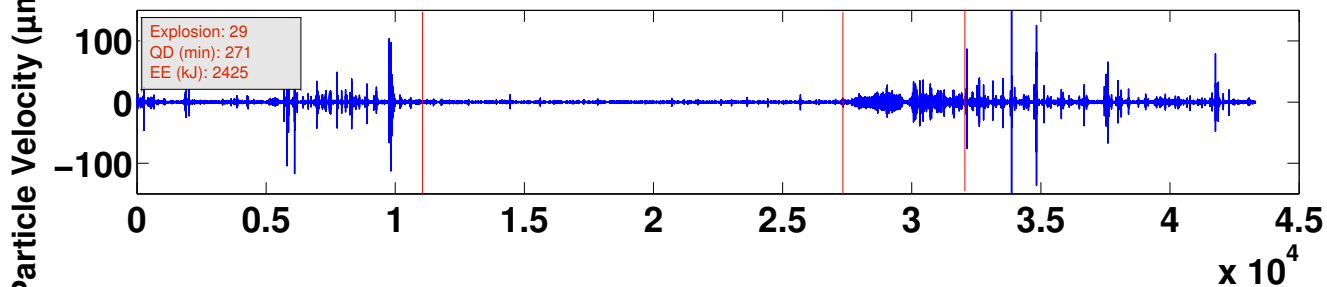


Median-Filtered Seismic Intensity (blue) and changepoint analysis (red)

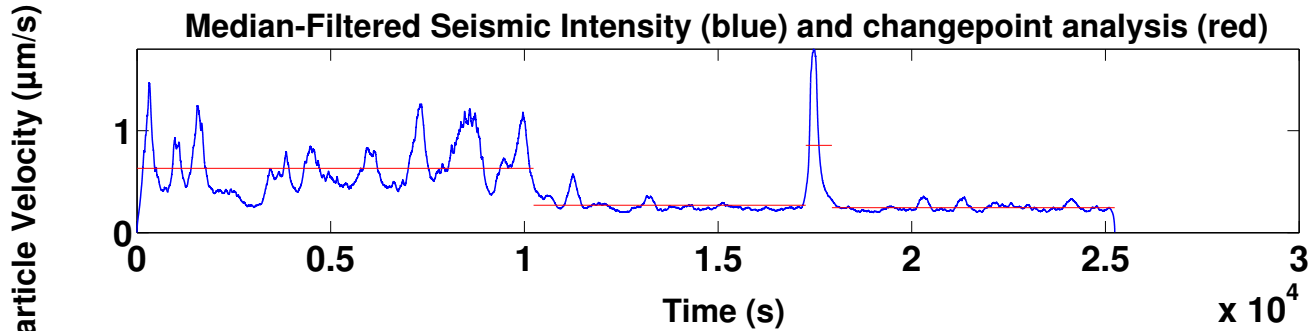
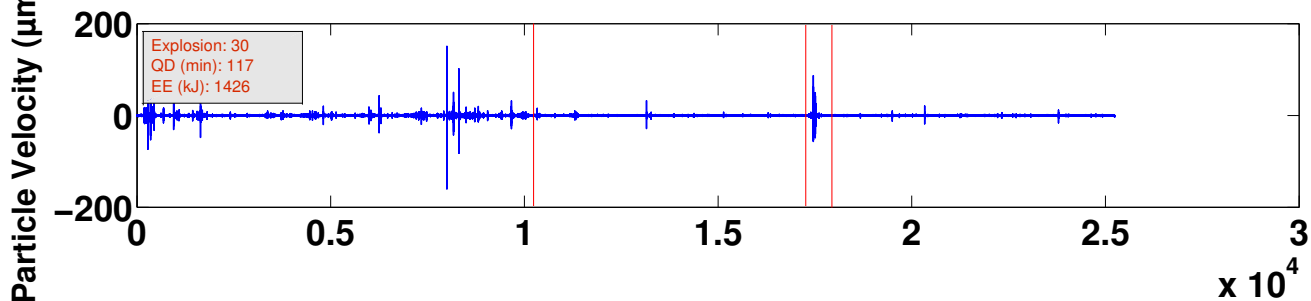


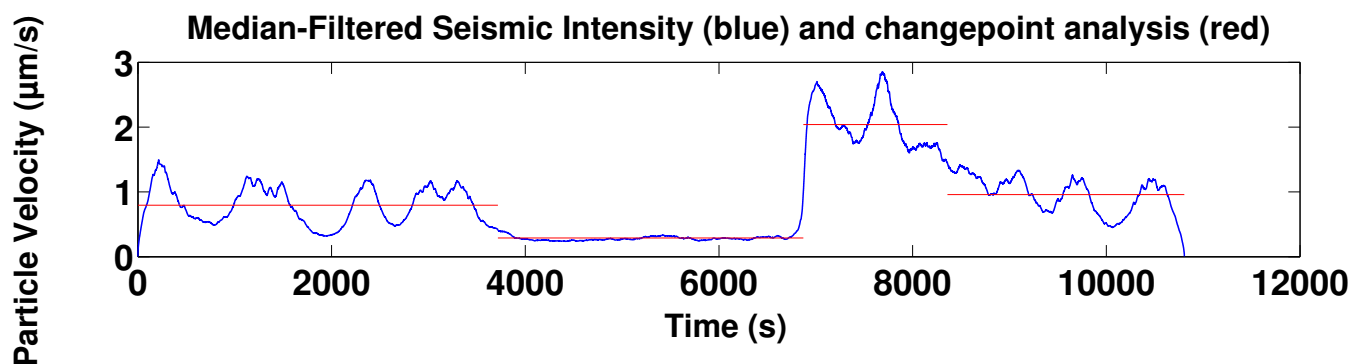
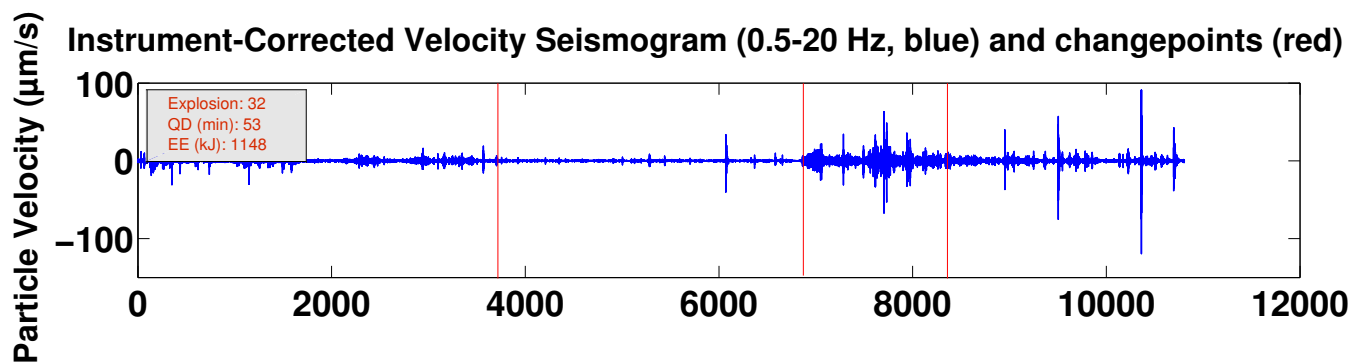
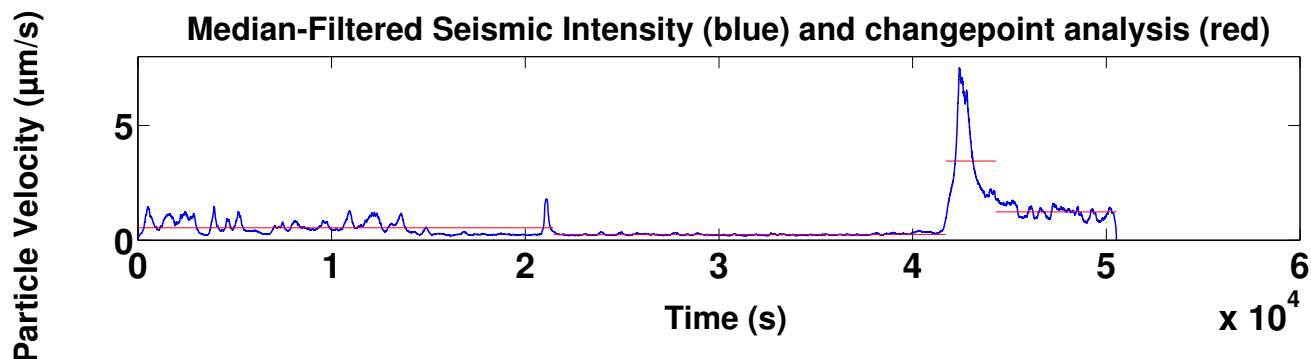
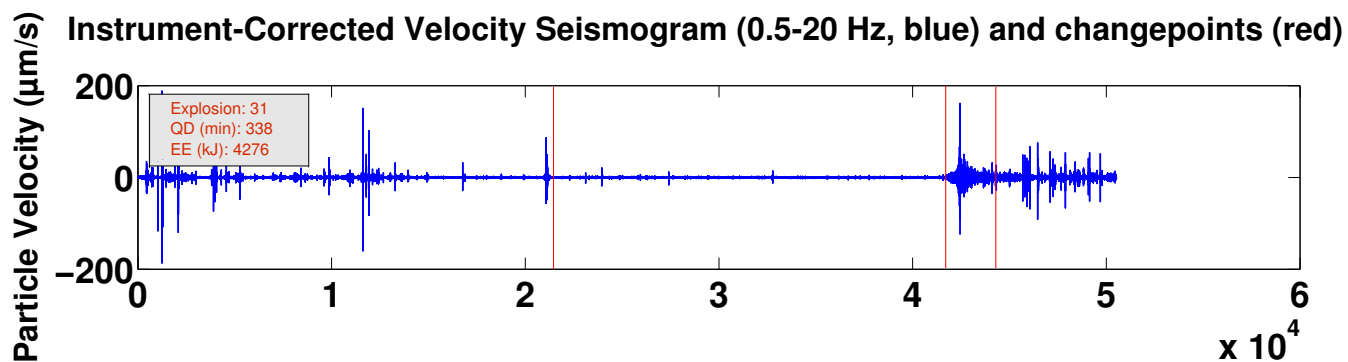


Instrument-Corrected Velocity Seismogram (0.5-20 Hz, blue) and changepoints (red)

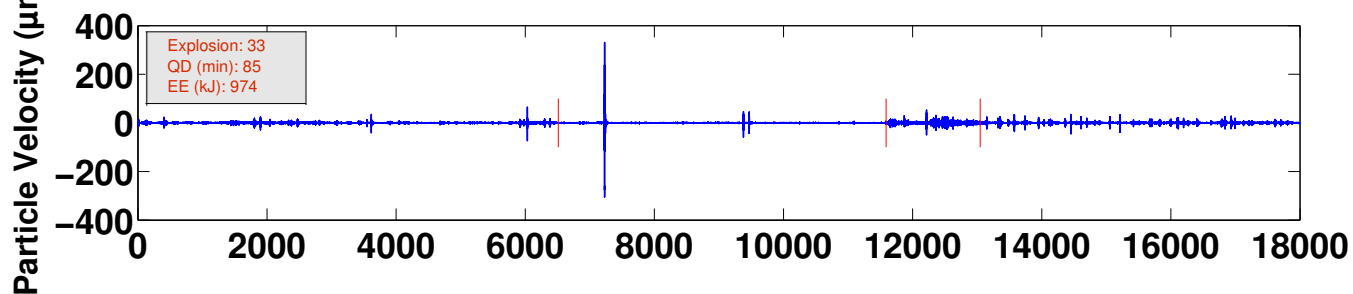


Instrument-Corrected Velocity Seismogram (0.5-20 Hz, blue) and changepoints (red)

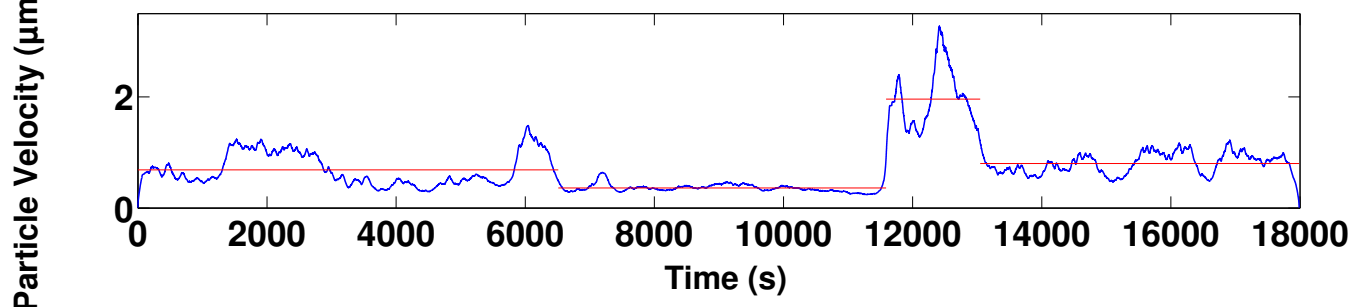




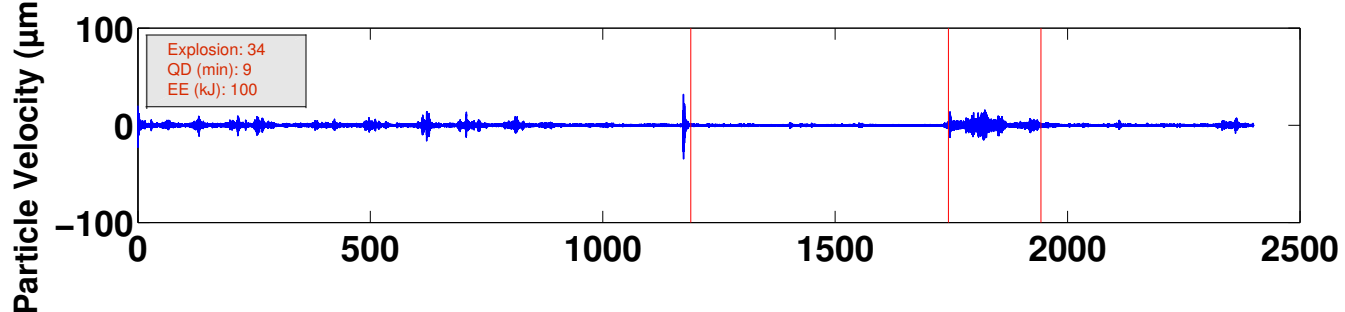
Instrument-Corrected Velocity Seismogram (0.5-20 Hz, blue) and changepoints (red)



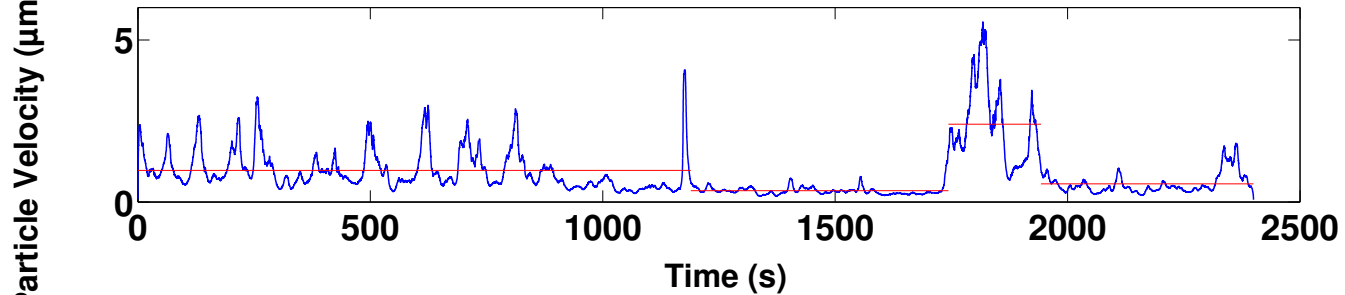
Median-Filtered Seismic Intensity (blue) and changepoint analysis (red)



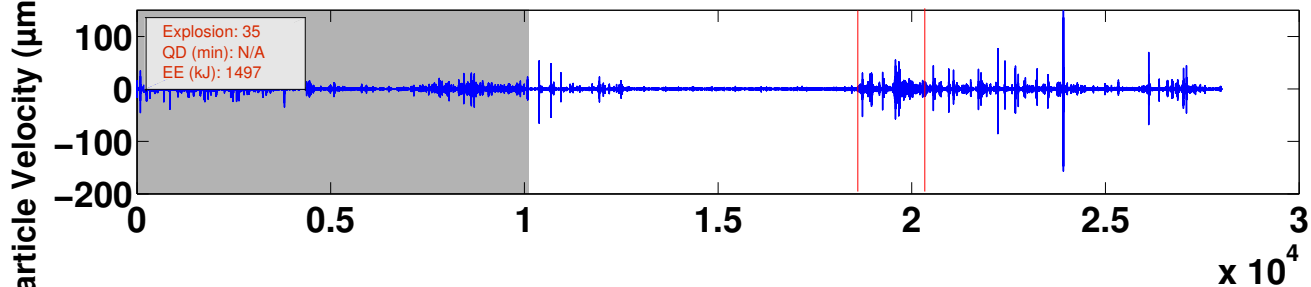
Instrument-Corrected Velocity Seismogram (0.5-20 Hz, blue) and changepoints (red)



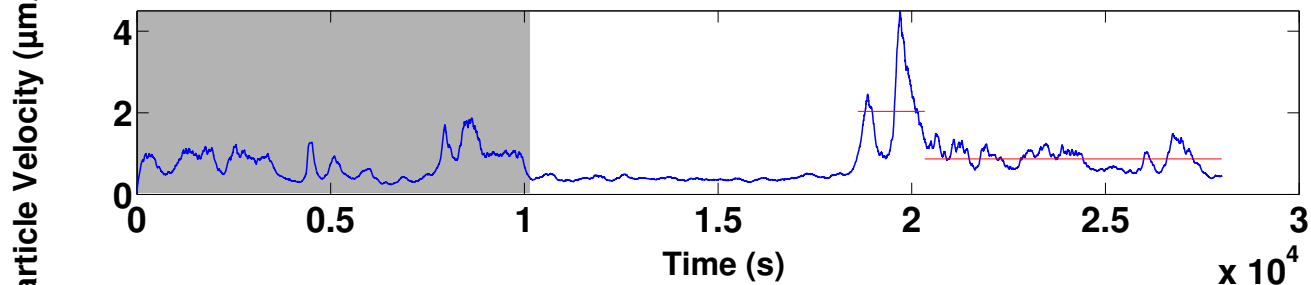
Median-Filtered Seismic Intensity (blue) and changepoint analysis (red)



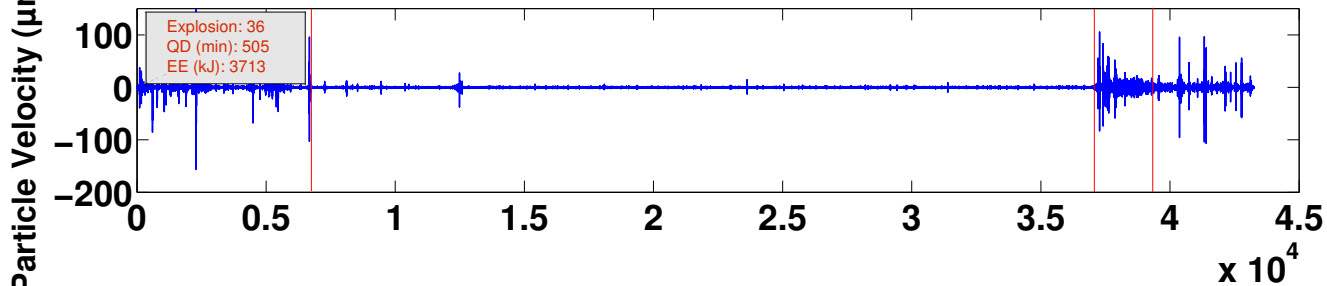
Instrument-Corrected Velocity Seismogram (0.5-20 Hz, blue) and changepoints (red)



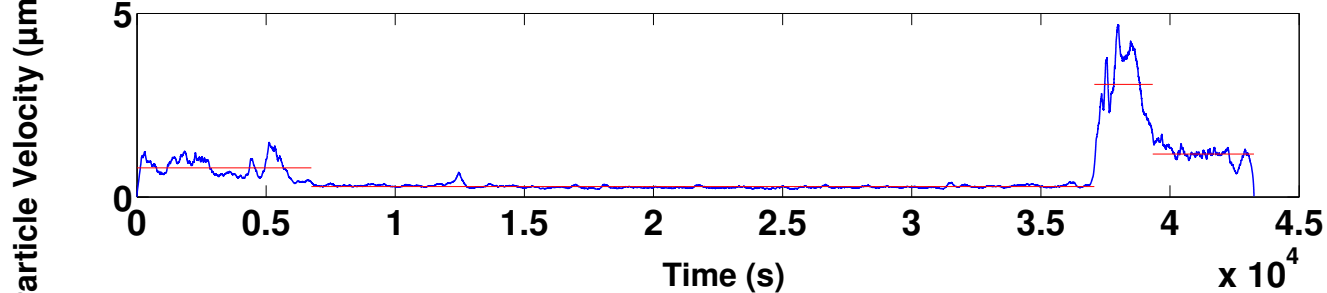
Median-Filtered Seismic Intensity (blue) and changepoint analysis (red)

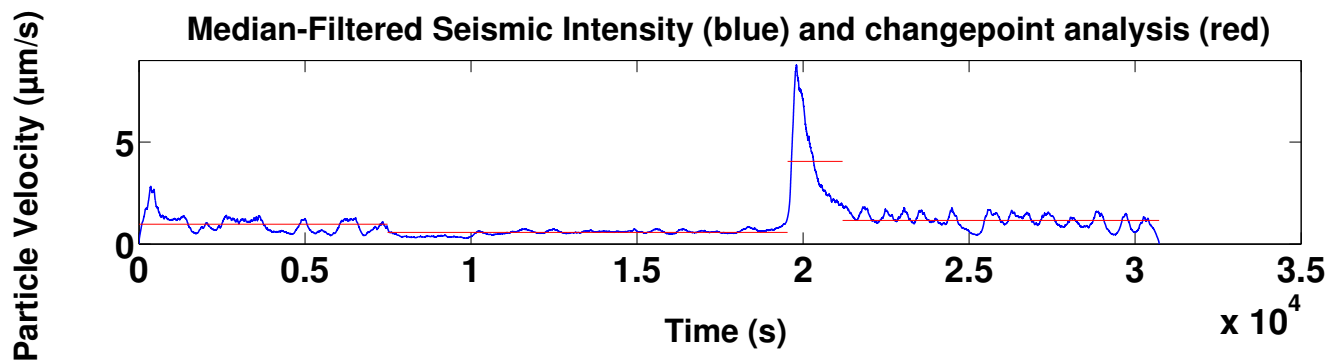
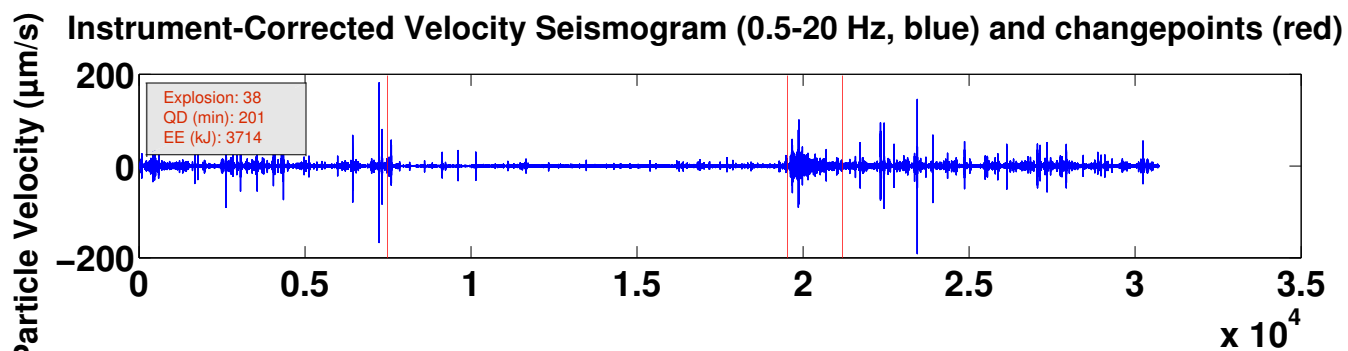
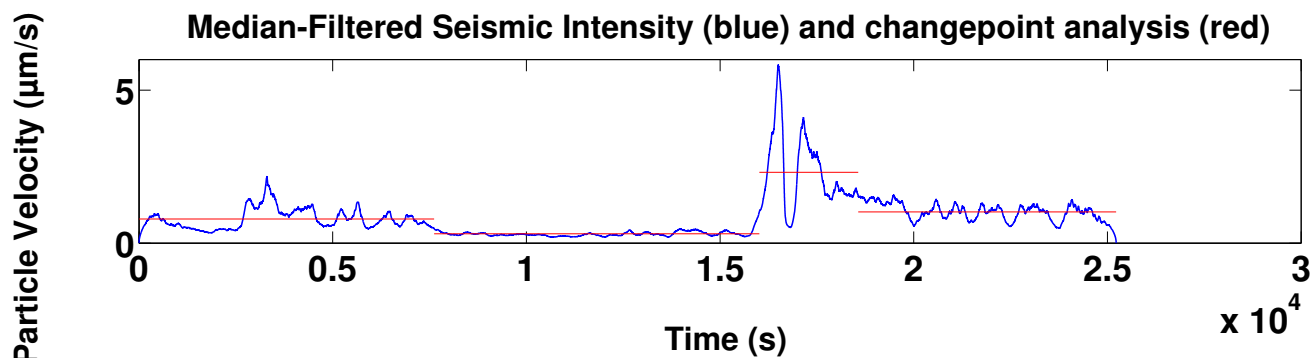
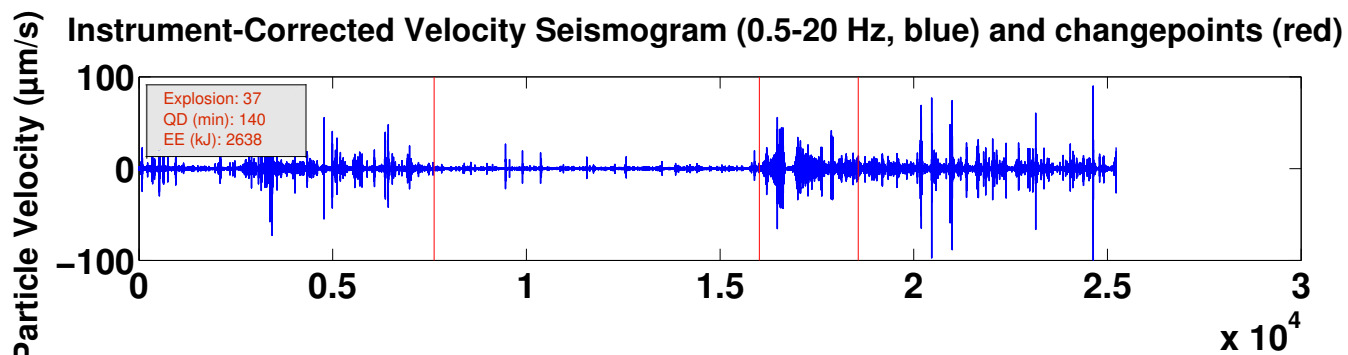


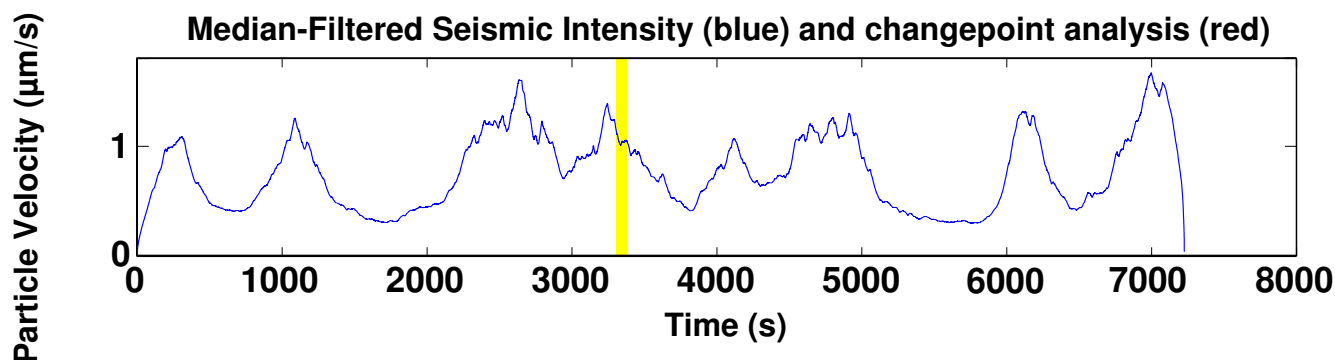
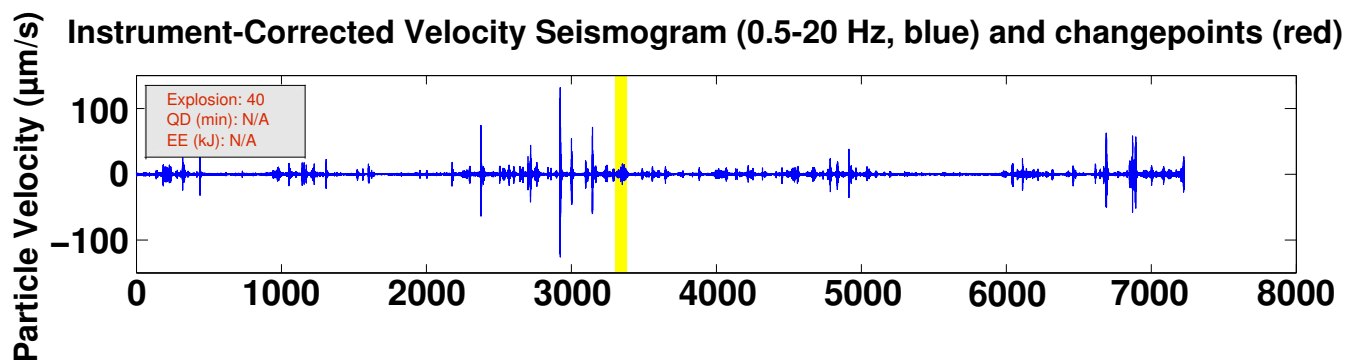
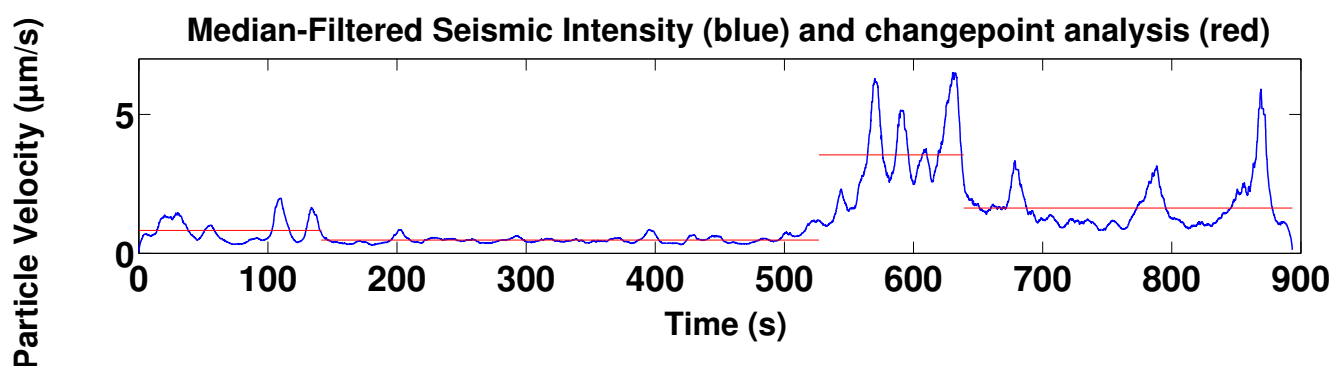
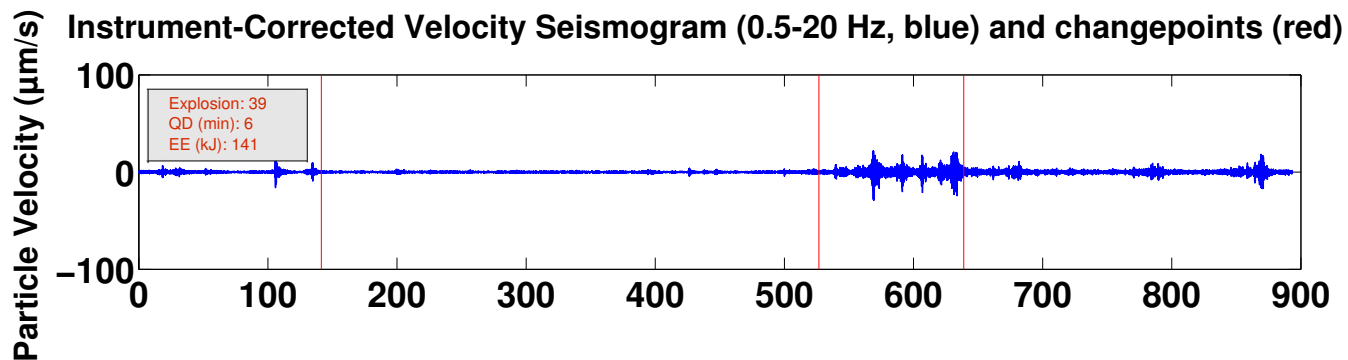
Instrument-Corrected Velocity Seismogram (0.5-20 Hz, blue) and changepoints (red)



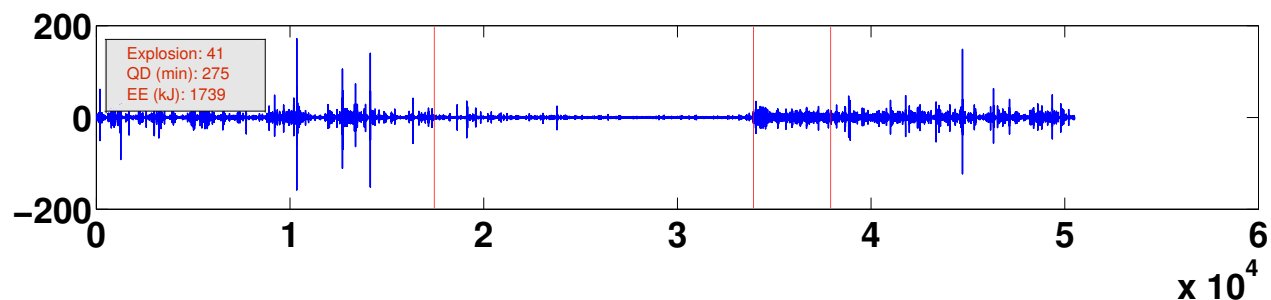
Median-Filtered Seismic Intensity (blue) and changepoint analysis (red)



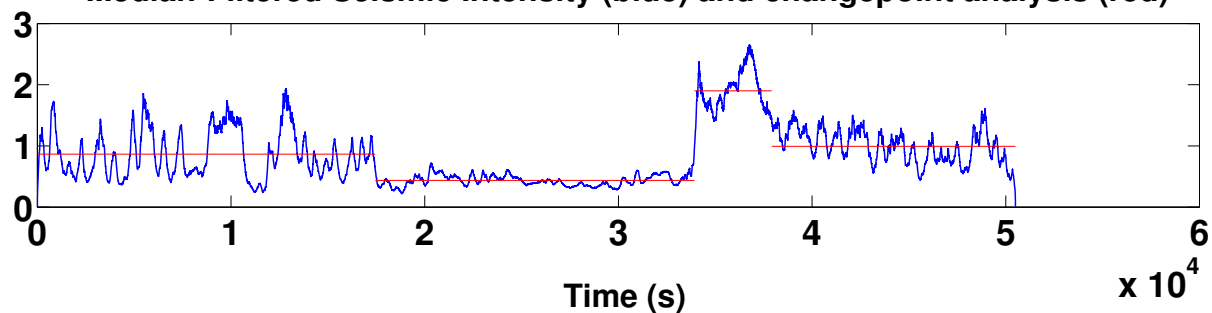




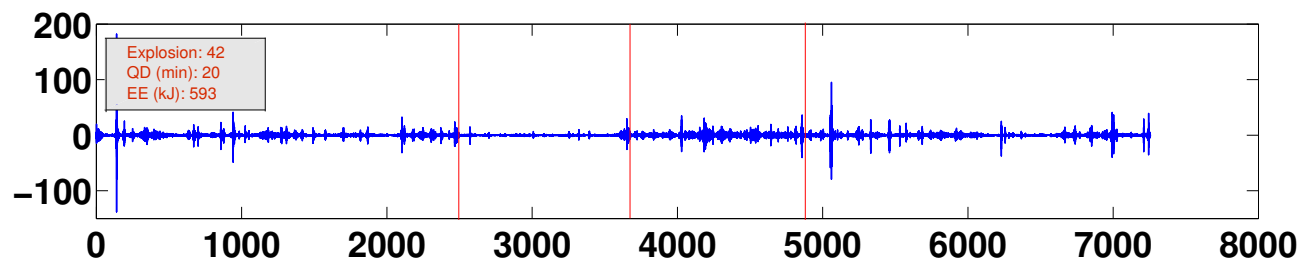
Instrument-Corrected Velocity Seismogram (0.5-20 Hz, blue) and changepoints (red)



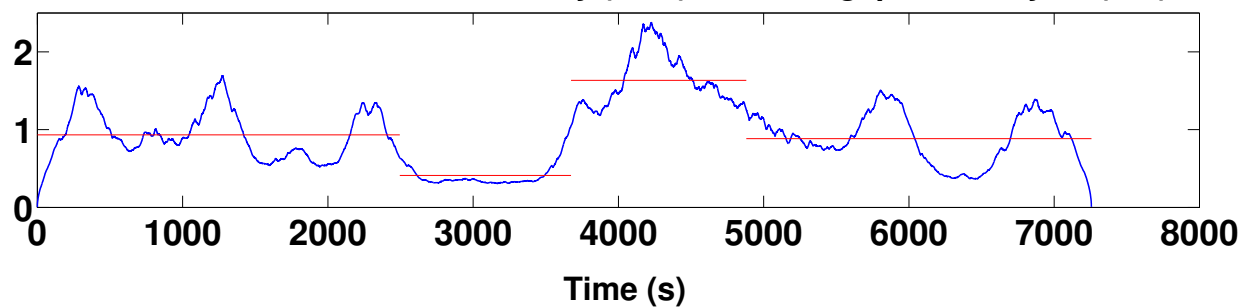
Median-Filtered Seismic Intensity (blue) and changepoint analysis (red)

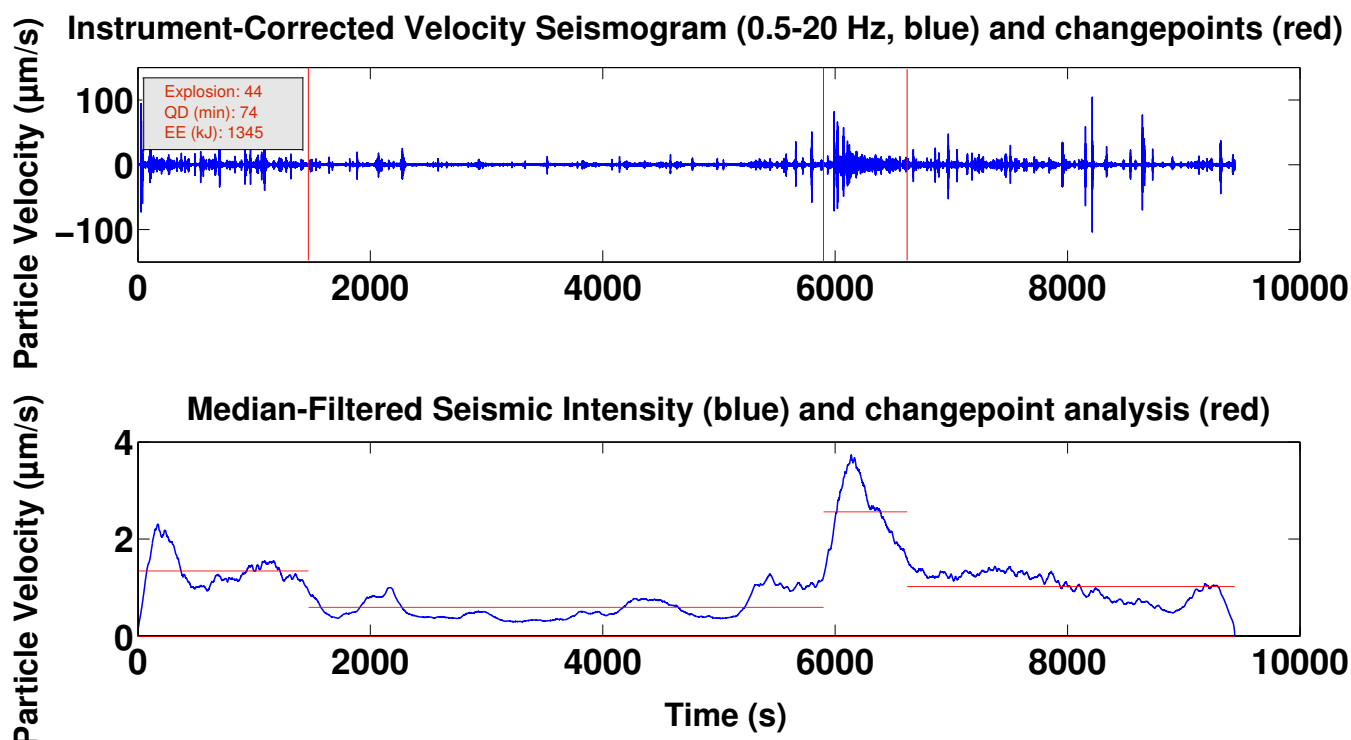
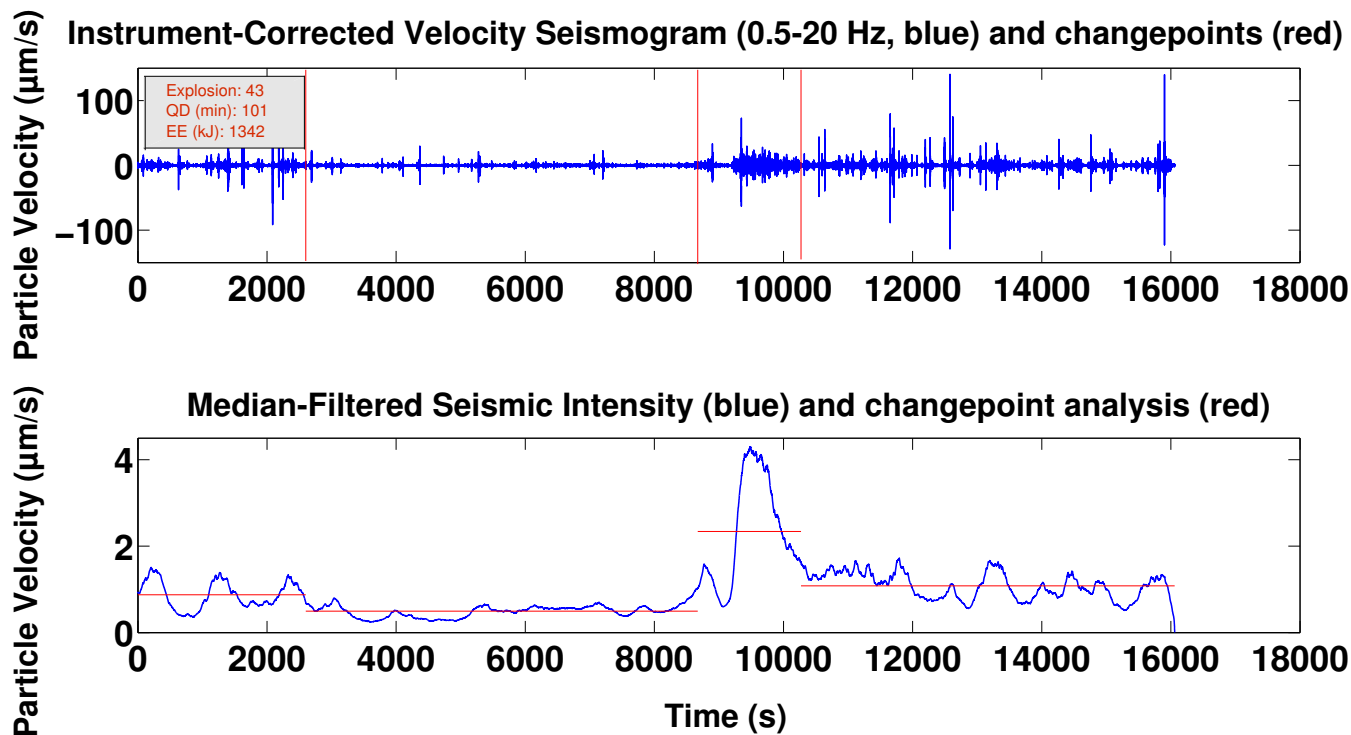


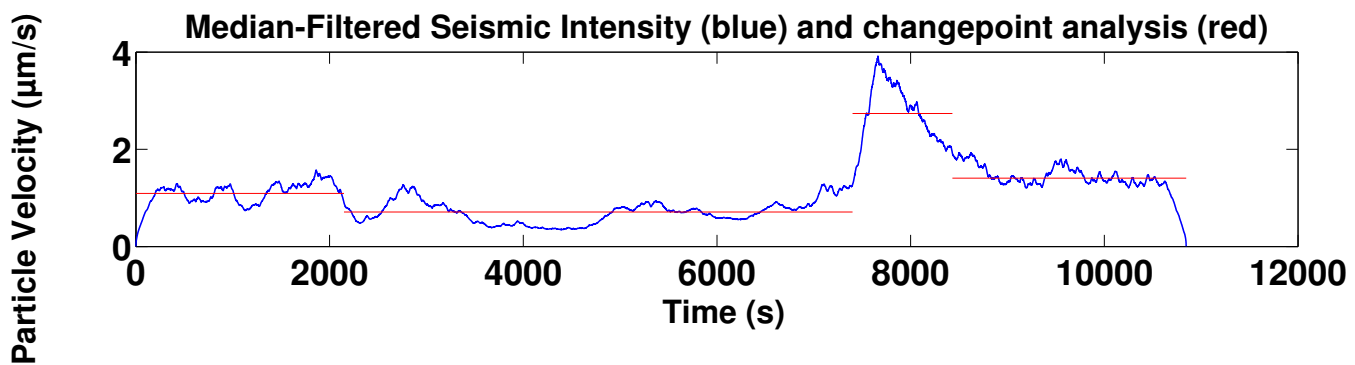
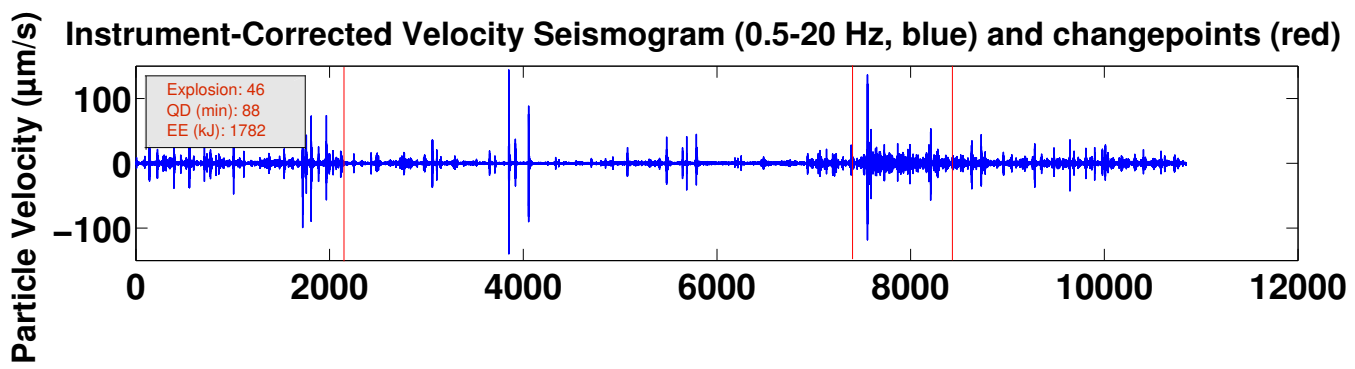
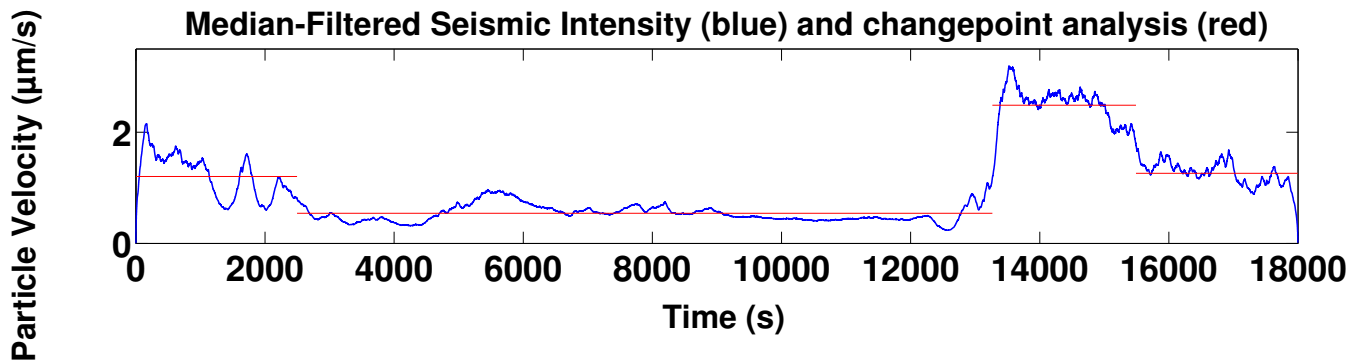
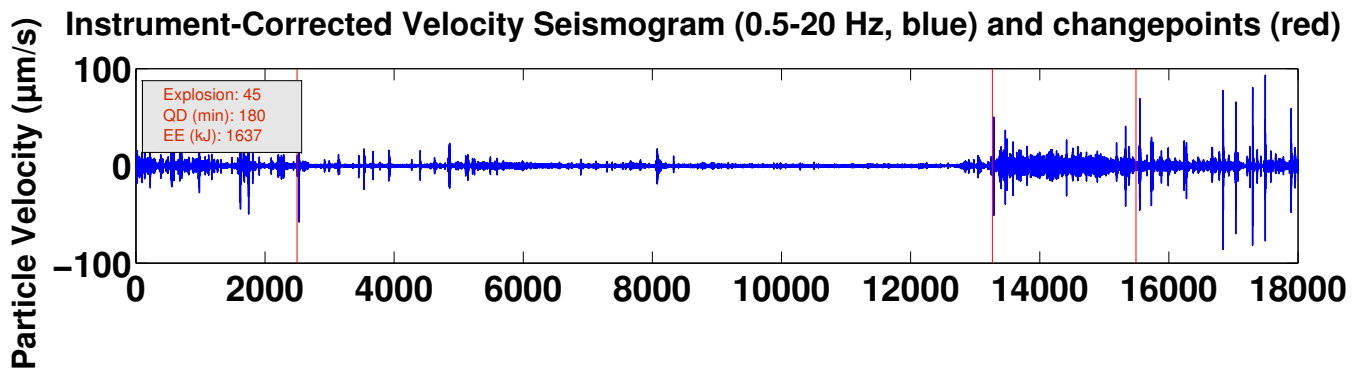
Instrument-Corrected Velocity Seismogram (0.5-20 Hz, blue) and changepoints (red)



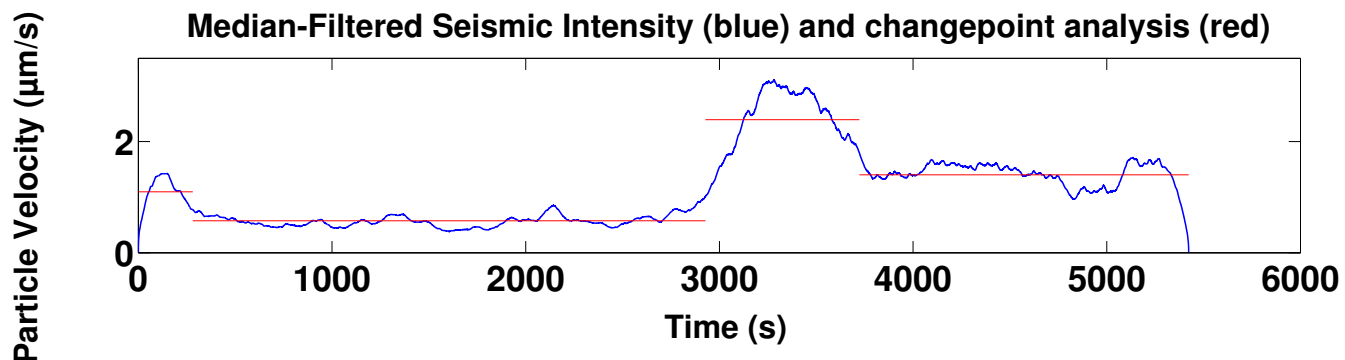
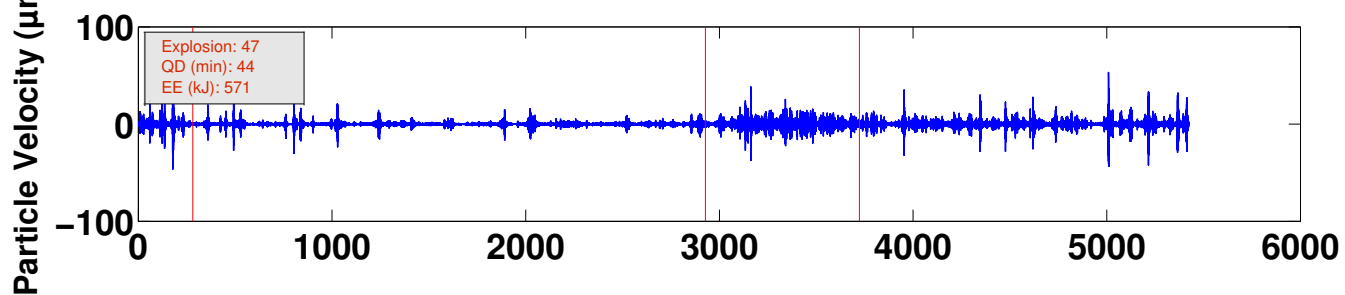
Median-Filtered Seismic Intensity (blue) and changepoint analysis (red)







Instrument-Corrected Velocity Seismogram (0.5-20 Hz, blue) and changepoints (red)



Instrument-Corrected Velocity Seismogram (0.5-20 Hz, blue) and changepoints (red)

